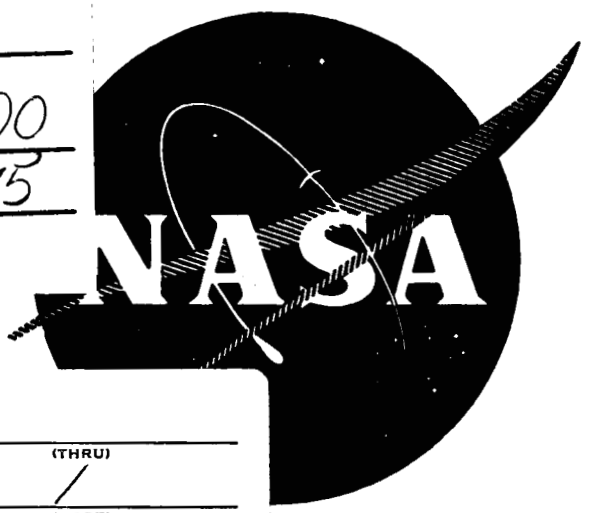

WANL-PR(P)-008
NAS CR54723

DETERMINATION OF THE WELDABILITY AND ELEVATED TEMPERATURE STABILITY OF REFRACTORY METAL ALLOYS

Eighth Quarterly Report

by

G. G. Lessmann and D. R. Stoner

prepared for
National Aeronautics and Space Administration
Lewis Research Center
Space Power Systems Division
Under Contract NAS 3-2540

Astronuclear Laboratory
Westinghouse Electric Corporation

NOTICE

This report was prepared as an account of Government-sponsored work. Neither the United States nor the National Aeronautics and Space Administration (NASA), nor any person acting on behalf of NASA:

A) Makes any warranty or representation, expressed or implied, with respect to the accuracy, completeness, or usefulness of the information contained in this report, or that the use of any information, apparatus, method, or process disclosed in this report may not infringe privately-owned rights; or

B) Assumes any liabilities with respect to the use of, or for damages resulting from the use of any information, apparatus, method or process disclosed in this report.

As used above, "person acting on behalf of NASA" includes any employee or contractor of NASA, or employee of such contractor, to the extent that such employee or contractor of NASA or employee of such contractor prepares, disseminates, or provides access to, any information pursuant to his employment or contract with NASA, or his employment with such contractor.

Copies of this report can be obtained from:

National Aeronautics & Space Administration
Office of Scientific and Technical Information
Washington 25, D. C.
Attention: AFSS-A

Astronuclear Laboratory

WANL-PR-(P)-008

NASA CR-54723

DETERMINATION OF THE WELDABILITY AND ELEVATED TEMPERATURE STABILITY OF REFRACTORY METAL ALLOYS

by

G. G. Lessmann

and

D. R. Stoner

Eighth Quarterly Report

Covering the Period

March 21, 1965 to June 20, 1965

Prepared for

NATIONAL AERONAUTICS AND SPACE ADMINISTRATION
Contract NAS 3-2540

Technical Management
Paul E. Moorhead
NASA - Lewis Research Center
Space Power Systems Div.

Astronuclear Laboratory
Westinghouse Electric Corporation
Pittsburgh 36, Pa.

FOREWORD

This report describes work accomplished under Contract NAS 3-2540 during the period March 21, 1965 to June 20, 1965. This program is being administered by R. T. Begley of the Astronuclear Laboratory, Westinghouse Electric Corporation. G. G. Lessmann and D. R. Stoner are responsible for the performance of this investigation.

Mr. P. E. Moorhead of the National Aeronautics and Space Administration is Technical Manager of this program.

TABLE OF CONTENTS

LIST OF FIGURES

LIST OF FIGURES (Continued)

LIST OF TABLES

1. INTRODUCTION

This is the Eighth Quarterly Progress Report describing work accomplished under Contract NAS 3-2540. The objective of this program is to determine the weldability and long time elevated temperature stability of promising refractory metal alloys in order to determine those most suitable for use in advanced alkali-metal space electric power systems. Alloys included in this investigation are listed in Table 1. A detailed discussion of the program and program objectives was presented in the First Quarterly Report. As an addition to this program, an evaluation of the effect of oxygen contamination on the weldability and thermal stability of refractory metal alloys has been undertaken. Three alloys, including T-111, T-222, and FS-85 will be evaluated. A detailed discussion and outline of this study was presented in the Seventh Quarterly Report.

Process and test controls employed throughout this program emphasize the important influence of interstitial elements on the properties of refractory metal alloys. Stringent process and test procedures are required, including continuous monitoring of the TIG weld chamber atmosphere, electron beam welding at low pressures, aging in furnaces employing hydrocarbon free pumping systems providing pressures less than 10^{-8} torr, and chemical sampling following successive stages of the evaluation for verification of these process controls.

Equipment requirements and set-up, and procedures for welding and testing, have been described in previous progress reports. Any improvements in processes, changes in procedures, or additional processes and procedures are described in this report.

II. SUMMARY

During this period the weldability study phases of this program were completed for the columbium and tantalum alloys. This completes a major portion of this study as outlined in Figure 1, and permits initiation of the elevated temperature thermal stability studies.

A weldability study of yttrium modified D-43 was completed. As with C-129Y and AS-55, yttrium additions to D-43 resulted in improved weld ductility. The net improvement is evident in the bend transition summary shown in Figure 2. This figure shows the range of bend ductile-brittle transition temperatures obtained in testing twelve welds for each of two welding processes for each alloy. For this summary weld parameters were varied over a broad range and welds were bend tested in both the longitudinal and transverse directions. In addition to the improved performance of yttrium modified D-43 (D-43Y), shown in this figure, the post weld annealing response for 1 hour anneals at 1900°F, 2100°F, and 2400°F of D-43Y was considerably different than for D-43. Annealing resulted in moderately improved weld ductility for D-43Y whereas D-43 responded to increased annealing temperature by displaying a severe loss and then recovery of ductility through an apparent age-overage reaction. D-43Y displayed a hot tearing tendency in TIG welding, the cause of which has not been determined.

A study to determine the causes and effects of weld porosity in refractory metal alloys was completed. Porosity appears to result from the degassing during welding of a pickling residue (or adsorbed hydrogen) from the surfaces of the joint interface. Hence, minimizing the joint surface area and eliminating crevices at the interface is desirable. In this respect, machined edges are better than sheared edges. Considerable variation in porosity sensitivity is observed between alloys. Overall alloy fabricability and porosity sensitivity appear to be closely related. The most fabricable alloys can be welded using sheared edges, whereas the less fabricable alloys require machined edges and vacuum degassing following pickling. No significant effects of weld porosity on weld ductility were observed.

Nine program alloys were included in a plate weldability evaluation which was completed during this period. As in the sheet material evaluation, weld ductility was emphasized. The alloys evaluated, in order of decreasing plate weld ductility, were: Ta-10W, T-111, T-222, SCb-291, FS-85, C-129Y, D-43, Cb-752, and B-66. The tantalum alloys, as a group, were considerably more ductile than the columbium alloys. All were readily weldable with the exception of B-66 which has a tendency to hot tear, making thick section welding difficult.

The three alloys included in the study of the effect of oxygen contamination on weldability were doped to the first test level and evaluated. The first contamination level is 500 ppm in FS-85 and 350 ppm in T-111 and T-222, providing approximately equal contamination in atomic percent. Evaluation at this level has been completed. The results tend to confirm preliminary data. T-111 was least sensitive. T-222 was most sensitive, significantly more so than T-111. The difference in T-111 and T-222 remains surprising in view of their close similarity in chemistry. Process control of the doping apparatus has been improved. Numerous process surveillance tests were run to ascertain the adequacy of the doping process.

III. TECHNICAL PROGRAM

A. WELDING EVALUATIONS

1. Weldability of Yttrium Modified D-43 (D-43Y) - The alloys C-129Y and AS-55, evaluated in this program, contain minor additions of the rare earth element yttrium. As an addition to columbium alloys, this element provides an interesting modification of mechanical properties resulting primarily in improved fabricability. The beneficial effect of yttrium has been demonstrated in the weldability evaluation of C-129Y and AS-55, see Figure 1, substantiating the claims by the developers of these alloys[1,2,3]. C-129Y base and weld metal bend ductile-to-brittle transition temperatures are among the lowest of the columbium alloys despite its relatively high solute content. AS-55, even though produced with a high and normally detrimental oxygen level, exhibits reasonably good ductility. Further, both alloys are only moderately sensitive to weld parameter variations as compared with the other columbium alloys. The beneficial effect of yttrium is apparently instrumental in providing the improved ductility in these alloys.

Yttrium is essentially insoluable in columbium, and very reactive with oxygen[4,5]. Hence, the most probable mechanisms for improved fabricability are an effective reduction in matrix oxygen level by preferential combination with yttrium, purification of the base metal during original melting and during welding by slagging of the yttrium oxide, and grain refinement resulting from the presence of the highly stable oxide. To a lesser extent nitrogen levels are also reduced during melting[5] and welding, probably by volatilization as YN, further explaining the improved ductility.

There was no reason to assume that the beneficial effect of yttrium would be limited to AS-55 and C-129Y. Hence, determining the effects of yttrium on other alloys might prove to be an interesting and promising endeavor. D-43 was selected for this evaluation. D-43 has twice the solute level of AS-55 and is nominally a low interstitial alloy. Properly heat treated, D-43 is a promising high strength, high temperature alloy.

Considerable variability in weld ductility is observed in this alloy. This variability reflects the effect of the carbide phase(s) morphology, which is altered considerably during welding, on strength and ductility. This heat-treat sensitivity characteristic was also clearly evident in the post weld annealing study[6] in which D-43 TIG welds displayed a pronounced aging response, Figure 10. A 1900°F, 1 hour age raised the weld transition temperature above 475°F. This loss of ductility was partially recovered after 1 hour at 2200°F, and completely after 1 hour at 2400°F. Obviously any improvement in this alloy resulting from the addition of yttrium would be fairly easily observed.

Four square feet of 0.035 inch thick D-43Y sheet were obtained from the Wah-Chang Corp. for this evaluation. The analyses of this material is shown in Table 2. This sheet has the lowest oxygen level among the columbium alloys indicating both the beneficial affect of yttrium and that adequate production process controls were employed. The sheet was in the recrystallized condition as received with an ASTM grain size of 9 and a DPH hardness of 151, resulting from a final anneal of 2 hours at 2400°F. For comparison the D-43 sheet evaluated in this program had a final anneal of 1 hour at 2600°F, a hardness of DPH 220, and a grain size of 5.

The microstructure of the as-received sheet, Figure 3, show that the D-43 sheet has an aged structure containing predominantly mono-metal carbides transformed in situ from the dimetal carbide. The D-43Y base metal also contains the stable mono-metal carbides but not in an aged structure. These structures account for differences in grain size and hardness for the two alloys and indicate that D-43 was optimized for high temperature strength through strain induced precipitation hardening[7], whereas D-43Y was not. This difference in structure may also be largely responsible for differences in base metal bend ductility, but not for differences in the weld bend test results discussed below. For both alloys weld bend specimen failures occurred in thermally distrubed areas (weld or heat affected zone) not in the unaltered base metal, demonstrating that the base metal condition did not influence weld bend test results.

The weldability evaluation of D-43Y followed the procedure standardized for this program and reported in previous reports[8]. Weld parameters were chosen to ascertain the effects of variation in weld freezing rate, cooling rate, and unit weld length heat input. This is accomplished in TIG welding by varying the welding speed, clamp spacing, and weld size (amperage) and maintaining other factors, including arc gap and electrode configuration, constant. Essentially the same procedure was employed in EB welding except that weld size is influenced also by the cyclic beam deflection and beam current is restricted for any one weld speed-beam deflection combination because of the physical effect of the beam power density on the weldment.

Weld parameters are given in Tables 3 and 4 while bend test results for the individual welds are shown in Figures 5 to 8. The base metal bend test curves are shown in Figure 4. Some difficulty was encountered in TIG welding D-43Y. Weld No. 11, Table 4, had a transverse crack through the weld. This is an unusual failure with no apparent explanation. Initially welds 5, 7, and 10 hot tore during welding but reruns of these were satisfactory. The significance of the hot tears is not clear since these occurred in joining narrow specimens, one-half inch wide, which probably permits more walking during welding than would be encountered in wide, and more restrained, sections. Undoubtedly these tests demonstrate a tendency toward hot tearing, but perhaps not as severely as a cursory examination of these results would indicate. There was no hot tearing noted in the bead-on-plate patch test run on this alloy. In this respect, these results are similar to those described for welds in oxygen doped T-111, see Section III-B of this report. Hot tearing of the T-111 welds was unexpected, thereby tending to also raise the question of significance with D-43Y. In addition to the hot tears, several D-43Y welds contained porosity which, as described in Section III-A-3 of this report, results primarily from inadequate joint preparation even though innate alloy characteristics are also partially responsible. In both TIG and EB welds, improved ductility was slightly favored by moderate weld speeds and small TIG welds were slightly more ductile than large ones. Among the TIG welds, the transverse transition temperature tends to decrease

with increased welding speed while the longitudinal transition temperature increases. This could indicate that weld strength increases slightly with increased speed causing, by non-uniform bending, a transference of strain in transverse tests from the weld to more ductile base metal resulting in an apparent lowering of the DBTT. With the uniform straining of longitudinal tests, however, the increased weld strength causes an apparent increase in the DBTT. These trends are not particularly strong. Hence, the spread in transition temperatures observed appears to represent an alloy characteristic more than a measure of the effect of welding variables. This observation is in basic agreement with the results which have been obtained on the other alloys. In this respect Figure 1, which compares the alloys on the basis of total spread in bend transition temperatures provides a comparison of an actual alloy characteristic, the variability of weld ductility. From this figure alloys can be compared on the basis of both the lowest transition temperature obtainable and the variability involved in obtaining consistent ductility, namely the spread in ductile-to-brittle transition temperatures. A considerable improvement in ductility is apparent for D-43Y as compared with D-43. Both the transition temperatures and their variability are less for D-43Y.

An interesting improvement in alloy behavior also occurred in the post weld annealing study. The response of D-43Y weld ductility, as measured by the ductile-to-brittle transition temperature, to annealing is shown as a function of temperature in Figure 9. The corresponding behavior for D-43 is shown in Figure 10. A significant loss and then recovery of weld ductility with increasing temperature was observed for D-43, while D-43Y responded primarily with moderately improved ductility. D-43Y is apparently considerably less sensitive to the selected post weld anneals than D-43 indicating that the presence of yttrium, or Y_2O_3, appreciably alters the morphology and/or kinetics of carbide precipitation.

This evaluation has demonstrated that the beneficial effect on ductility of minor yttrium additions can be realized in D-43 as well as in C-129Y and AS-55. In total, a great deal more information is required to understand this phenomena with respect to its effect on the kinetics of metallurgical reactions, phase morphology, and consequently

physical and mechanical properties. The tendency of D-43Y to hot tear could be a disadvantage although the cause of these tears is not obvious. In this respect, however, an unusual weld failure also occurred in a C-129Y program weld (one prepared using optimized TIG weld parameters for the thermal stability study). This weld fractured along its centerline in a virtually flat plane from the weld start for about 2 inches. The fracture appeared to occur upon removal from the welding fixture. It was easily extended another 2 inches by hand bending the two halves of the weld demonstrating the existence of a plane of weakness in this weld. The tearing was identified as a grain boundary fracture. This failure is suspicious in that it was unique for a weld in as-received sheet and may therefore be related to the yttrium which could be preferentially concentrated as a largely incoherent oxide at weld centerline grain boundaries. A similar defect in oxygen contaminated T-111 has occurred. Preliminary electron metallography data indicates that the T-111 fracture surface does in fact contain a high precipitate concentration. (See Section III-B of this report).

2. Manual TIG Weld Evaluation - Manual TIG welding has been employed in this program for restraint tests in 0.035 inch thick sheet and 0.375 inch thick plate, and for butt welding plate test specimens. The welding for both of these efforts has been completed and the results are presented in this section.

Restraint Tests - Bead-on-plate patch tests and circular groove restraint tests were used in evaluating hot or cold cracking tendencies in sheet and plate thicknesses respectively. Sketches of the specimens employed in these tests are shown in Figure 11. Actual welded specimens were shown in previous reports. Sheet and plate specimens were inspected visually and by dye penetrant. Sheet specimens were also radiographed. Test results are summarized in Table 5. A measure of the relative strain introduced in these tests is provided by the distortion measurements listed in this table. Considerable distortion occurred in all specimens indicating the severity of these tests. Because of experimental variability, as noted particularly by differences in weld width, the distortion per se is probably not a valid basis for alloy comparison. Also, distortion is routinely encountered and accommodated in welding fabrication. Hence, the primary significance of these tests lies in demonstrating simple weldability

as measured by the ability to produce sound welds using conventional welding practices.

All patch tests showed NDT indications at weld craters but these were not listed as "positive" in Table 5 since they could have been eliminated by weld current tailing. The B-66 patch test had a positive indication of a 1/8 inch weld start crack by both radiographic and dye-penetrant testing. This crack is probably a hot tear since this problem has been previously observed in welding B-66. Positive indications in FS-85 radiographs were traced to weld texture, not defects.

No defects were detected in the circular groove plate weld specimens. These specimens were welded with a fusion root pass to increase the effective weld depth. Two filler passes were required to fill the groove. Filler was manually added to the weld using 0.082 inch diameter wire of the same composition as the base material. No particular difficulty was encountered and, based on this test, all alloys appear to have satisfactory weldability in plate thicknesses.

Plate Butt Welding - To ascertain the effect of increased section thickness on weldability, a plate butt welding evaluation has been included in this program. In general, weldability requirements tend to become more stringent with increased section thickness and the effect of welding on mechanical properties becomes exaggerated. Hence, the plate weld evaluation represents an important phase of this program complementing the previously reported sheet weld study. Because of the large size of plate weldments, and thus high material cost, the scope of this effort was more restricted than for the sheet weld evaluation. Nine alloys were included in the plate welding study. These included all the tantalum alloys and all the columbium alloys except D-43Y and AS-55. The tungsten base alloys will not be welded in plate thicknesses. Approximately thirty-six feet of plate welding was required.

The plate weld program followed for each alloy is outlined in Figure 12. All specimens were prepared with the same double "U" joint configuration (see Figure 13). This is not necessarily an optimized design but proved satisfactory for all the alloys investigated. Welds were evaluated by bend testing, post weld annealing, tensile testing, and optical metallography. Both longitudinal and transverse tests were run. Chemical analyses were

obtained to aid in evaluating the welding process controls.

Welding Procedures - Welding procedures for the different alloys were generally the same. Tungsten arc, direct current straight polarity, manual welding in a helium atmosphere was used. The root of the welds were tacked together with zero joint clearance, and the fusion root pass was made without the addition of filler metal. Additional passes, two for the columbium base alloys and two or three for the tantalum based alloys, on each side with filler wire added manually completed the butt weld. The filler wire diameter was 0.082 inches. Typical weldment configurations are shown in the macro-sections of Figure 15. Weldment flatness was controlled by alternate welding on opposite sides of the weld joint, and by introducing a camber into the joint (by adjusting the tack weld holding fixture) before applying the root pass. These actions taken at the discretion of an experienced welder proved adequate for flatness control. Amperage and welding speed were both controlled by the welder. These were approximately the same for a particular alloy group. Hence, the welding schedule of Figure 14 for SCb-291 plate is typical of columbium alloys. Higher welding currents and slower welding speeds were used for tantalum alloys. Support blocks of either columbium or tantalum were placed under the specimens during welding to avert contact with and, hence, pickup of copper from the water cooled work platen.

All welding was accomplished in the vacuum purged weld box following a sixteen hour (overnight) pumpdown to approximately 10^{-6} torr. Backfilling was accomplished using ultra-high purity helium providing total active impurity levels of about 1 ppm. Atmosphere monitors were employed and welding was halted when the oxygen level reached 5 ppm or the moisture level reached 10 ppm. The acceptable moisture level for plate welding was set higher than for sheet welding (10 ppm vs. 5 ppm). This was necessary for practical reasons since increased outgassing of interior weld chamber surfaces, the primary source of water vapor, occurred with the high heat input of plate welding.

To minimize moisture outgassing and for operator comfort, extensive internal chamber cooling was employed. A water cooled convection heat exchanger, Figure 16, and specially designed water cooled welding torch and platen, Figure 17, were used. All flexible water

connections on this tooling, including the torch coolant lines, were constructed from convoluted stainless steel tubing providing essentially zero moisture permeability. Integrally spined copper tubing was used in the heat exchanger providing excellent heat transfer characteristics. The installed exchanger was baffled and canted in a manner which enhances convection. The heat exchanger provided a comfortable chamber atmosphere temperature. The water cooled platen and torch maintained adequately low temperatures in the work area for operator comfort and to avoid overheating, evaporation, or decomposition of gloves and torch insulators.

Two torch styles are shown in Figure 17. One torch is equipped with an outer plastic insulating sheath while the other uses nylon standoffs to insulate the stainless hose from the torch and feed through assembly (not shown). The sheath design has proved less satisfactory than the standoff design. Plastic sheaths tends to outgas and decompose during a moderate temperature, chamber evacuation, bakeout. The torch is equipped with a radiation shield. This protects the operator's hand from the radiant heat of the weldment. The use of a shield has proven to be a necessity because of the increased thermal radiation of the high melting point refractory metal alloys. The tantalum alloys in particular, with melting points above 5000°F, have been troublesome in this respect.

Mechanical Test Procedures - Tensile tests were conducted according to recommended Material Advisory Board procedures[9]. A strain rate of 0.005 in/in/min was used through the 0.6 percent offset yield point, then 0.05 in/in/min to specimen fracture. Tensile specimen designs are shown in Figures 18 and 19. Two inch gage lengths were used except for longitudinal plate weld tensiles which had one and a half inch gage lengths. Tensile test results for plate welds are listed in Table 6. For comparison, sheet tensile results for base metal and transverse welds are listed in Table 7. All tensile tests were run on post weld annealed specimens. The annealing temperatures were chosen on the basis of post weld annealing studies reported in the Seventh Quarterly Progress Report. Pre-treatment for base metal tensile specimens was the same as for weld specimens to assure that comparable data was obtained.

All plate weld bend testing was done at room temperature, using single point loading over a fixed test span. Each specimen was tested in three stages using successively sharper punch radii. The three punches have radii of 16t, 8t, and 3t. These are used to produce successive respective bend angles of approximately 25°, 40°, and 140°, and calculated outer fibre tensile strains of 3%, 6%, and 14%. Bend specimens were of conventional size, 1-1/2 inches wide by 6 inches long. Welds were tested in the as-welded condition. The test fixture and typical bend tested weldments were shown in the Sixth Quarterly Progress Report. Welded plate bend test data are summarized in Tables 8 and 9. A proportional limit stress was calculated for most of the bends shown on these tables. Since contact points at the punch and supports translate along the surfaces throughout the bend test, the proportional limit calculation was based on an arbitrary selection of the load moment arm length. Hence, while they are useful in ascertaining the relative resistance of the various alloys to bending by correcting for specimen section variations, they do not represent accurate values of absolute stress.

For each alloy and each of two weld operators, specimens were bend tested in both the longitudinal and transverse directions. Also, bend tests were run on annealed specimens. Selected annealing temperatures, as with the tensile specimens, were based on results obtained in the sheet welding evaluation and are therefore not necessarily optimum for plate welds.

RESULTS

The plate welding study results are summarized for each alloy in the following discussion. Alloys are discussed in order of decreasing ductility. The tantalum alloys are superior in this respect to the most ductile columbium alloy.

Ta-10W - This alloy has excellent as-welded ductility in plate and sheet thickness as demonstrated in tensile and bend tests. Its performance in this respect was the best among the alloys tested. The as-welded longitudinal plate tensile test had an elongation at 24%, easily sufficient to accommodate the highest strain requirements on the 3t bend tests. Ta-10W was not tested in the post weld annealed condition since there is no apparent benefit to be gained by annealing. Comparing the plate weld tensiles to sheet base tensiles, a joint

efficiency of greater than 90% can be assumed.

T-111 - This alloy was only slightly inferior to Ta-10W producing full ductile bends as welded except that both a transverse and longitudinal bend had slight tension surface weld tearing. No defects were noted in the 2400°F annealed specimens. The annealed longitudinal plate weld tensile had 22% elongation. Metallography revealed slight weld grain boundary precipitation and also a heat affected zone-base metal interface precipitate which was previously observed in sheet welds and identified as hafnium monocarbide[6]. The tensile joint efficiency for T-111 appears to be about 100%.

T-222 - This alloy also exhibited good ductility and proved nearly equal to T-111 while exhibiting greater strength. Slight weld tension surface tearing was noted in all the as-welded bend specimens. This was eliminated by post-weld annealing for 1 hour at 2400°F. The plate weld strength exceeded the sheet base metal strength for this alloy.

SCb-291 - As expected, because it is solid solution strengthened and only of moderate strength, SCb-291 proved to be the most ductile columbium base alloy. The single failure occurring in this alloy was a full section fracture in a longitudinal specimen which bent through the nominal 140° before failure. Other specimens, including two stress relieved at 1900°F, produced defect free bends. A lower temperature anneal was employed for the plate than was used on the sheet since the higher temperature, 2200°F, might impair the ductility of this alloy through grain growth and it was felt that an overage anneal should be unnecessary. The difference in annealing temperatures probably accounts for the lower tensile strength of the sheet as compared with the plate weld tensile strength.

FS-85 - This alloy exhibited improved strength with a weld joint efficiency exceeding 90%, while retaining reasonably good as-welded ductility. The annealed longitudinal plate weld tensile specimen had 21% elongation corresponding with the full ductile 140° bends obtained in the annealed welds. Both as-welded longitudinal bends failed, at 40° and 125°, by sudden, severe transgranular cleavage. Weld ductility was recovered by annealing for 1 hour at 2400°F. The cleavage failures are typical of columbium alloys. This behavior

contrasts with the tantalum base alloys in which failures occurred as ductile tears indicating a total strain limitation rather than a loss of resistance to fracture propagation. The effect of annealing on welded FS-85 plates was similar to that observed for sheet welds, Figure 20. Weld precipitation occurred in solute rich weld areas, but only in the final weld pass indicating that successive weld passes tend to homogenize the cast structure of the previously applied passes. Annealing also resulted in slight grain boundary precipitation in the heat affected zone and base metal.

C-129Y - As compared with FS-85, increased strength at room temperature is realized with a moderate loss in ductility. The ductility is recoverable through a 2400°F, 1 hour anneal. The as-annealed plate weld strength is at least equal to the annealed sheet base metal strength implying nearly a 100% joint efficiency. The metallurgical structure appears relatively stable with only minor second phase precipitation occurring during annealing in the solute rich intercellular areas of the weld. The base and heat affected zone contain a dispersed and also agglomerated second phase(s). Weld bend test failures occurred catastrophically by full section transgranular cleavage as typical of the columbium alloys.

D-43 - The strength of welds in this alloy is not significantly higher than for C-129Y even though a more severe ductility loss is encountered which was not recovered by the single post-weld annealing treatment investigated. Strength and ductility in this system are dependent on the morphology of dispersed carbide precipitates which is controllable through heat treatment. Hence, these results are not likely optimized, and, in fact, the data reported by Roche[10] indicate that a considerable loss in ductility in this alloy can be recovered by thermal treatment.

Based on Roche's results, the as-welded structure in the weld and heat affected zone contains Cb_2C platelets, Figure 11. These are stable above 2900°F but tend to transform to low temperature mono-metal carbides on slow cooling, as would be encountered in plate weldments, causing loss of ductility. Annealing in the 2300°F range should result in eventually completing the transformation of the Cb_2C platelets to a finely dispersed cubic

columbium-zirconium carbide and restoration of ductility. Evidence of this transformation is apparent in the annealed weld microstructure, also shown in Figure 21. Weld joint efficiency for the specific conditions of these tests was approximately 100%.

Cb-752 - Plate weld ductility in this alloy is marginal in the as-welded condition, and also after annealing at 2200°F. As with D-43, there is no particular reason to assume that the single annealing treatment is optimum for recovery of ductility. The 2200°F anneal was chosen on the basis of the weld results in sheet material. EB weld results (reference Seventh Quarterly) and data reported by Bewley and Schussler[11] indicate that a 2400°F or higher anneal might have provided greater ductility recovery. Also, the annealed plate weld tensile strength is considerably higher than sheet tensile strength implying that overaging and full restoration in ductility has not been realized during the 2200°F anneal. Considerable precipitation occurred in the weld and heat affected zone during annealing, Figure 22.

B-66 - A minimal room temperature plate weld ductility was obtained in this alloy with only slight recovery resulting from a 1900°F stress relief anneal. Both tensile and bend test results indicated that the ductile-to-brittle transition temperature was above room temperature. The annealed transverse plate weld tensile specimen fractured with zero elongation at a stress level less than the transverse sheet yield strength. Considerable second phase intercellular precipitation occurred in the weld during annealing, Figure 23.

3. Weld Porosity - As discussed in the Sixth Quarterly Progress Report, several welds in the T-222 parameter evaluation series contained x-ray detectable porosity. This was unexpected and the need for an evaluation of this problem was indicated. At first the porosity seemed confined to T-222, since T-111 welds were defect free. However, an examination of thirty welds in each of the program alloys prepared for the thermal stability studies indicated that the problem was more widespread. In this check no porosity was noted in Ta-10W welds and only minor amounts in T-111, T-222, FS-85, and SCb-291. Moderate amounts of porosity (2-3 pores/in) were noted in C-129Y, Cb-752, and B-66, and severe porosity occurred in D-43 (and D-43Y in the parameter series). These results, showing a comparison of porosity sensitivity, are summarized in Table 10.

Since this problem proved to be of a general nature, variables associated with joint preparation and welding were investigated. Obviously, with the considerable alloy to alloy variability, porosity formation is also dependent on differences in innate alloy characteristics. These differences are not clearly defined, and, since their definition would probably require an evaluation beyond the scope of this program, were not directly evaluated in this investigation. However, to circumvent this limitation, the most sensitive alloy, D-43, was generally employed to investigate this problem. This approach appeared rational since it would provide a more sensitive measure of minor process variation, and it was assumed that a solution to porosity in the worst alloy would be fully applicable to the others.

The relative importance of joint preparation and welding procedures was easily determined by producing bead-on-plate welds. Since these are welds produced without a joint, they provide an independent evaluation of the welding process. A preliminary check using D-43, D-43Y, C-129Y, Cb-752, and SCb-291 showed that bead-on-plate welds contained no porosity. These tests were conducted on new material and also on used material adjacent to defected welds providing a built-in pentrameter for radiographic inspection. This demonstrated clearly that butt joint edge preparation, not welding procedure, was the source of porosity.

D-43 was selected for evaluating the effect of joint edge preparation variables on TIG weld porosity. Mechanical and chemical edge preparations were evaluated. These tests are summarized in the flow chart of Figure 24 while the respective pickling and rinsing procedures are listed in Table 11. The results, as determined by a porosity count are also shown in Figure 24.

Test number 4 (see Figure 24) represents the normal shear-pickle-rinse-weld sequence employed in the early phases of this program. The improvement in porosity over the thermal stability welds (3.2 per inch vs 8.4 per inch, see Table 10) probably resulted from greater care in rinsing. Interestingly, elimination of pickling, tests 1 and 2, using only sheared and scrubbed edges nearly eliminates porosity. Hence, pickling is essential for the formation of porosity. Edge grinding, test 5, resulted in a measureable decrease in porosity. Machined edges, test 6, proved to be better than ground edges and reduced porosity to a level where it could well be

overlooked in routine inspection. Among the pickling solutions those containing sulfuric acid proved superior. The rinsing procedures proved to be about equal. Porosity in pickled samples was eliminated only by vacuum baking prior to welding tests 8 and 9.

The following conclusions were made based on this series of tests:

1. The direct cause of porosity was not identified but porosity appears to result from the degassing during welding of a pickling residue (or adsorbed hydrogen) from the surfaces of the joint interface.

2. Mechanical preparation is important to the extent of minimizing the joint interface surface area. Hence, machined edges are considerably better than sheared edges. However, if pickling is not required, sheared edges are satisfactory.

3. The difference between alloys probably also reflects a difference in joint interface area. The more fabricable alloys (more easily formed, welded, and with lower bend transition temperatures) had less porosity in welds produced on sheared blanks. Apparently the more fabricable alloys had less edge tearing from shearing and, hence, less edge area and less porosity. With the exception of C-129Y, bend transition temperatures increase with increasing porosity sensitivity. Hence, porosity as measured in these tests, like bend ductility, is a measure of alloy fabricability.

4. For D-43 vacuum degassing of components following pickling and prior to welding is required to prevent porosity. The less sensitive alloys, particularly T-111, T-222, FS-85, Ta-10W, and SCb-291 most likely do not require the vacuum degassing while for the intermediate alloys (Cb-752, B-66, and C-129Y) degassing is probably desirable.

5. Pickling solutions containing sulfuric acid proved advantageous. This indicates that fluoride residues, whose removal is enhanced by including sulfuric acid in the pickling solution, are at least partially responsible for the occurance of porosity.

The results of these experiments provide guidelines for the edge preparation of these alloys. Naturally, specific refinements are probably required to optimize these procedures for any particular alloy. As demonstrated with D-43, optimization of joint preparation in severe cases requires vacuum degassing. This strongly implicates hydrogen as the source of weld porosity. Atomic hydrogen tends to be absorbed during pickling and, because of its low

solubility at elevated temperatures, is released upon subsequent heating during welding. Entrapment of gaseous hydrogen during weld freezing then produces porosity. The evolution of hydrogen from pickled refractory metals observed in vacuum annealing runs (reference, Fifth Quarterly) lends support to this conclusion. Pickling and welding did not result in a detectable hydrogen contamination. Ten welds were chemically analyzed and found to be essentially free of hydrogen. The highest value was 1.6 ppm while eight values were less than 1 ppm.

As a cross-check on the effect of edge preparation and welding procedures on weld properties, bead-on-plate welds were made using parameters previously employed for butt welding. The bend transition temperatures of bead-on-plate welds and butt welds produced from sheared blanks are compared in the following table:

	Bend Transition Temperatures, °F			
	Butt Weld*		Bead-on-Plate Weld	
Alloy	Long. Test	Trans. Test	Long. Test	Trans. Test
D-43	+200	+50	+400	+300
C-129Y	-175	-250	-200	-175
AS-55	+75	+175	+200	-100
D-43Y	0	-200	+75	-150

* Edge preparation as per Table II, P2-R1.

Considering the bend test variability, these appear to be comparable. The larger variance in D-43 is probably a reflection of its greater sensitivity to welding.

A complimentary test, to determine if thermal response of the bead-on-plate welds would differ from the butt welds was also run. In this test, bend tests of annealed D-43 welds were compared and the following results were obtained:

Post Weld Annealing Conditions	Bend Transition Temperature, °F			
	Butt Weld*		Bead-on-Plate Weld	
	Long. Test	Trans. Test	Long. Test	Trans. Test
1 Hr. at 1900°F	+475	+400	+800	+400
1 Hr. at 2200°F	+400	+125	+300	0
1 Hr. at 2400°F	+100	+25	+25	+25

*Edge preparation as per Table 11, P2-R1.

Again, these tests seem to be in good agreement with both butt and bead-on-plate welds responding in like manner to post weld annealing. These tests indicate that the edge preparation had no significant effect on weld properties or weld thermal response.

B. EFFECT OF OXYGEN CONTAMINATION ON THE WELDABILITY OF REFRACTORY METAL ALLOYS

The effect of oxygen contamination on the weldability and thermal stability of three selected refractory metal alloys (FS-85, T-111, and T-222) is being evaluated as an additional program to the overall weldability study. Gaseous oxidation with a low partial pressure of oxygen in helium carrier gas is being used to contaminate 0.035 inch alloy sheet. At the doping temperatures employed, 800°F for FS-85 and 1100°F for T-111 and T-222, an adherent oxide film is produced which is subsequently diffusion annealed at higher temperatures. The apparatus and process control are described in detail in a preceding report[6]. Figure 25 outlines the overall contamination program.

1. Oxidation Process Control - Although chemical analysis for oxygen content is used to measure the contamination level, the "in-process" control is weight gain which is measured following the oxidation process.

Figures 26 and 27 show the correlation between weight gain and actual change in oxygen content for FS-85 and the tantalum base alloys respectively. Referring to Figure 25, the 1:1 correlation line falls along the points representing the calculated net change in oxygen content based on weight gain, rather than on the net change plus the initial, as-received oxygen content, which for FS-85 is 105 ppm.

The apparent bias between the calculated oxygen content and chemical analysis may be due to greater oxygen pickup at the specimen edges since the samples reported are from the specimen interior, where the physical test samples comprising the evaluation program will be obtained. Chemical analysis of edge and corner samples have consistently shown a higher analyzed oxygen content than calculated for possibly two reasons; the greater surface area to volume ratio existing at a corner, (the oxidation reaction is a surface area phenomenon) and a genuine higher reaction rate near the edge because of surface condition or higher

oxygen partial pressure. (The center surfaces are shielded by other specimens). In any case, the bias will not jeopardize the use of weight gain as a process control tool. Better correlation was obtained for the tantalum base alloys, Figure 27, particularly at the higher contamination levels. In this case the anticipated 1:1 line falls midway between the net change and net change plus initial oxygen content.

As part of the process control and evaluation, analyses have been made for nitrogen, carbon, and hydrogen which may be picked up as extraneous contamination during the oxygen contamination process. Substantial changes in interstitial composition could jeopardize test results since these interstitials significantly effect refractory metal alloy mechanical properties[12]. Table 12 lists the results of chemical analyses made for extraneous contamination. Other than the increase in carbon content shown for the FS-85 specimen annealed in an oil pumped vacuum system, there has been no evidence of significant undesirable contamination. Freedom from such contamination is necessary and considerable care is employed in process control. Ultrapure helium, analyzed for trace impurities of hydrocarbons, nitrogen, and water vapor is used as the carrier gas for the oxygen contamination. The oxidation retorts are evacuated to less than 5×10^{-6} torr prior to each run and diffusion annealing is done in sputter ion pumped furnaces operating at from 10^{-7} to 10^{-9} torr.

The chemical analyses in the oxidation program were obtained from samples representing the entire specimen cross section; the surfaces are solvent cleaned prior to analysis, but no material is removed since both oxygen and extraneous contamination may be unevenly distributed through the cross section.

The oxygen contamination is being done in batches, with eight, 4 inch long specimens in each batch, amounting to 100 square inches of surface area. Figure 28 shows the specimen to specimen variation for the first oxidation level (500 ppm by weight for FS-85 and 350 ppm by weight for the tantalum base alloys). A top view of the specimen position is shown at the top of the figure with the oxygen pickup (calculated from weight gain) shown below. The variation (from 20 to 10%) between eight specimens may be compared to a variation of 5% obtained between three FS-85 specimens using vacuum oxidation at 1700°F[13].

2. Test Results

Weld Restraint Tests - As part of the first screening phase of the alloy evaluation program, patch type, bead-on-plate, weld restraint specimens are made of the three alloys at each oxygen doping level. The normal size of patch test used in this program is 4 inches square, but the doping apparatus size limitation is 2 inches x 4 inches. Consequently, a fabricated patch specimen is used with the first weld being an automatic butt weld joining the two 2 inch x 4 inch pieces together. Following this operation, the specimens are handled in the normal manner, manually welding the 2 inch diameter circle and the final straight weld. Figures 29, 30, and 31 show the patch tests of the as-received and oxygen contaminated material, both as-welded and dye penetrant inspected. No cracks were observed in the patch tests except for small dye indications in weld craters at the end of weld beads.

A considerable amount of black smut was observed on the as-welded patch test specimens and on the T-111 bead-on-plate welds produced for tensile and bend ductility testing. Since the smut was observed only on oxygen doped T-111 bead-on-plate specimens, and all three alloys were welded in the same weld chamber load in a random sequence, an attempt was made to identify the surface deposit. A solid source mass spectrometer[14] at the Westinghouse Central Research Laboratory was used in a scanning surface analysis. A high concentration of tantalum and hafnium oxides was observed in the smut area as compared to the clean surface areas. The presence of oxides in the discolored areas correlates well with the greater amount of smut observed on patch specimens of contaminated material.

Bend Ductility - Bend ductility tests are the primary means being used to establish the degredating effects of oxygen contamination on mechanical properties, with both welded and unwelded material being evaluated. Four longitudinal bend specimens are obtained from each 4 inch long by 1 inch wide specimen. Figures 7 and 8 are the bend ductility curves obtained from the as-received material and material doped to the first oxygen level. The oxygen contamination level is 500 ppm for FS-85 and 350 ppm for T-111 and T-222, the differing oxygen percent by weight providing equivalent atomic concentrations of oxygen. It is important to note that the "as-received" material received the same thermal treatment as the doped material, i. e., a 50 hour diffusion annealing treatment at 1800°F for the bend ductility specimens and 1500°F and 2200°F for elevated temperature test specimens with a

corresponding testing temperature. This precaution was taken to separate thermal aging effects from the effect of oxygen contamination in combination with time-temperature treatments.

The bend ductile-brittle transition temperatures, Figure 32, obtained for the as-received material agree well with previous tests performed on identical material[6] showing no significant aging at 1800°F. Oxygen doped material, Figure 33, shows a significant increase in the ductile-brittle transition temperature in both the welded and unwelded condition. All three alloys showed an upward shift in ductile-brittle transition temperature with T-222 showing extreme loss of ductility. Some doubt is placed on bend tests above 600°F however, since the testing is done in air and in situ contamination of the bend test samples may be misleading. Likewise, the bend ductility temperature of welded T-222 doped to 330 ppm O_2 was increased although the transition temperature was not bracketed.

Preliminary data[6] on contaminated T-222 indicated that higher diffusion annealing temperatures (2200°F) restored the bend ductility of material doped to 260 ppm O_2. The higher temperature either alters the form or distribution of the oxides to produce a more ductile material.

Bend Ductility Summary - A considerable amount of bend ductility data was obtained in preliminary process evaluation. A summary of this data and new data obtained in the full scale program is presented in Figures 34 and 35 which relate bend ductile-brittle transition temperature to the oxygen content. Figure 34 compares the three alloys in the unwelded condition while Figure 35 represents bend tests of longitudinal weld specimens. The data obtained from the first full scale phase of the program is marked with an "N" on the two figures.

For the most part, the new data continues the trends observed in the preliminary data except that ductile-brittle transition points were not obtained for the higher oxygen level (over 300 ppm) tantalum alloy welds. The T-111 specimen split down the weld centerline during welding and the transition point was missed with the four available specimens on the T-222 weld. FS-85 shows the least change in bend ductility properties, both in the welded and unwelded condition, with oxygen contamination either on a weight percent or atomic percent basis. Of the tantalum base alloys, there is a considerable and unexpected difference

in the response of T-111 and T-222 to oxygen contamination. Although the behavior of T-222 may be strongly influenced by the form and distribution of oxygen, (see previous discussion on 2200°F diffusion treatment), a comparison of welded specimens of the two alloys, (a complete redistribution occurs in the weld metal), still shows the T-111 alloy to be markedly superior to T-222 at oxygen contamination levels up to 250 ppm.

Metallography - Hardness traverses were obtained across contaminated 0.035 inch sheet for background information relating to oxygen concentration gradients. Hardness data, as related to oxygen content, must be judiciously applied to gettered alloys because of several competing effects[15]. The hardness level, per se, generally cannot be directly related to oxygen content since increasing the oxygen level can result in the formation of incoherent oxides of Zr and Hf causing an actual decrease in the hardness of the matrix through the loss of Hf and Zr as solid solution strengtheners. The softening may continue until the getter additions are consumed, theoretically between 2000-3000 ppm oxygen for the alloys investigated, assuming ZrO_2 or HfO_2 are formed. After the reactive solutes are largely removed, the solid solution hardening effects of oxygen would predominate and an increase in hardness would be expected.

Figures 36, 37, and 38 are cross sectional hardness traverses of the as-received alloys and oxygen contaminated alloys diffusion annealed at 1800°F and 2200°F. The hill and valley variation observed between adjacent hardness values is normal with the small sized Knoop indenter and normally represents changes in grain orientation between impressions. FS-85, Figure 36, shows a higher hardness at the edges following the 1800°F diffusion anneal although the 2200°F anneal traverse is comparable to as-received material. The hardness depression in the 1800°F anneal traverse for FS-85 may represent an advancing oxygen front combining with the zirconium getter and producing an initial softening. With this reasoning, the center area represents the as-received hardness, indicating low oxygen content and the edges have a high oxygencontent, exceeding the amount needed to combine with the getter addition. The 2200°F diffusion treatment has apparently leveled the oxygen concentration gradient. These suppositions will be tested in layer by layer chemical analysis through the material cross section. The 2200°F diffusion anneal will not be used as a general leveling

treatment since the oxygen concentration gradients expected in hardware operating at 1500°F to 1800°F is not known and a gradient of some degree may be more typical.

The tantalum base alloys display a similar leveling of the hardness gradient following the 2200°F anneal. The overall general softening of T-222 following the 2200°F-50 hour diffusion anneal is unexpected and may represent an overaged condition.

Figure 39 compares Vickers hardness traverses across TIG welds in as-received and oxygen contaminated material of the three alloys. The similarities in the traverse values is striking with an increase in the weld metal hardness for all of the contaminated welds. The actual decrease in base metal hardness for the contaminated T-222 alloy is reasonable since the contaminated T-222 was diffusion annealed 50 hours at 2200°F, (note the decrease in hardness following the 2200°F anneal shown in Figure 38), and the base metal would be expected to be softer than the as-received T-222 base metal which was solution annealed 1 hour at 3000°F. All three contaminated alloys shown in Figure 14 were diffusion annealed at 2200°F.

Photomicrographs of the as-received and oxygen doped alloys are shown in Figures 40, 41, and 42. Although the contaminated material is shown following a 50 hour 2200°F diffusion anneal, no significant differences were noticed following the lower temperature diffusion treatments. No visual evidence of oxygen concentration gradients was observed using the metallographic preparations and magnifications shown. Future work will include higher magnification and anodizing-straining techniques as a means of phase identification. Recent work at the Astronuclear Laboratory[16,17] has indicated that staining techniques may be useful in oxide particle identification. There appears to be a greater amount of grain boundary precipitate in oxygen doped FS-85, Figure 40. No concentration was noticed near the surface. A slight increase in grain boundary and general precipitate is observed in T-111, Figure 41, and T-222, Figure 42, displays a more marked increase, especially in general and flow line precipitate. Extraction and x-ray diffraction techniques will be used in the future, especially if the precipitate concentration continues to increase with oxygen contamination level.

3. Work in Progress - The three alloys, T-111, T-222, and FS-85 have been oxygen doped to the second level, 1000 ppm O_2 for FS-85 and 700 ppm O_2 for T-111 and T-222. Work on the third level has been started with FS-85 being contaminated to 200 ppm O_2. The equivalent atomic oxygen content for the tantalum base alloys will be 140 ppm, (see Table 13).

Tensile specimens have been machined for the room temperature and elevated temperature tests for the as-received and the 500/350 ppm O_2 doping levels for the three alloys.

Chemical analysis specimens have been obtained from representative samples of the first two evaluation levels, the as-received material and the first contamination level. Analyses are in process for both oxygen level and nitrogen and carbon content to keep close control over extraneous contamination and in the case of carbon, the intentional alloying addition for T-222. Over 36 analyses are represented in this first full size group, and a more complete story of the weight gain-chemical analyses correlation will be obtained. Oxygen analyses are being made of both the base and weld metal to follow any oxygen decrease in the weld metal as was observed in the overall weldability evaluation program[6]. Sections of as-received and contaminated welds and base metal are being prepared for metallographic examination and hardness surveys.

Following the completion of oxidation to the third level in progress, 200 ppm for FS-85 and 140 ppm for T-111 and T-222, the fourth and final oxidation level will be completed for the screening phase of the program. In view of the deterioration of bend ductility at moderate oxygen contamination levels, especially for T-222, it is anticipated that a low oxidation level of 100 ppm O_2 for FS-85 and 70 ppm O_2 for T-111 and T-222 will be substituted for the originally intended level of 2000 ppm. Table 2 shows the oxidation levels by weight and atomic percent oxygen.

In conjunction with the regular chemical analyses run as a check on in-process weight gain measurements, two evaluations will be made to determine oxygen contamination uniformity both from point to point on a given specimen and also through the specimens cross-section. This data should answer the questions posed by the weight gain-chemical analysis bias shown in Figures 26 and 27 and by the hardness traverses through the material thickness.

Since both the distribution and form of the oxides introduced into contaminated material may be dependent on the contamination process used, material oxidized by alternate processes will be evaluated. Three samples of FS-85 have been vacuum oxidized[13] to 500 ppm O_2 at 1700°F and these will be evaluated for mechanical properties and oxide distribution as compared to the low temperature oxidation and diffusion annealing treatment used in this program. Samples of each alloy have also been electro-chemically anodized[18] and will be diffusion annealed and similarly evaluated.

IV. FUTURE WORK

Baseline tensile testing at room and elevated temperatures will be completed and reported for the columbium and tantalum alloys. Both weld and base metal tests at 1800°F, 2100°F, and 2400°F will be included.

Preliminary data of the thermal stability study will be obtained including tests following a 100 hour 1700°F screening anneal.

Additional doping levels will be completed and evaluated in the contaminated alloy weldability study.

V. REFERENCES

1. R. T. Torgerson, "Development and Properties of Cb-10W-10Hf Alloy", Paper presented at AIME Meeting, New York, November 1, 1962.

2. Wah Chang Corporation Alloy Data Sheet, "Columbium Alloy C-129Y".

3. R. G. Carlson, D. N. Miketta, R. G. Frank, and J. W. Semmel, Jr., "Evaluation of a High Strength Columbium Alloy (AS-55) for Alkali Metal Containment", GE 62FPD365, Missile and Space Division, General Electric Company.

4. A. Taylor, W. M. Hickam, and N. J. Doyle, "Solid Solubility Limits of Y and Sc in the Elements W, Ta, Mo, Nb, and Cr", February 5, 1965, Contract AF 33(616)-8315, Westinghouse Research Laboratories.

5. C. E. Carlson, and E. J. Delgrosso, "Utilization of Yttrium in Gettering Oxygen and Nitrogen in Columbium Base Materials", Pratt and Whitney Aircraft, Contract AT(30-1)2789, PWAC 441, June 24, 1965.

6. G. G. Lessmann and D. R. Stoner, "Determination of the Weldability and Elevated Temperature Stability of Refractory Metal Alloys", Seventh Quarterly Progress Report, NASA-CR-54434, Westinghouse Electric Corporation.

7. A. L. Mincher, "Development of Optimum Manufacturing Methods for Columbium Alloy Sheet", Contract AF 33(600)39942, Interim Report IX, E. I. duPont deNemours and Co., Inc.

8. G. G. Lessmann and D. R. Stoner, "Determination of the Weldability and Elevated Temperature Stability of Refractory Metal Alloys", Fourth Quarterly Progress Report, NASA-CR-54166, Westinghouse Electric Corporation.

9. "Evaluation Test Methods for Refractory Metal Sheet Materials", MAB 192-M.

10. T. K. Roche, "Aging of Columbium Alloy D-43", Notes for paper for presentation at Annual Meeting AIME, February 14-18, 1965, Chicago, Illinois.

11. James G. Bewley and Mortimer Schussler, "Final Report on Process Improvement of Columbium (Cb-752) Alloy", Technical Report AFML-TR-65-63, Contract AF 33(657) 11210, Union Carbide Corporation, March, 1965.

V. REFERENCES (Continued)

12. R. L. Ammon and R. T. Begley, "Pilot Production and Evaluation of Tantalum Alloy Sheet", WANL-PR-004, June 15, 1963.

13. Work performed by C. A. Barrett - NASA Lewis Research Center, Cleveland, Ohio.

14. W. M. Hickam and G. G. Sweeney, "Mass Spectrograph for the Analysis of Solids", The Review of Scientific Instruments, Vol. 34, No. 7, pp. 783-787, July, 1963.

15. R. T. Begley, et al, "Development of Niobium Base Alloys", Technical Report No. WADC-TR-57-344, Part 6, February, 1963.

16. Personal Communication with R. C. Goodspeed, Westinghouse Astronuclear Laboratory.

17. R. S. Crouse, "Identification of Carbides, Nitrides, and Oxides of Niobium and Niobium Alloys by Anodic Staining", ORNL-3821.

18. M. J. Leadbetter and B. B. Argent, "The Effect of Oxygen on the Mechanical Properties of Zone-Refined Niobium", Journal of Less Common Metals, Vol. 3, No. 1, February, 1961.

TABLE 1 - Alloys Included in the Weldability and Thermal Stability Evaluations

Alloy	Nominal Composition Weight Percent
AS-55	Cb-5W-1Zr-0.2Y-0.06C
B-66	Cb-5Mo-5V-1Zr
C-129Y	Cb-10W-10Hf+Y
Cb-752	Cb-10W-2.5Zr
D-43	Cb-10W-1Zr-0.1C
FS-85	Cb-27Ta-10W-1Zr
SCb-291	Cb-10W-10Ta
D43 + Y	Cb-10W-1Zr-0.1C+Y
T-111	Ta-8W-2Hf
T-222	Ta-9.6W-2.4Hf-0.01C
Ta-10W	Ta-10W
W-25 Re	W-25Re
W	Unalloyed
Sylvania "A"*	W-0.5Hf-0.02C

* NOTE: All alloys from arc-cast and/or electron beam melted material except Sylvania "A"

TABLE 2 - Chemistry of As-Received Material

Alloy	Form	Heat	Certified Analysis (Avg.) w/o Zr	Hf	Mo	V	Y	Re	W	Ta	Cb	ppm C	O	N	Check Chemistry ppm C	O_2	N_2
AS-55	Sheet	430-7	1.07				0.02-0.3		4.74		Bal.	306	190-600	155	440	630-930	200
B-66	Plate	DX-609	1.00		5.17	4.89					Bal.	95	110	63	37	120	70
	Sheet	DX-609	1.00		5.17	4.89					Bal.	95	110	63	44	150	30
	Wire	DX-569	1.10		5.23	5.61					Bal.	17	70	64	130	140	90
		DX-603	0.92		4.55	4.85					Bal.	40	82	75	130	190	60
C-129Y	Plate	6.6-57033		10.25					10.8		Bal.	65	160	15	58	200	30
		610-57204		10.10					10.85		Bal.	80	50	58			
	Sheet	46-70617		9.5			0.105		9.8	0.135	Bal.	85	105	50	36	102	60
	Wire	6.6-57033		10.25					10.8		Bal.	65	160	15	52	120	50
Cb-752	Plate	52165	2.70						9.8		Bal.	50	76	10	16	84	70
	Sheet	52208	2.90						9.9		Bal.	40	143	102	21	180	80
	Wire	52183	2.90						9.6		Bal.	30	60	120	51	120	90
D-43	Plate	43-398-13	0.97						10.3		Bal.	835	63	32	930	64	20
	Sheet	43-398-13	1.00						9.9		Bal.	1046	200	32	1100	180	10
	Wire	43-372-1	0.88						9.7		Bal.	810	52	33		85	60
D-43Y	Sheet	95065	0.99				0.26		9.5		Bal.	960	<50	26	1040	64	40
FS-85	Plate	85D-740	0.94						10.6	28.1	Bal.	20	90	60			
	Sheet	85D-739	0.95						10.43	27.61	Bal.	40	40	52	12	98	50
	Wire	85D-695	0.97						10.2	28.0	Bal.	20	40	30	24	73	40
SCb-291	Plate	2255							10.0	9.83	Bal.	20	110	40	22	101	20
	Sheet	1991							9.9	9.6	Bal.	12	65	76	17	110	50
	Wire	1825							10.1	9.2	Bal.	10	67	70	12	130	50
Ta-10W	Plate	60B-758							9.90	Bal.		50	40	20	5	10	10
	Sheet	60B-758							9.90	Bal.		50	40	20	12	66	100
	Wire	60B-609															
T-111	Plate	2691		1.7					7.05	Bal.		18.5	10	26	27	34	10
	Sheet	6-65042-Ta		2.0					8.8	Bal.		80	50	35	48	15	18
	Wire	DX-571		2.01					8.12	Bal.		10	20	10	17	23	20
T-222	Plate	5.510-65041		2.55					9.2	Bal.		115	50	20			
	Sheet	5.510-65041		2.55					9.2	Bal.		115	50	20	100	29	10
W-Re	Sheet	3.5-75002						25.6	Bal.			40	50	35	8	8	10
W	Sheet	KC-1350							Bal.						6	10	10
		KC-1353							Bal.						9	15	10

TABLE 3 - D43Y Sheet. EB Butt Weld Record

Weld No.	Speed (ipm)	Deflection[1] (Inches)	Current (ma)	Chill Spacing (Inches)	Power (Watts)	Watt-Sec. Per Inch	Weld Bead Width (Inches)		Average Weld Bead Width (In.)	Vacuum Torr
							Top	Bottom		
1	15	0	2.4	3/16	360	1450	.027	.020	.023	3.4×10^{-6}
2	15	L-.050	3.6	3/16	540	2160	.026	.016	.021	3.4×10^{-6}
3	15	T-.050	3.6	3/16	540	2160	.044	.040	.042	3.4×10^{-6}
4	25	L-.050	3.6	3/16	540	1300	.041	.025	.033	3.4×10^{-6}
5	15	L-.050	3.3	1/2	495	1980	.030	.024	.027	3.4×10^{-6}
6	25	L-.050	3.3	1/2	495	1190	.041	.031	.036	3.4×10^{-6}
7	50	L-.050	4.0	1/2	600	720	.036	.022	.029	3.4×10^{-6}
8	100	L-.050	5.2	1/2	780	468	.034	.022	.028	3.4×10^{-6}
9	50	L-.050	4.3	3/16	645	775	.034	.027	.030	4.1×10^{-6}
10	50	L-.050	4.8	3/16	720	865	.041	.031	.036	4.1×10^{-6}
11	50	L-.100	5.5	3/16	825	990	.038	.027	.032	4.1×10^{-6}
12	100	L-.050	6.1	3/16	915	550	.031	.027	.029	4.1×10^{-6}

All welds made at 150 kv.

1. L is longitudinal

   T is transverse

TABLE 4 - D43Y Sheet. TIG Butt Weld Record

Weld No.	Clamp Spacing (Inch)	Speed (ipm)	Current Amperes	Weld Width Top/Bottom (Inches)	Q Joules/Inch	Atmosphere Monitor Readings O_2(1) ppm	O_2(2) ppm	H_2O(3) ppm	Comments Visual Inspection	Dye Check	Radiography
1	1/4	7.5	65	0.114/0.100	7800	--	2.4	0.1	Negative	Neg.	Slight Porosity
2	1/4	7.5	82	0.150/0.135	9200	--	1.9	0.15	Negative	Neg.	Negative
3	1/4	15	72	0.105/0.075	4320	--	1.9	0.19	Negative	Neg.	Negative
4	3/8	15	65	0.120/0.075	3640	--	2.2	0.20	Negative	Neg.	Porosity (5)
5	1/4	15	117	0.195/0.180	7010	--	3.0	2.9	Negative(4)	Neg.	Negative
6	1/4	30	100	0.099/0.090	3000	--	2.4	0.2	Negative	Neg.	Negative
7	1/4	15	117	0.165/0.150	7010	--	1.3	0.1	Negative(4)	Neg.	Negative
8	3/8	30	78	0.090/0.036	2180	--	3.8	0.3	Negative	Neg.	Porosity(5)
9	3/8	15	83	0.165/0.150	4980	--	4.0	0.3	Negative	Neg.	Negative
10	1/4	30	128	0.135/0.120	4090	--	3.0	2.9	Negative(4)	Neg.	Negative
11	3/8	60	160	0.111/0.105	2880	--	4.3	0.4	(6)	(6)	(6)
12	1/4	60	215	0.180/0.159	4090	--	3.0	3.0	Negative	Neg.	Negative

(1) Westinghouse oxygen gage.
(2) Lockwood & McLorie oxygen gage.
(3) CEC moisture monitor.
(4) Rerun, first try hot tore severely along weld centerline.
(5) Welds rejected for further test, porosity attributed primarily to edge preparation rather than material characteristics.
(6) One transverse crack through weld.

TABLE 5 - Restraint Test Summary

Alloy	Bead-on-Plate Patch Test (Sheet)						Circular Groove (Plate)		
	Visual	Weld Width	Dye Check	X-ray	Distortion		Visual	Dye Check	Distortion (inches)[2]
					Angle (Max)	Inches[1]			
AS-55	Neg.	0.24	Neg.	Negative	13°	0.75	(5)	---	---
B-66	Neg.	0.23	Neg.	Positive[3]	31°	0.63	Neg.	Neg.	0.075
C-129Y	Neg.		Neg.	Negative	30°	0.63	Neg.	Neg.	0.10
Cb-752	Neg.	0.34	Neg.	Negative	28°	0.73	Neg.	Neg.	0.195
D-43	Neg.	0.23	Neg.	Negative	32°	0.60	Neg.	Neg.	0.08
D-43Y	Neg.	0.11	Neg.	Neg.	25°	0.70	(5)	---	---
FS-85	Neg.	0.15	Neg.	Positive[4]	36°	0.76	Neg.	Neg.	0.04
SCb-291	Neg.	0.20	Neg.	Negative	32°	0.69	Neg.	Neg.	0.10
Ta-10W	Neg.	0.17	Neg.	Negative	30°	0.70	Neg.	Neg.	0.10
T-111	Neg.	0.22	Neg.	Negative	26°	0.60	Neg.	Neg.	0.14
T-222	Neg.	0.25	Neg.	Negative	18°	0.65	Neg.	Neg.	0.10

1. Closest distance between two parallel planes on opposite sides of weldment.
2. Holding one corner flat, measure lift from flat plane at diagonally opposite corner.
3. 1/8 inch starting crack identified on one leg of weld.
4. Positive x-ray indication not identified in consequent examination.
5. This alloy not evaluated as plate.

TABLE 6 - Room Temperature Tensile Properties for Welded Plate

Alloy	Type	1 Hr. Post Weld Anneal Temp. (°F)	0.2% Offset Yield Pt., psi x 10^{-3}	Ultimate Stress psi x 10^{-3}	R.A. (%)	Elongation (%)	Fracture Location
T-111	Trans.	2400	73.70	86.99	76.0	17.4	Weld
T-111	Long.	2400	76.20	89.85	64.7	22.3	--
Ta-10W	Trans.	None	61.16	77.71	82.2	21.9	Weld
Ta-10W	Long.	None	65.85	81.30	70.0	24.3	--
T-222	Trans.	2400	88.21	101.01	74.4	18.7	Weld
T-222	Long.	2400	87.99	100.74	68.3	21.9	--
B-66	Trans.	1900	(1)	68.36	0.0	0.0	Weld
B-66	Long.	1900	77.79	88.81	2.6	6.6	--
D-43	Trans.	2400	59.40	79.74	70.7	5.2	Weld
D-43	Long.	2400	54.86	88.22	28.7	17.4	--
FS-85	Trans.	2400	60.21	76.72	9.7	9.4	Weld
FS-85	Long.	2400	61.81	79.82	66.6	21.0	--
Cb-752	Trans.	2200	56.32	75.90	79.7	24.9	Base
Cb-752	Long.	2200	61.00	79.30	46.2	20.7	--
SCb-291	Trans.	1900	47.03	62.70	88.9	22.5	Weld
SCb-291	Long.	1900	46.86	62.47	77.5	21.2	--
C-129Y	Trans.	2400	70.07	87.38	16.9	12.7	Weld
C-129Y	Long.	2400	68.10	86.90	44.7	22.0	--

(1) Brittle Fracture

TABLE 7 - Sheet Material Room Temperature Tensile Properties

Alloy	Type[1]	Pre-Test 1 hr Anneal Temp.(°F)[2]	Specimen No.	0.2% Offset Yield Strength Psi x 10^{-3}	Ultimate Tensile Strength Psi x 10^{-3}	El. %	Comments	Joint Efficiency %
T-111	Base	2400	T1-80	83.20	89.20	16		
T-111	Weld	2400	T1-31	82.50	92.00	14	Weld Fracture	103
TA-10W	Base	None	T2-80	71.50	84.41	29		
TA-10W	Weld	None	T2-31	69.99	81.43	9	Weld Fracture	96
T-222	Base	2400	T3-80	80.10	88.00	18		
T-222	Weld	2400	T3-31	83.20	90.10	14	Base Fracture	102
B66	Base	None	C1B-38	79.88	104.73	22.5		
B66	Weld	None	C1B-1	81.04	100.92	9	Weld Fracture	96
D43	Base	2400	C2-38	62.15	90.21	19.5		
D43	Weld	2400	C2B-1	63.75	90.26	18.0	Base Fracture	100
D43Y	Base	2400	C8-44	39.57	62.75	24.0		
D43Y	Weld	2400	C8-81	42.35	70.03	22.5	Base Fracture	112
FS85	Base	2400	C3-49	67.60	83.10	22.5		
FS85	Weld	2400	C3-2	61.90	78.60	10	Weld Fracture	95
Cb752	Base	2200	C4-38	55.50	73.10	27		
Cb752	Weld	2200	C4B-1	48.80	64.80	12.5	Weld Fracture	89
SCb291	Base	2200	C5-37	47.53	59.57	23.5		
SCb291	Weld	2200	C5-4	45.90	57.20	9	Weld Fracture	96
C129Y	Base	2400	C6-38	72.06	85.97	26.5		
C129Y	Weld	2400	C6B-1	66.54	74.93	5.5	Weld Fracture	87

(1) Transverse to rolling direction for base, to weld direction for weld specimens. Weld direction parallel to rolling direction.

(2) Post weld annealing treatments applied to both weld and base metal specimens. Reference post-weld annealing studies, Sec. IIIA2, Seventh Quarterly Progress Report.

TABLE 8 - Welded Plate Bend Test Results

Alloy	Specimen No.	Type	Condition[1]	1st Bend, 16 t Bend Rad.		2nd Bend, 8t Bend Rad.		3rd Bend, 3t Bend Rad.	
				Free Bend Angle[2]	Proportional Limit, Psi	Free Bend Angle[2]	Proportional Limit, Psi	Free Bend Angle[2]	Proportional Limit, Psi
B-66	1-2	Long.	AW	4° F	N.D.	- - -	- - -	- - -	
	5-6	Long.	AW	0° F	66,950	- - -	- - -		- - -
	7-8	Long.	PWA 1 hr/1900°F	17° B	99,730	50° B	107,140	67° F	108,560
	9-10	Trans.	AW	4° F	N.D.	- - -	- - -	- - -	- - -
	11-12	Trans.	AW	22° B	103,090	37° F	119,960	- - -	- - -
	13-14	Trans.	PWA 1 hr/1900°F	0° F	76,580	- - -	- - -	- - -	- - -
C129Y	1-2	Long.	AW	25° B	N.D.	49° B	133,740	132° B	128,950
	3-4	Long.	AW	22° B	90,540	60° B	110,390	135° B	103,420
	7-8	Long.	PWA 1 hr/2400°F	17° B	95,520	40° B	95,060	137° B	97,620
	9-10	Trans.	AW	22° B	N.D.	27° F	147,490	- - -	- - -
	13-14	Trans.	AW	25° B	79,100	60° B	95,880	- - -	91,020
	11-12	Trans.	PWA 1 hr/2400°F	15° B	88,840	50° B	94,760	137° F	88,170
Cb752	1-2	Long.	AW	29° F	N.D.	- - -	- - -	- - -	- - -
	3-4	Long.	AW	0° F	79,560	- - -	- - -	- - -	- - -
	7-8	Long.	PWA 1 hr/2200°F	22° B	65,030	52° F	74,320	- - -	- - -
	9-10	Trans.	AW	26° B	N.D.	45° F	90,490	- - -	- - -
	13-14	Trans.	AW	20° B	81,360	62° B	98,610	140° B	79,960
	11-12	Trans.	PWA 1 hr/2200°F	20° B	80,500	30° F	83,930	- - -	- - -
D43	1-2	Long.	AW	23° B	N.D.	39° F	122,730	- - -	- - -
	3-4	Long.	AW	25° B	97,220	60° B	86,580	- - F	78,340
	5-6	Long.	PWA 1 hr/2400°F	17° B	82,580	45° B	82,540	130° F	83,600
	9-10	Trans.	AW	23° B	N.D.	36° B	106,280	47° F	105,770
	13-14	Trans.	AW	23° B	75,200	60° B	87,890	-- F	67,790
	11-12	Trans.	PWA 1 hr/2400°F	17° B	71,780	35° B	85,980	135° B	87,450

(1) AW - As-welded, PWA - Post-Weld Annealed (Time-Hrs/Temp-°F Indicated).
(2) Letters B & F in this column designate "Bend" or "Failed" (any tear or crack) Respectively.
ND — Not determined.

TABLE 8 - Welded Plate Bend Test Results (Continued)

Alloy	Specimen No.	Type	Condition[1]	1st Bend, 16t Bend Rad.		2nd Bend, 8t Bend Rad.		3rd Bend, 3t Bend Rad.	
				Free Bend Angle[2]	Proportional Limit, Psi	Free Bend Angle[2]	Proportional Limit, Psi	Free Bend Angle[2]	Proportional Limit, Psi
FS-85	1-2	Long.	AW	27° B	N.D.	40° B	160,290	125° F	135,500
	3-4	Long.	AW	25° B	79,370	40° F	95,240	- - -	- - -
	7-8	Long.	PWA 1 hr/2400°F	17° B	86,100	60° B	85,390	145° B	83,600
	9-10	Trans.	AW	26° B	N.D.	40° B	124,030	145° B	119,600
	11-14	Trans.	AW	25° B	75,610	62° B	87,580	140° B	69,790
	12-13	Trans.	PWA 1 hr/2400°F	17° B	84,440	55° B	81,880	140° B	81,990
SCb-291	1-2	Long.	AW	23° B	N.D.	44° B	97,820	160° F	80,200
	3-4	Long.	AW	22° B	70,300	58° B	73,040	140° B	66,630
	7-8	Long.	PWA 1 hr/1900°F	20° B	68,060	62° B	67,180	140° B	62,930
	9-10	Trans.	AW	22° B	N.D.	37° B	87,810	132° B	94,920
	13-14	Trans.	AW	20° B	68,720	60° B	78,720	140° B	66,720
	11-12	Trans.	PWA 1 hr/1900°F	22° B	73,060	55° B	68,030	140° B	67,000
TA-10W	3-4	Long.	AW	29° B	N.D.	57° B	N.D.	141° B	N.D.
	5-6	Long.	AW	28° B	95,240	60° B	103,900	140° B	86,000
	9-10	Trans.	AW	28° B	N.D.	54° B	N.D.	141° B	N.D.
	11-12	Trans.	AW	28° B	98,550	60° B	103,880	140° B	97,630
T-111	1-2	Long	AW	27° B	94,590	62° B	102,680	142° B	87,350
	3-4	Long.	AW	27° B	101,630	62° B	109,600	142° F	99,960
	7-8	Long.	PWA 1 hr/2400°F	30° B	102,330	55° B	92,610	140° B	88,310
	9-11	Trans.	AW	20° B	95,490	55° B	118,060	142° B	105,070
	10-12	Trans.	AW	25° B	73,200	63° B	104,170	120° F	82,410
	13-14	Trans.	PWA 1 hr/2400°F	29° B	122,540	55° B	106,480	136° B	94,770
T-222	1-2	Long.	AW	25° B	139,360	60° B	148,640	142° F	126,380
	3-4	Long.	AW	25° B	116,610	60° B	137,800	142° F	125,800
	7-8	Long.	PWA 1 hr/2400°F	28° B	123,790	50° B	115,750	137° B	107,310
	9-10	Trans.	AW	25° B	120,870	60° B	140,640	140° F	114,000
	11-12	Trans.	AW	25° B	101,600	60° B	135,470	143° F	111,800
	13-14	Trans.	PWA 1 hr/2400°F	20° B	111,000	50° B	128,220	130° B	114,110

TABLE 9 - Plate Weld Bend Test Visual Inspection

Alloy	Specimen No.	Type	Condition*	Comments
B-66	1-2	Long.	AW	Transgranular cleavage-full width failure
	5-6	Long.	AW	Transgranular cleavage-full width failure
	7-8	Long.	PWA	Transgranular cleavage-full width failure
	9-10	Trans.	AW	Full width transgranular cleavage, 25% weld centerline-75% weld interface
	11-12	Trans.	AW	Full width weld centerline transgranular cleavage
	13-14	Trans.	PWA	Full width weld centerline transgranular cleavage
C-129Y	1-2	Long.	AW	Full ductile weld bend-slight base tension side edge traps
	3-4	Long.	AW	Full ductile weld bend-slight base tension side edge traps
	7-8	Long.	PWA	Full ductile weld bend-slight base tension side edge tears
	9-10	Trans.	AW	Full width weld centerline transgranular cleavage
	13-14	Trans.	AW	Full width (90% HAZ-10% WELD) transgranular cleavage
	11-12	Trans.	PWA	Full ductile weld bend
Cb-752	1-2	Long.	AW	Full width transgranular cleavage
	3-4	Long.	AW	Full width transgranular cleavage
	7-8	Long.	PWA	Full width transgranular cleavage, slight lamination
	9-10	Trans.	AW	Full width weld centerline cleavage
	13-14	Trans.	AW	Full ductile bend
	11-12	Trans.	PWA	Full width weld interface cleavage

* AW - As-Welded
PWA - Post-Weld Annealed

TABLE 9 - Plate Weld Bend Test Visual Inspection
(Continued)

Alloy	Specimen No.	Type	Condition	Comments
D-43	1-2	Long.	AW	Full width tension side cleavage, slight lamination at base of crack
	3-4	Long.	AW	Severe tension surface cleavage, weld & HAZ, not to edge
	5-6	Long.	PWA	Full bend with sudden severe tension surface cleavage (90%) at outer end of bend
	9-10	Trans.	AW	Full width cleavage, 25% weld-75% HAZ
	13-14	Trans.	AW	Full width weld centerline cleavage
	11-12	Trans.	PWA	Full ductile bend
FS-85	1-2	Long.	AW	Full transgranular cleavage at outer end of bend
	3-4	Long.	AW	Full transgranular cleavage at center, slight lamination
	7-8	Long.	PWA	Full ductile bend
	9-10	Trans.	AW	Full ductile bend
	11-14	Trans.	AW	Full ductile bend
	12-13	Trans.	PWA	Full ductile bend
SCb-291	1-2	Long.	AW	Full transgranular cleavage at outer end of bend
	3-4	Long.	AW	Full ductile bend
	7-8	Long.	PWA	Full ductile bend
	9-10	Trans.	AW	Full ductile bend
	13-14	Trans.	AW	Full ductile bend
	11-12	Trans.	PWA	Full ductile bend

TABLE 9 - Plate Weld Bend Test Visual Inspection
(Continued)

Alloy	Specimen No.	Type	Condition	Comments
Ta-10W	3-4	Long.	AW	Full ductile bend
	5-6	Long.	AW	Full ductile bend
	9-10	Trans.	AW	Full ductile bend
	11-12	Trans.	AW	Full ductile bend
T-111	1-2	Long.	AW	Full ductile bend
	3-4	Long.	AW	Full ductile bend with slight weld surface tearing at base of weld ripple
	7-8	Long.	PWA	Full ductile bend
	9-11	Trans.	AW	Full ductile bend
	10-12	Trans.	AW	Full ductile bend with very slight weld crater tearing
	13-14	Trans.	PWA	Full ductile bend
T-222	1-2	Long.	PW	Full bend with tension side weld tears (1-1/4", others 1/16")
	3-4	Long.	AW	Full bend with tension side weld tears (8-12, 1/16" long)
	7-8	Long.	PWA	Full ductile bend
	9-10	Trans.	AW	Full ductile bend with slight weld crater tearing
	11-12	Trans.	AW	Full ductile bend with slight weld crater tearing
	13-14	Trans.	PWA	Full ductile bend with slight tears in apparent area where metallic pickup may have occurred (copper) during welding

TABLE 10 - TIG Butt Weld Porosity Count

Alloy	Pores/in.(1)
TA-10W	0
T-222	0.034
T-111	0.051
FS85	0.092
SCb291	0.83
C129Y	2.0
B66	2.6
Cb752	2.9
D43	8.4
D43Y	8.0

(1) Based on approximately 15 feet of weld using optimum weld parameters based on bend ductility, except D43Y for which the weld parameter series count is shown.

TABLE 11 - Pickling and Rinsing Schedules for Weld Porosity Evaluation (See Figure 24)

	Pickling Solution, v/o
P1	25% H_2NO_3, 25% HF, H_2O balance
P2	20% H_2NO_3, 15% HF, 10% H_2SO_4, H_2O balance
P3	25% H_2NO_3, 8% HF, 25% H_2SO_4, H_2O balance
P4	25% H_2NO_3, 15% HF, 25% H_2SO_4, H_2O balance
	Rinsing Schedules
R1	1. Fast transfer from pickle bath to rinse 2. 30-second boiling distilled water 3. 1-minute flowing cold water rinse 4. 5-minute boiling distilled water 5. Ethyl alcohol rinse 6. Hot air flash dry
R2	1. Fast transfer from pickle bath to rinse 2. 10-minute rinse in cold flowing tap water 3. 3-minute rinse in boiling distilled water 4. Ethyl alcohol rinse 5. Hot air flash dry

TABLE 12 - Extraneous Contamination

	Material	Sample	Ppm by Weight O_2	N_2	C	H_2
As-Received Material	FS-85	C3-C	104	38	23	
	T-111	T1-C	38	24	32	
	T-222	T3-C	75	8	110	
Oxygen Doped and Diffusion Annealed	FS-85	C3CD-102	260	41	32	
		C3CD-402	310	--	34	.22
		C3CD-402	310	--	33	
		C3-BL*	870	49	60	
		C3GL-1	920	40	21	
	T-111	T1CD-101	82	--	35	
		T1-CL	150	22	46	
		T1CD-303	210	--	36	.14
	T-222	T3-CL	180	10	120	
		T3CD-103	180	--	130	
		T3CD-302	275	--	120	.24

*Diffusion annealed in oil pumped system.

TABLE 13 - Selected Oxygen Contamination Levels

Chronological Order	F8-85		T-111 and T-222	
	Weight ppm	Atomic ppm	Weight ppm	Atomic ppm
4	100	780	70	780
3	200	1560	140	1560
1	500	3900	350	3900
2	1000	7800	700	7800

As-Received Oxygen Levels

	Weight ppm	Atomic ppm
FS-85	105	820
T-111	40	450
T-222	75	840

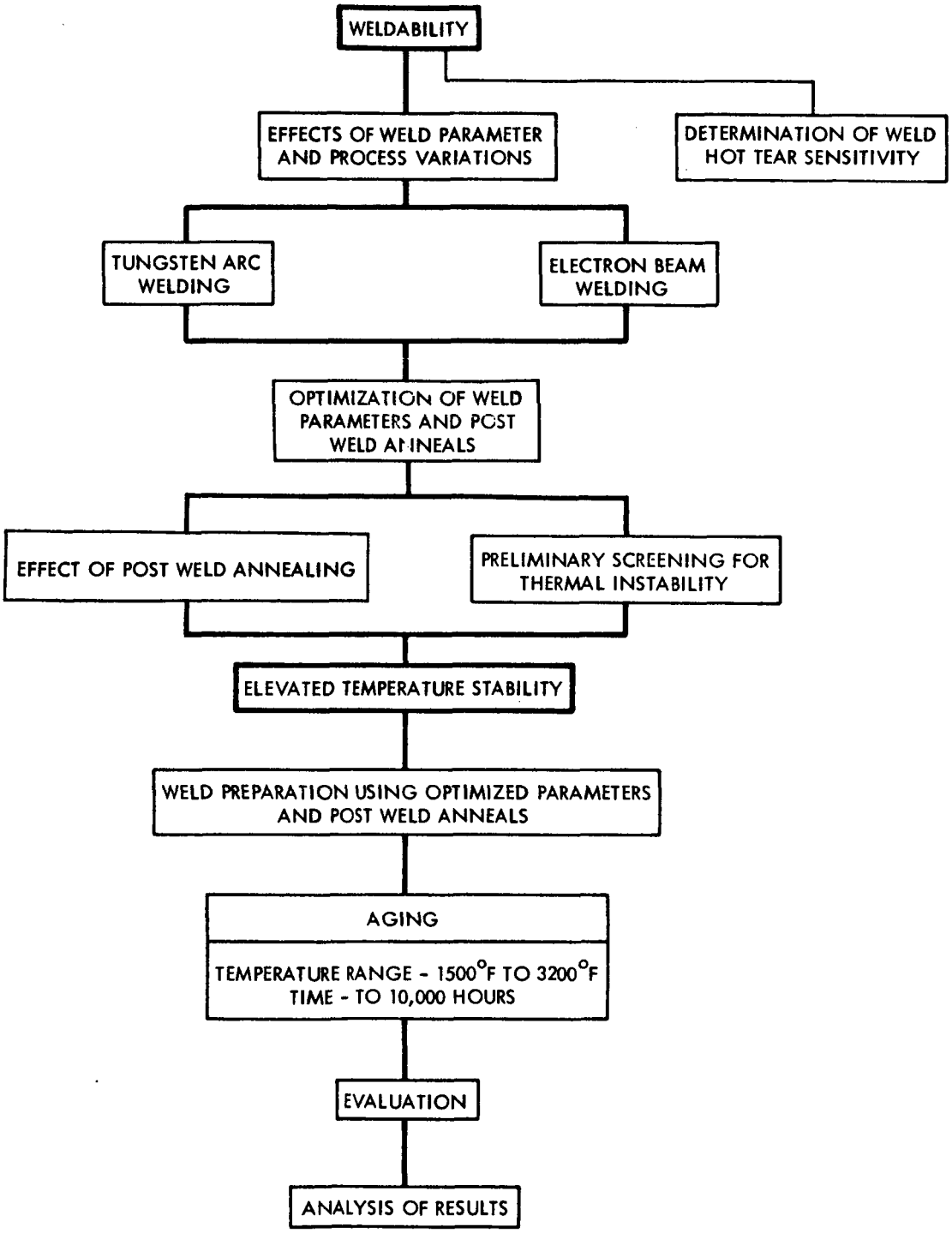

FIGURE 1 - Chronological Program Outline

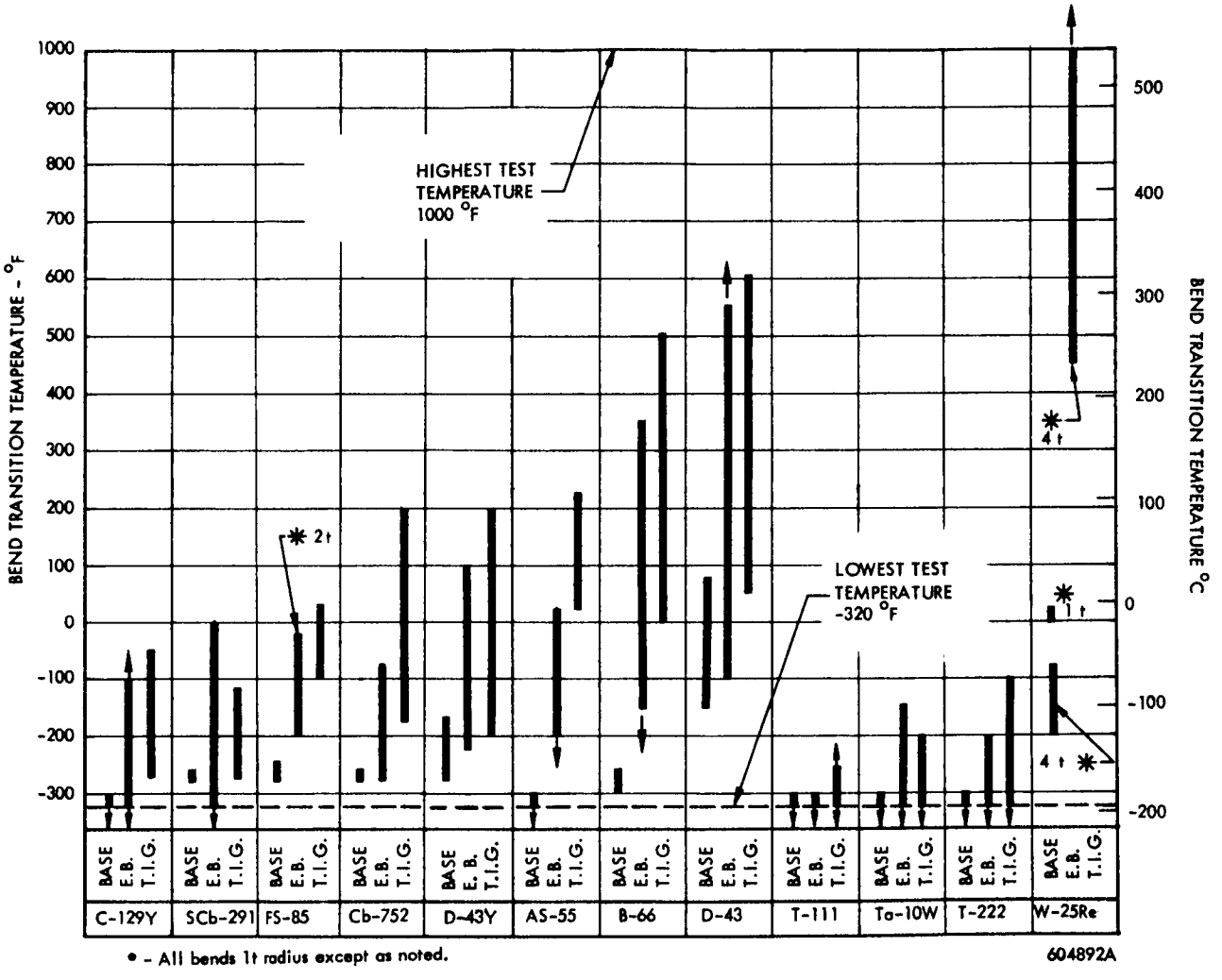

FIGURE 2 - Summary of Current Bend Test Results for Butt Welds in 0.035 Inch Sheet

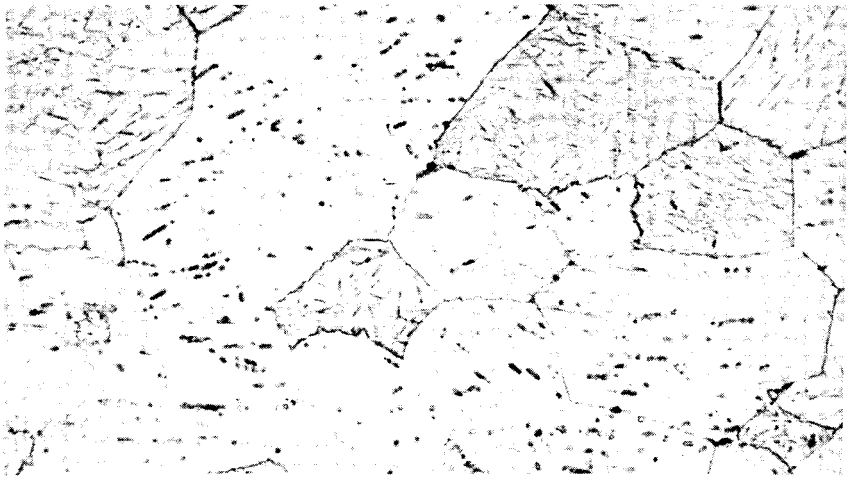

400X 8668

D-43

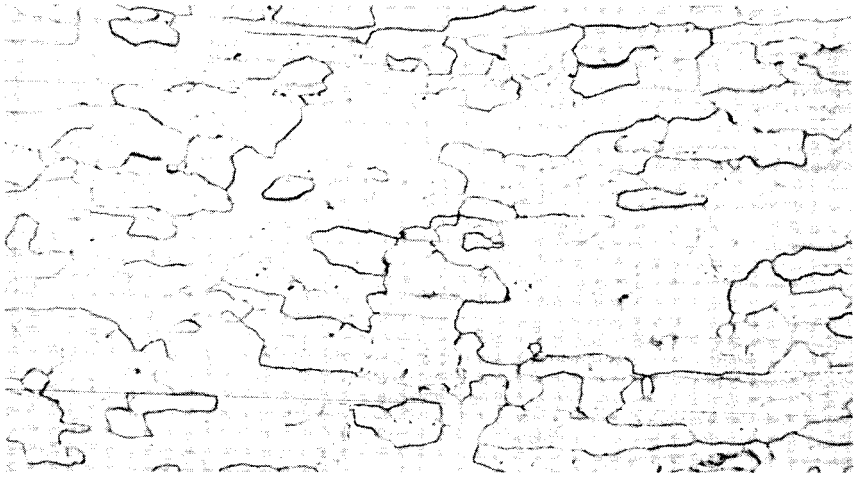

400X 9209

D-43Y

FIGURE 3 - As-Received Microstructures of D-43 and D-43Y Sheet

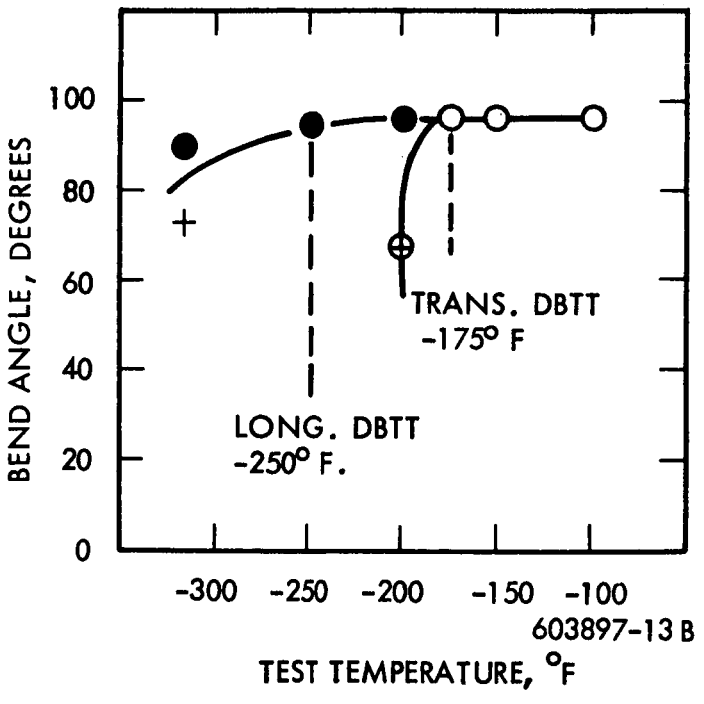

FIGURE 4 - D-43Y Base Metal Bend Test Results. 1t Bend Radius

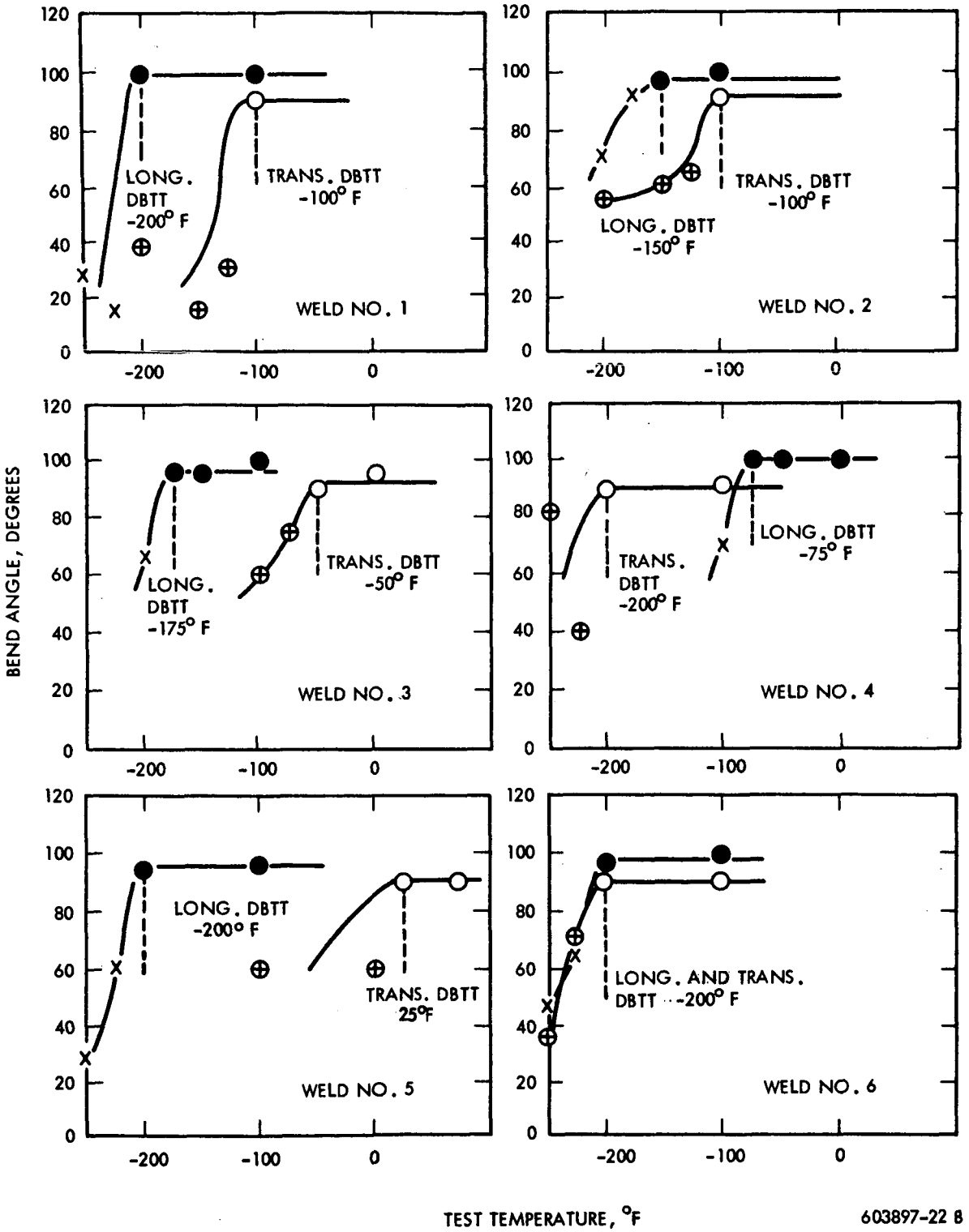

FIGURE 5 - D-43Y EB Weld Bend Test Results, 1t Bend Radius

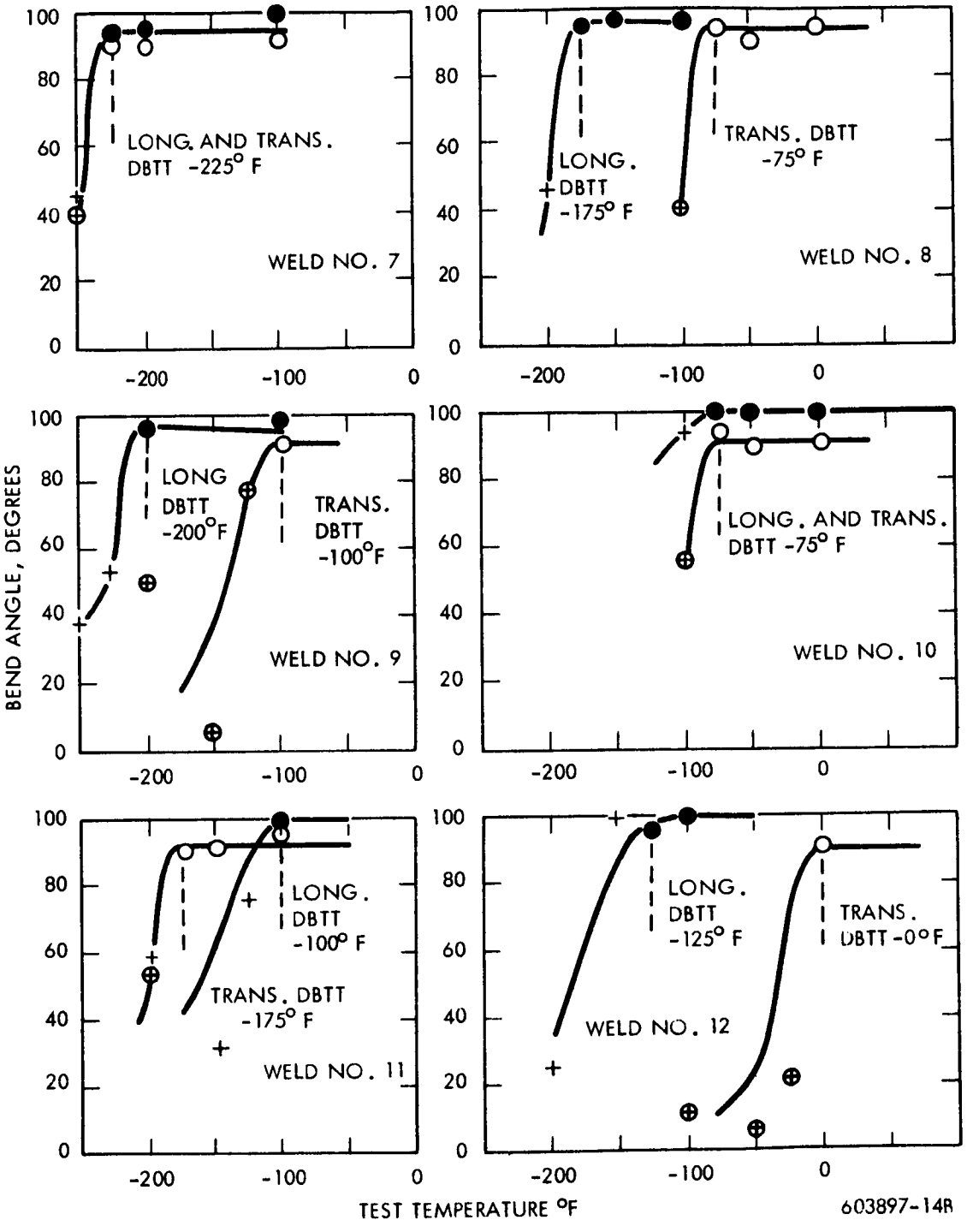

FIGURE 6 - D-43Y EB Weld Bend Test Results,
1t Bend Radius

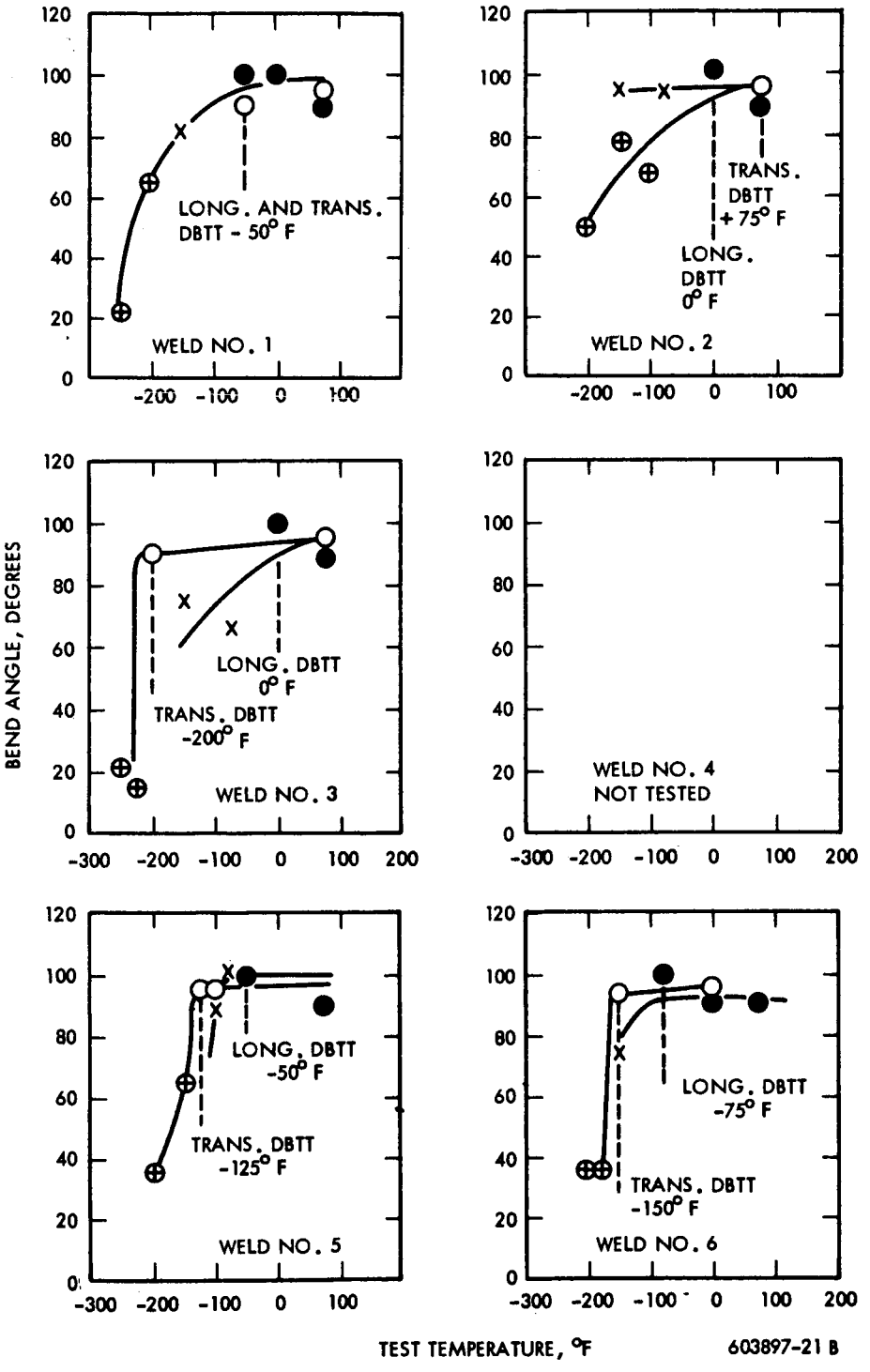

FIGURE 7 - D-43Y TIG Weld Bend Test Results, 1t Bend Radius

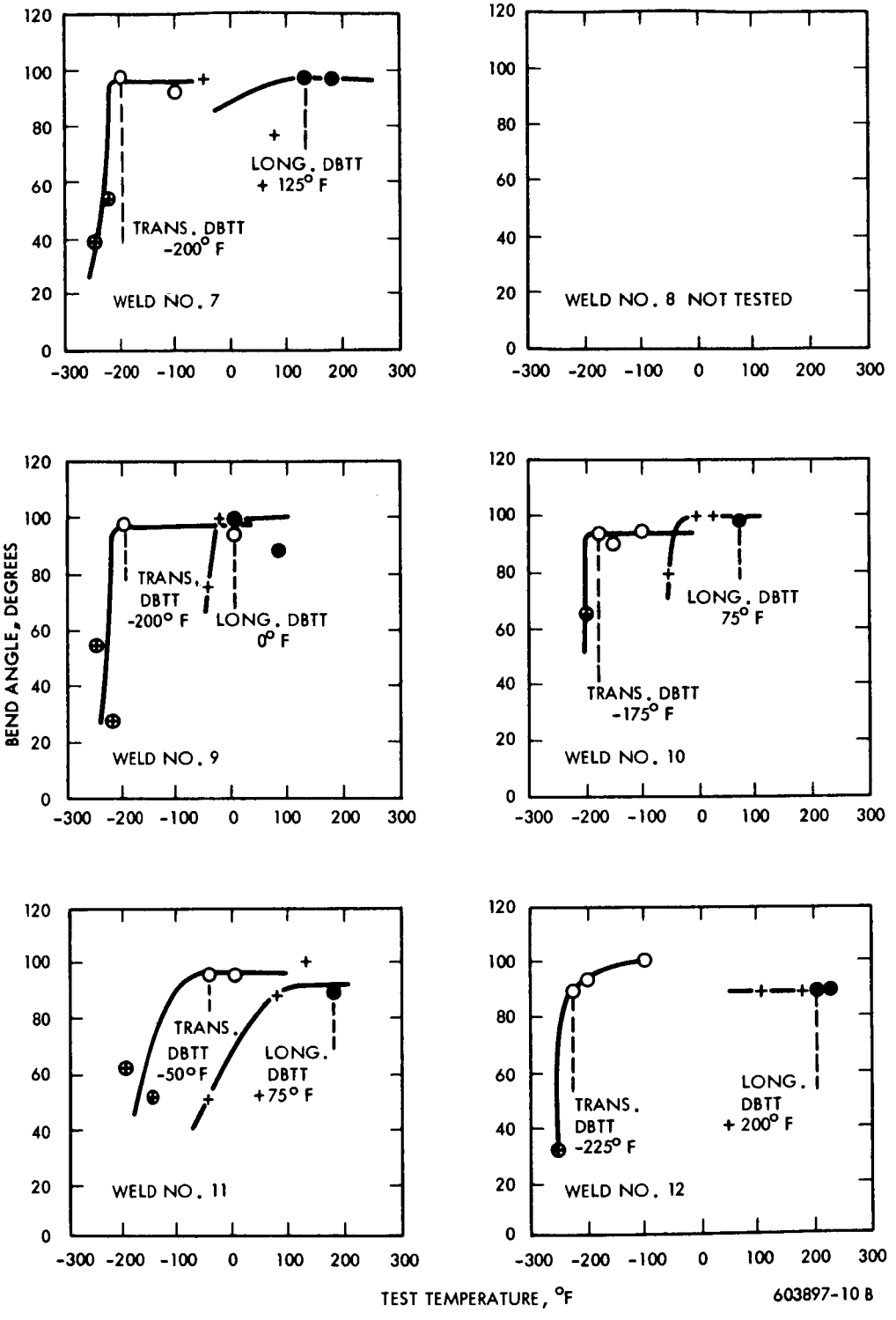

FIGURE 8 - D-43Y TIG Weld Bend Test Results, 1t Bend Radius

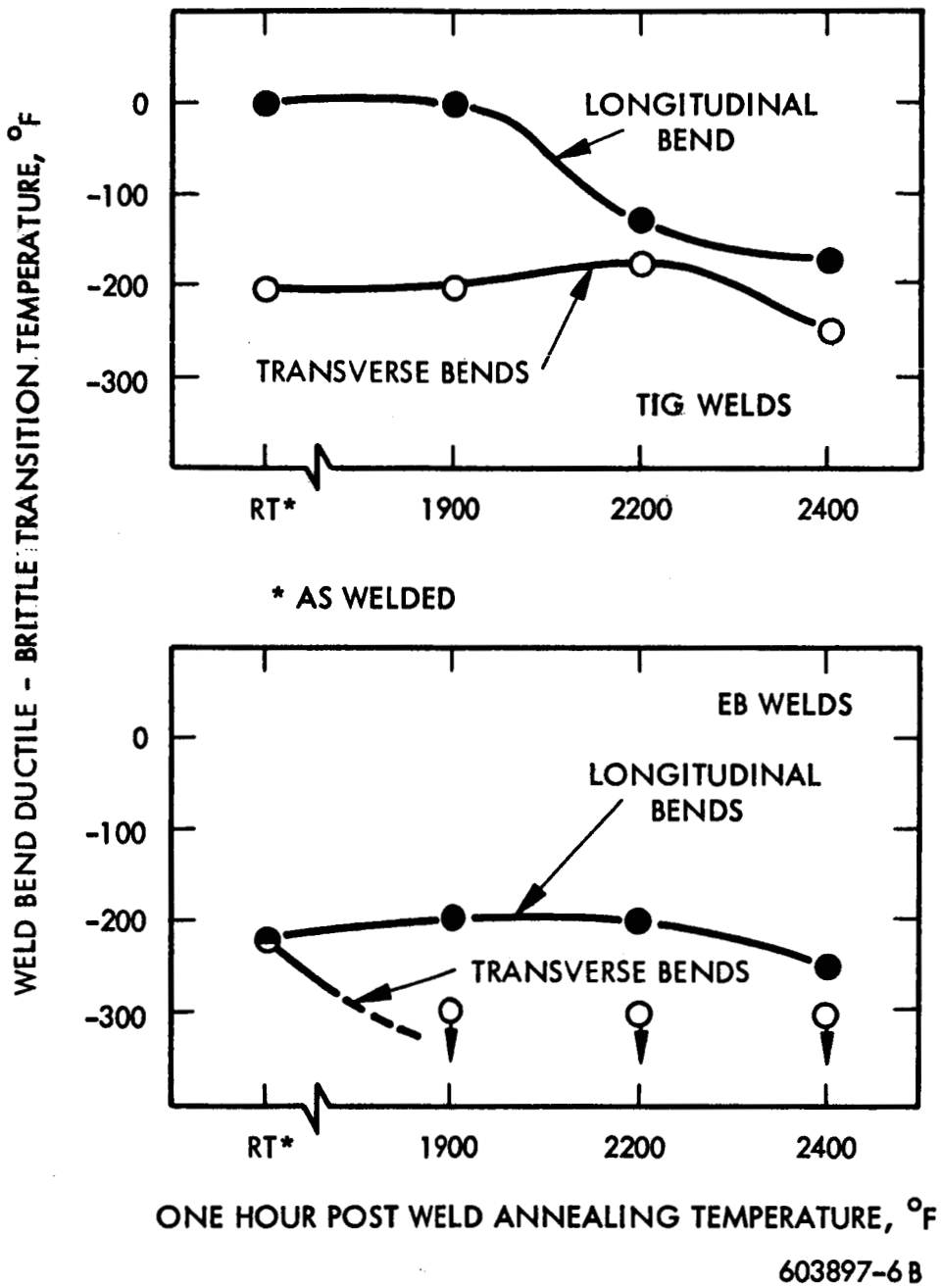

FIGURE 9 - Effect of Post Weld Annealing on D-43Y Weld Ductility

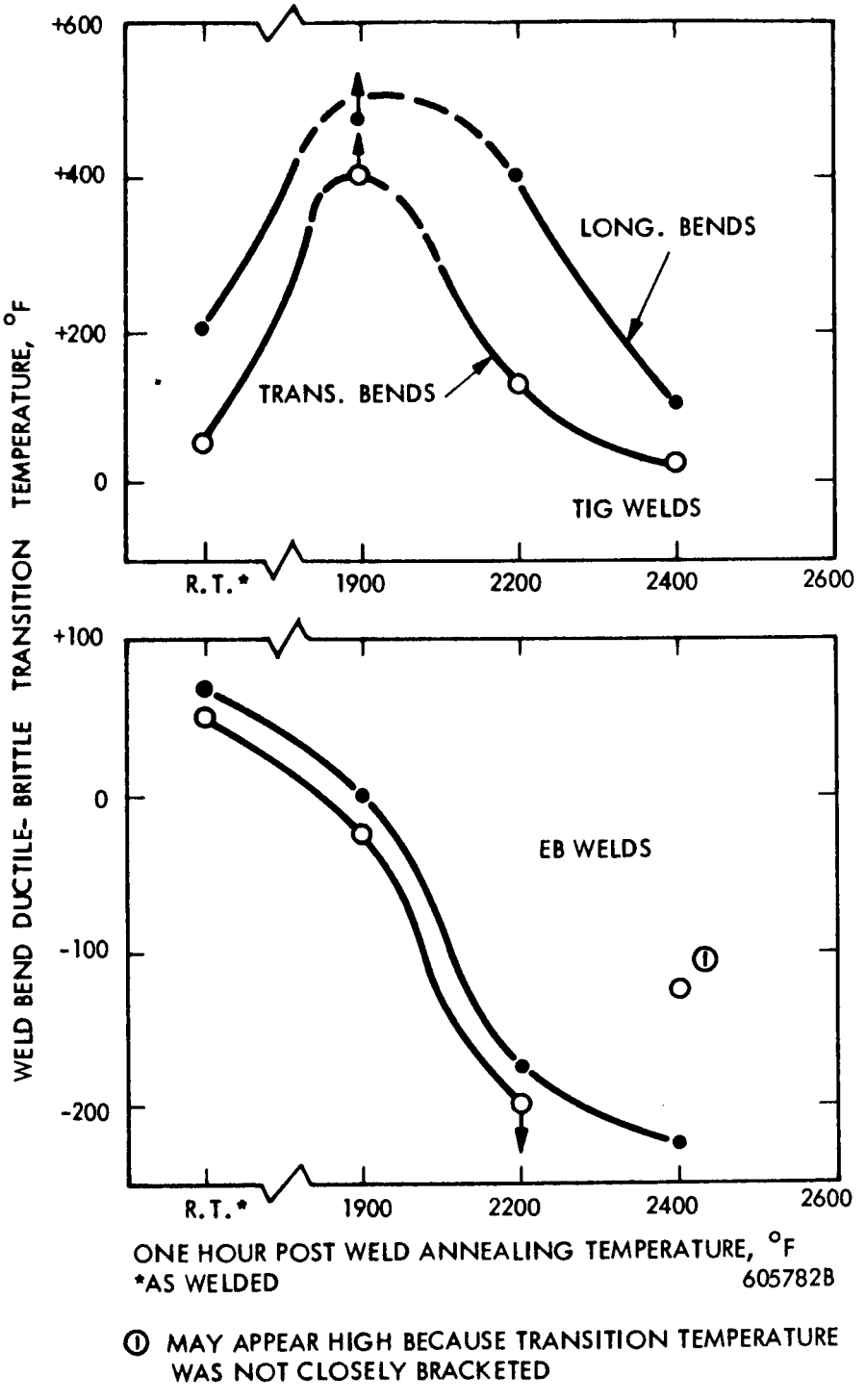

FIGURE 10 - Effect of Post Weld Annealing on D-43 Weld Ductility

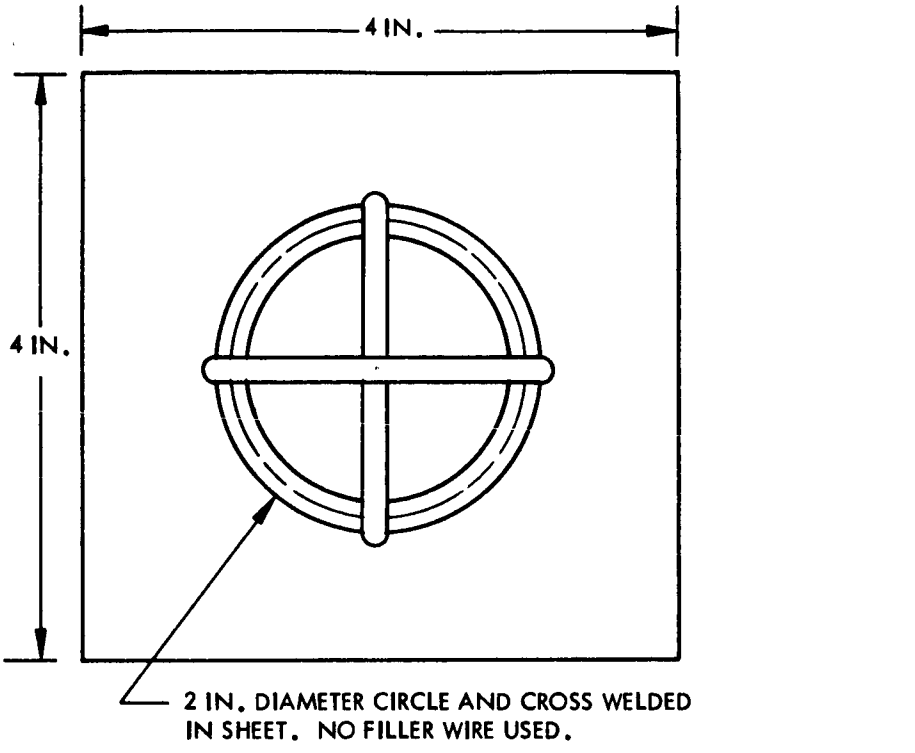

FIGURE 11 - Weld Restraint Test Specimens for 0.035 Inch Sheet (a), and 0.375 Inch Plate (b).

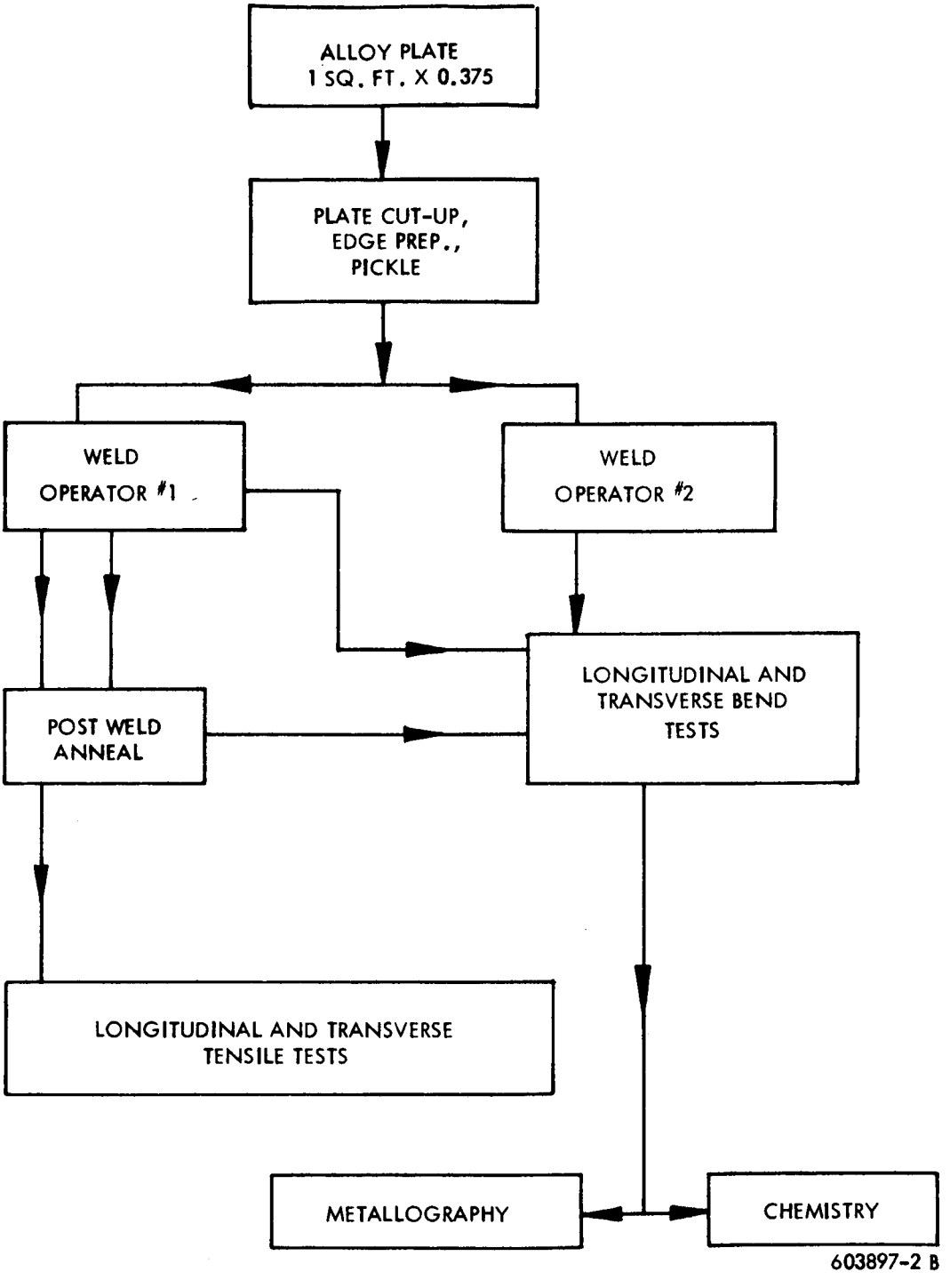

FIGURE 12 - Program Outline for Plate Weldability Evaluation

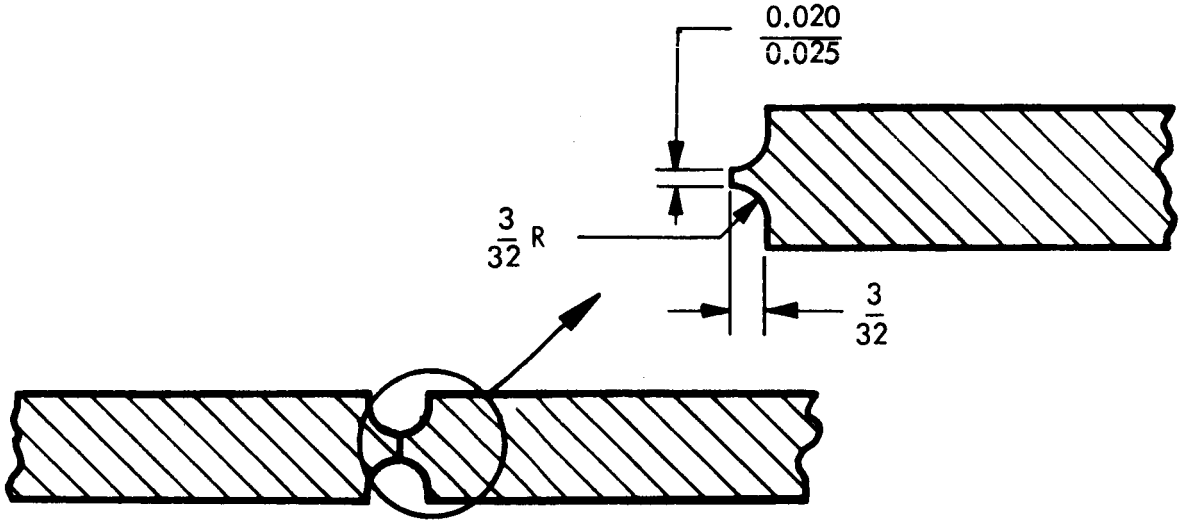

FIGURE 13 - Plate Butt Weld Joint Configuration

WELD 321 - SCb-291 Butt Weld, 3/8 Inch Plate.

1. Tack welded in center and at ends of joint. Positioned in clamp down fixture. 155 amperes.

2. Fusion pass on side No. 1. 300 amperes. Continuous weld from one end. One side of joint clamped, other side cantilevered.

3. Fusion pass on side No. 2. 280 amperes. Specimen supported along each edge on copper blocks. Continuous weld.

4. First filler pass on side No. 2. 300 amperes. Continuous weld.

5. First filler pass on side No. 1. 300 amperes. Continuous weld.

6. Second filler pass on side No. 2. 280 amperes. Continuous weld.

7. Second filler pass on side No. 1. 280 amperes. Continuous weld.

FILLER WIRE REQUIREMENTS: 2-1/2 inch of 0.082 diameter wire per inch of weld.

FIGURE 14 - Welding Schedule for SCb-291 Butt Weld in 3/8 Inch Plate Material

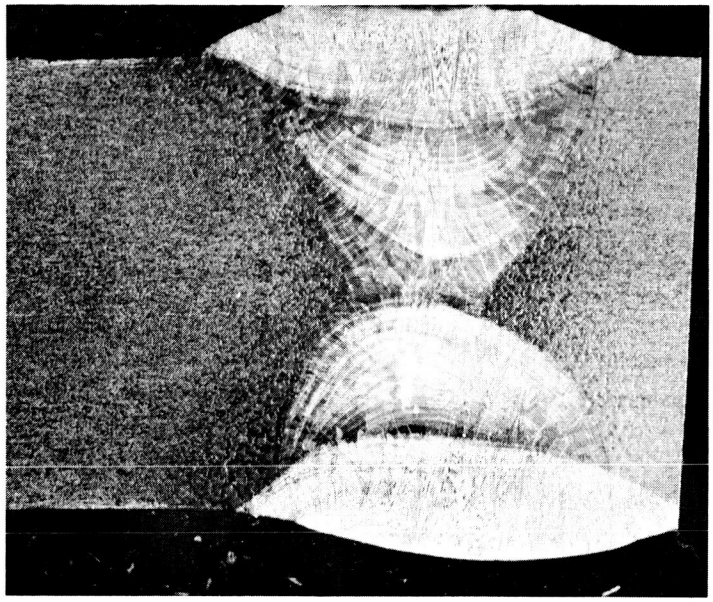

10,181 6X

FS-85

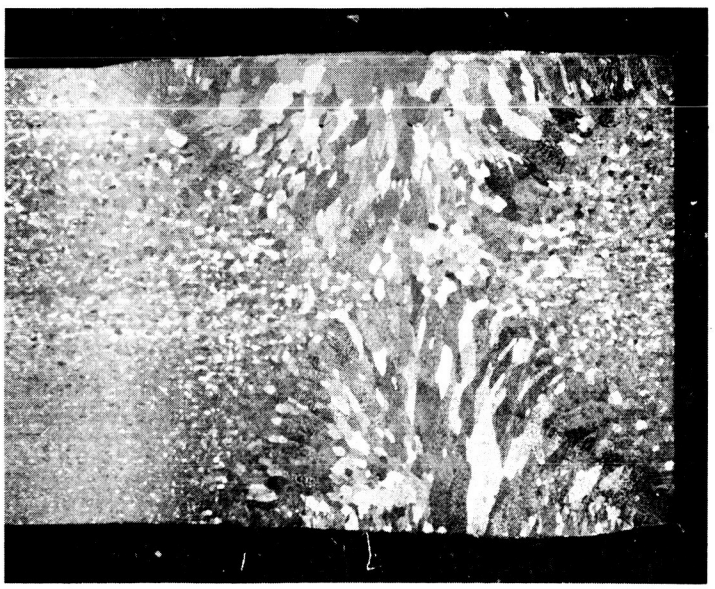

10,175 6X

D-43

FIGURE 15 - Typical Plate Weldment Macrosections

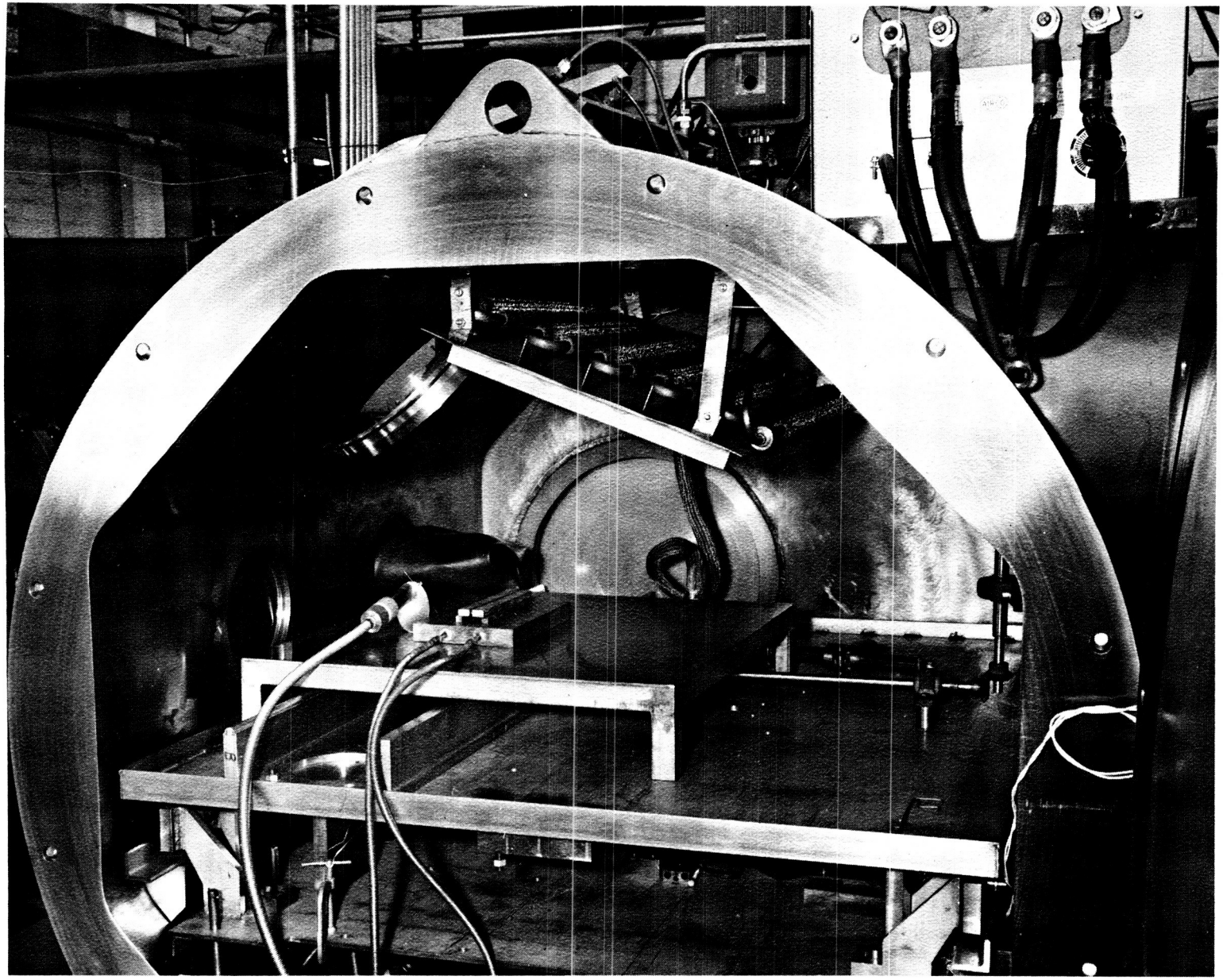

FIGURE 16 - Weld Chamber Internals Set-Up for Plate Welding. Baffled Convection Heat Exchanger Shown Installed in Top of Chamber

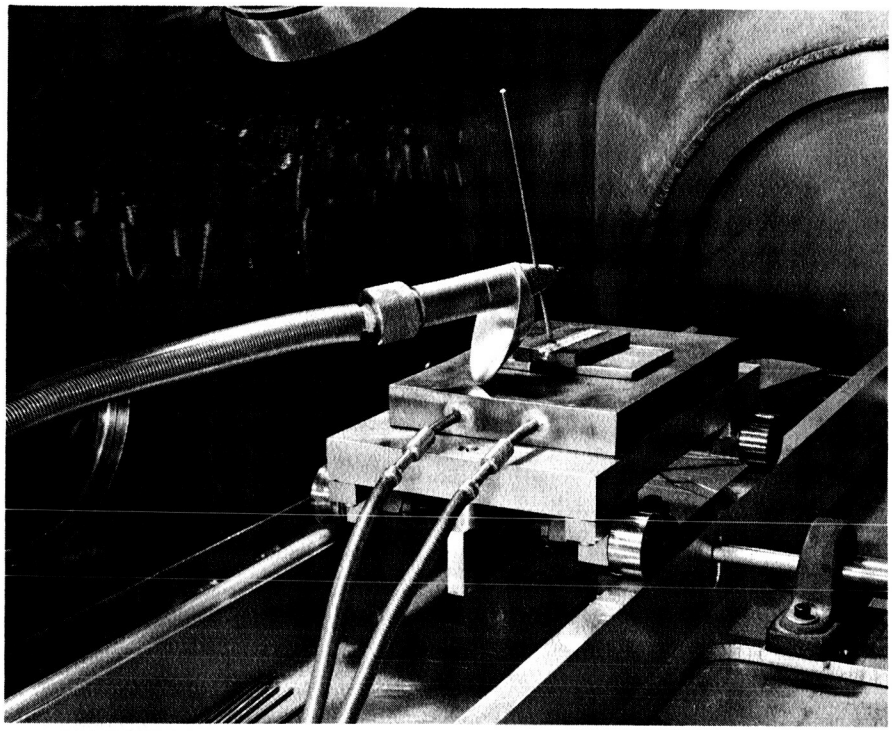

512-4

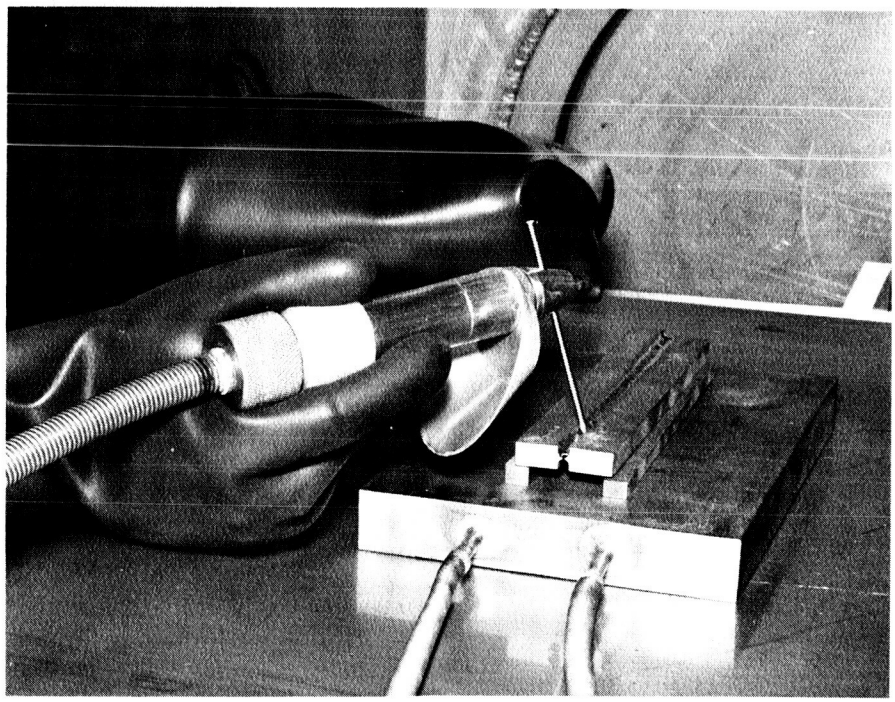

716-2

FIGURE 17 - Special Torch for Vacuum Purged Weld Chamber Top, Plastic Sheath Insulated. Bottom, Nylon Standoff Insulated.

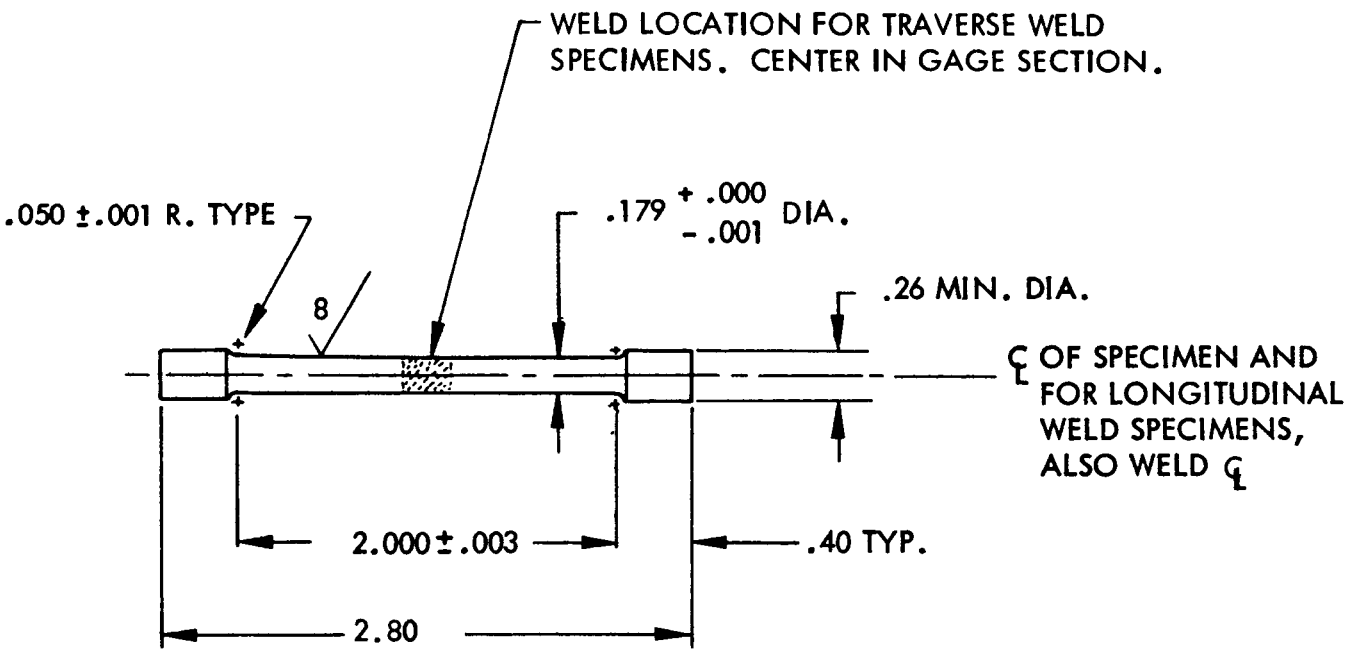

NOTES:

A- DIMENSIONAL TOLERANCES UNLESS OTHERWISE NOTED:
TWO PLACE DECIMALS - ± .02
THREE PLACE DECIMALS - ± .005

603897-16B

FIGURE 18 - Room Temperature Plate Weld Tensile Specimen Design

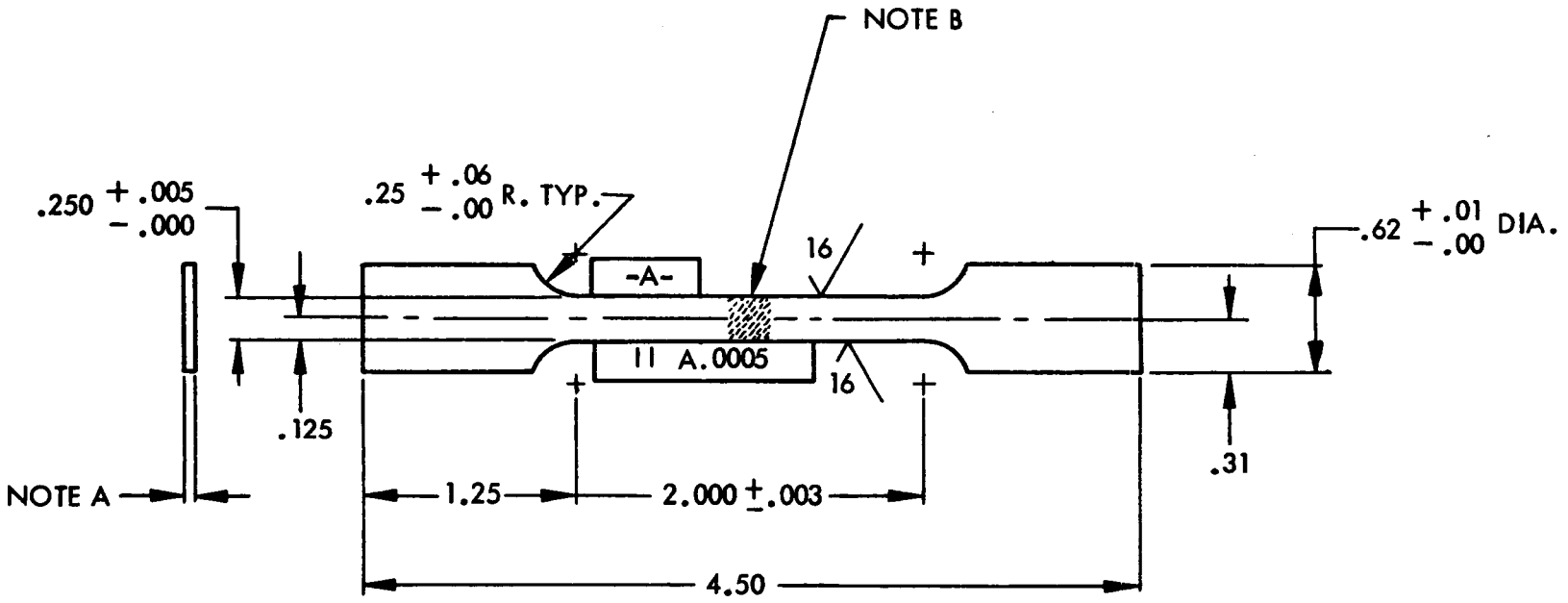

NOTES:

A. AS RECEIVED SHEET THICKNESS, EXCEPT WELDED SPECIMENS WHICH ARE GROUND TO BE FLAT AND PARALLEL WITHIN .0005

B. WELD LOCATION FOR WELD SPECIMENS - CENTER IN GAGE SECTION

C. DIMENSIONAL TOLERANCES UNLESS OTHERWISE NOTED:
TWO PLACE DECIMALS - ± .02
THREE PLACE DECIMALS - ± .005

603897-1 B

FIGURE 19 - Room Temperature Sheet Tensile Specimen Design

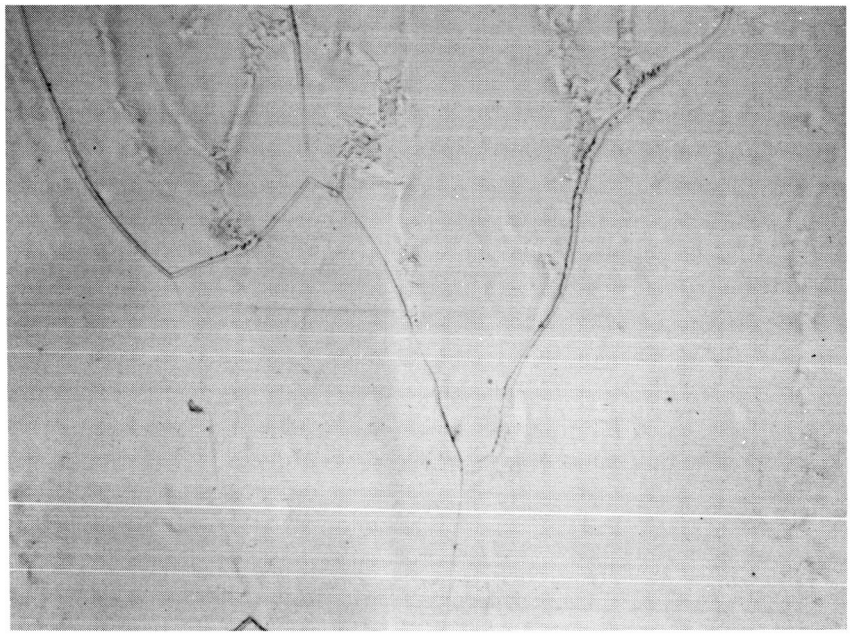

10,173 500X

As-Welded

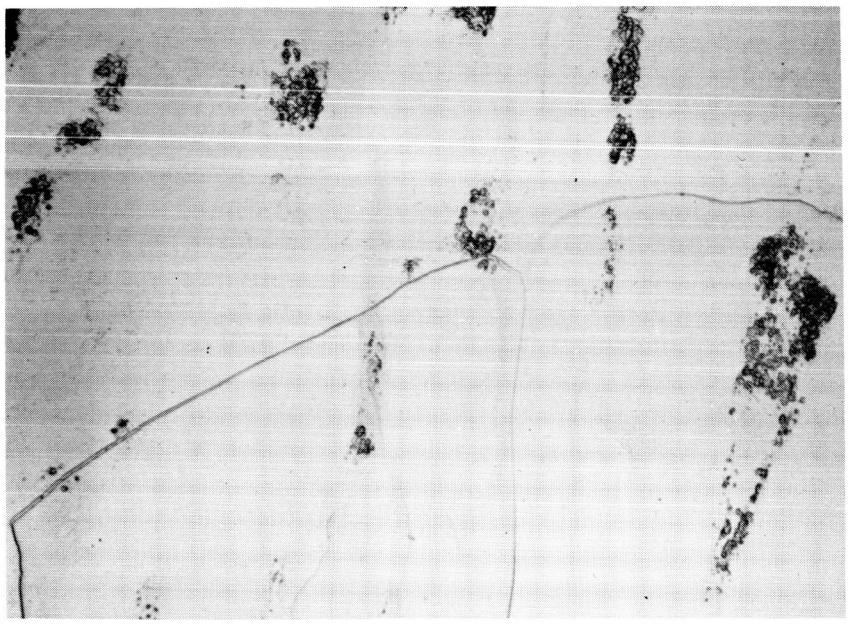

10,181 500X

Welded and Annealed for 1 Hr. at 2400°F (Second Phase in Final Weld Pass Only)

FIGURE 20 - FS-85 Welded Plate, Weld Microstructure

10,175 500X

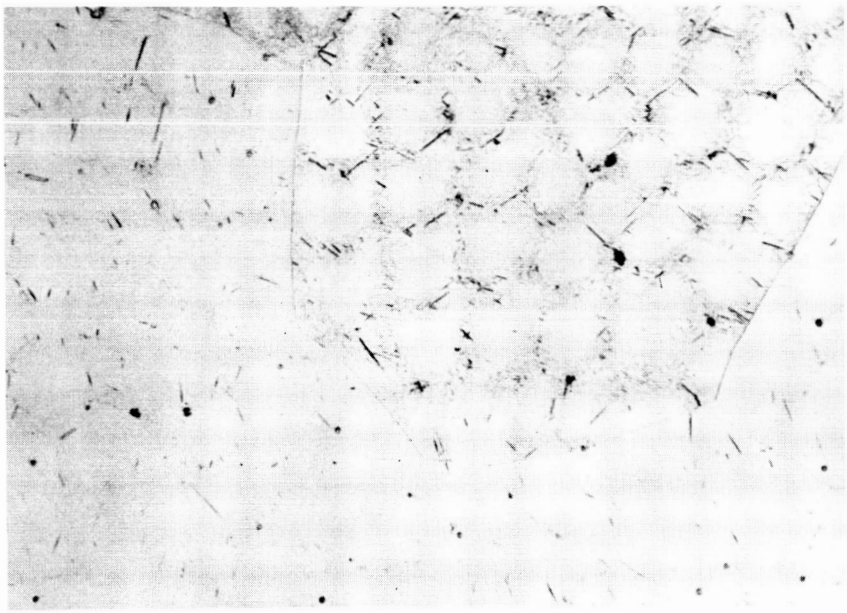

10,179 500X

Welded and Annealed for 1 Hr. at 2400°F

FIGURE 21 - D-43 Welded Plate, Weld Microstructure

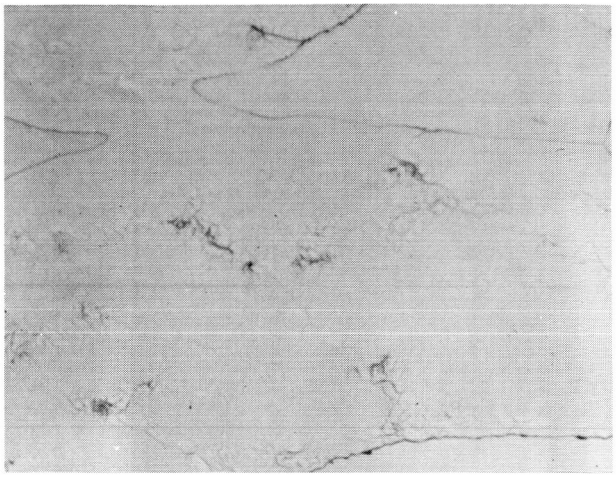

10,177 As-Welded 500X

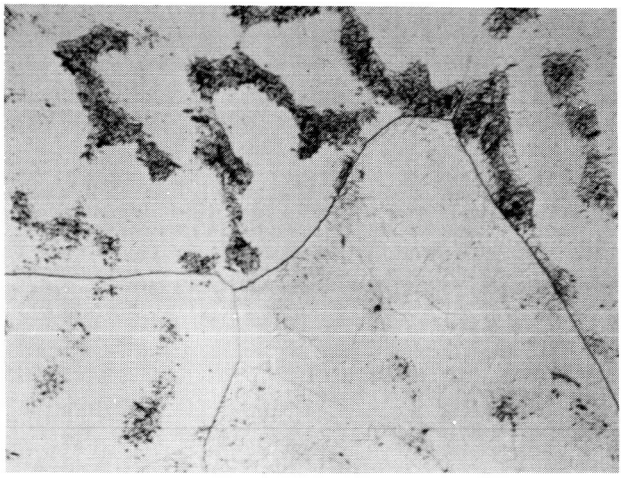

10,180 Annealed 1 Hr. at 2200°F 500X

Weld Area

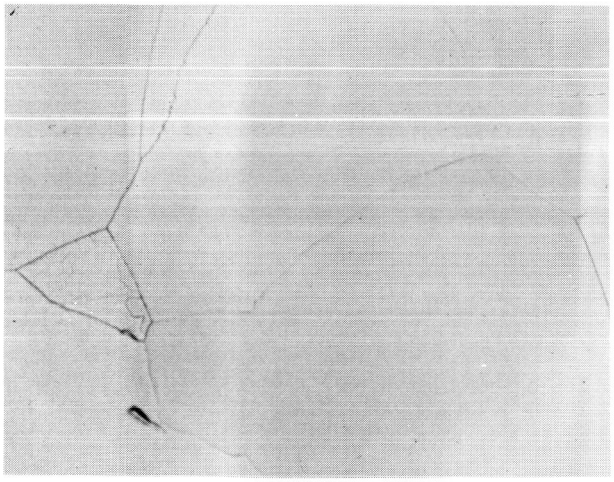

10,177 As-Welded 500X

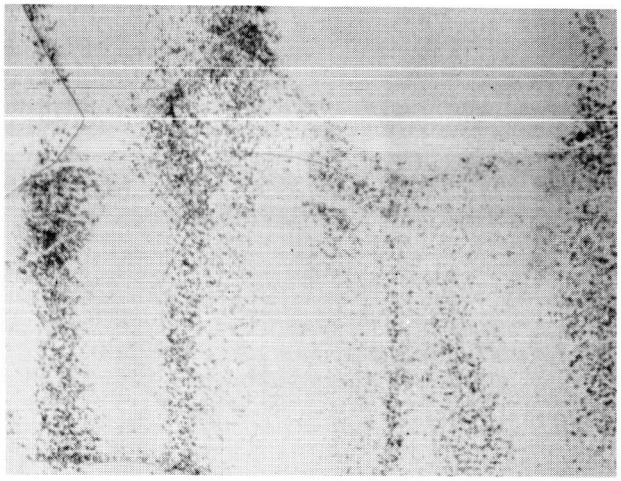

10,180 Annealed 1 Hr. at 2200°F 500X

Heat Affected Zone

FIGURE 22 - Weld and Heat Affected Zone Microstructure of Cb-752 Welded Plate

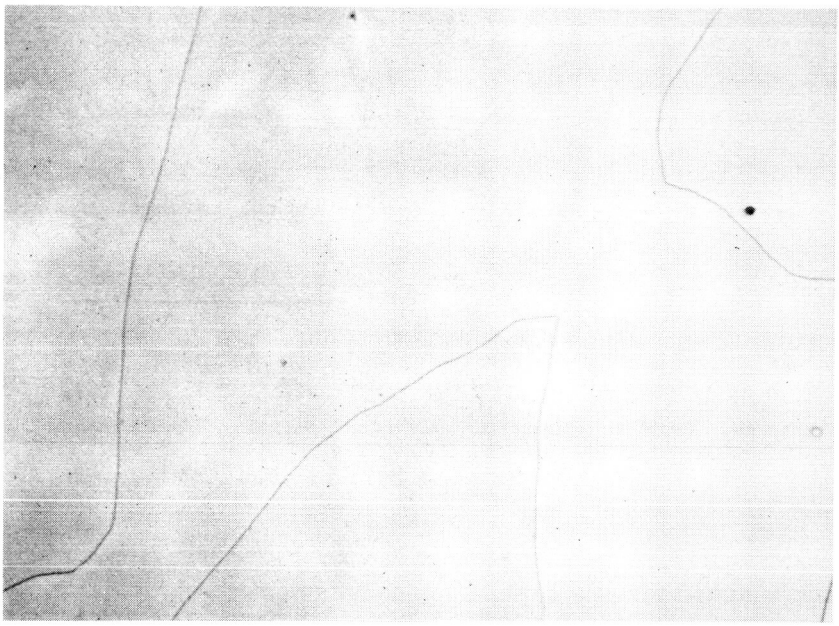

10,172 500X

As-Welded

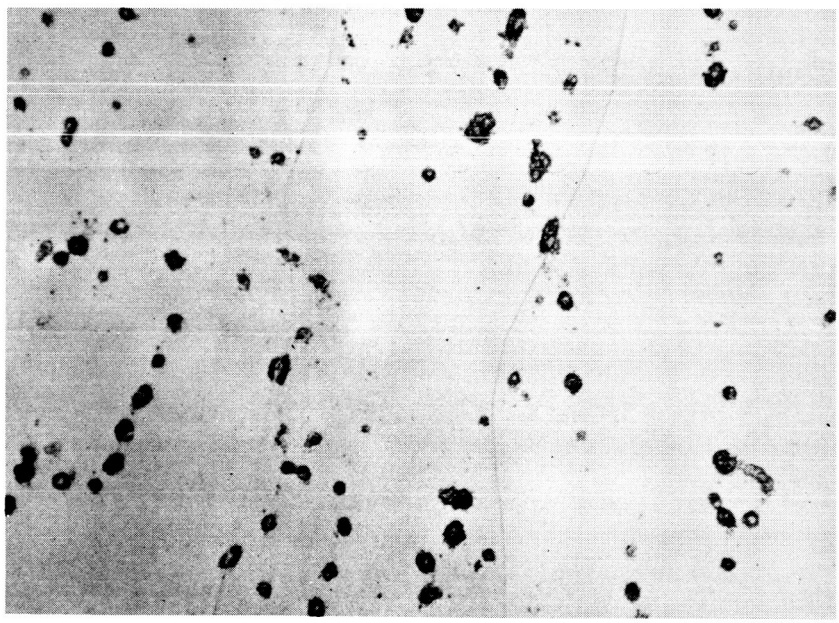

10,183 500X

Welded and Annealed 1 Hr. at 1900°F

FIGURE 23 - B-66 Welded Plate, Weld Microstructure

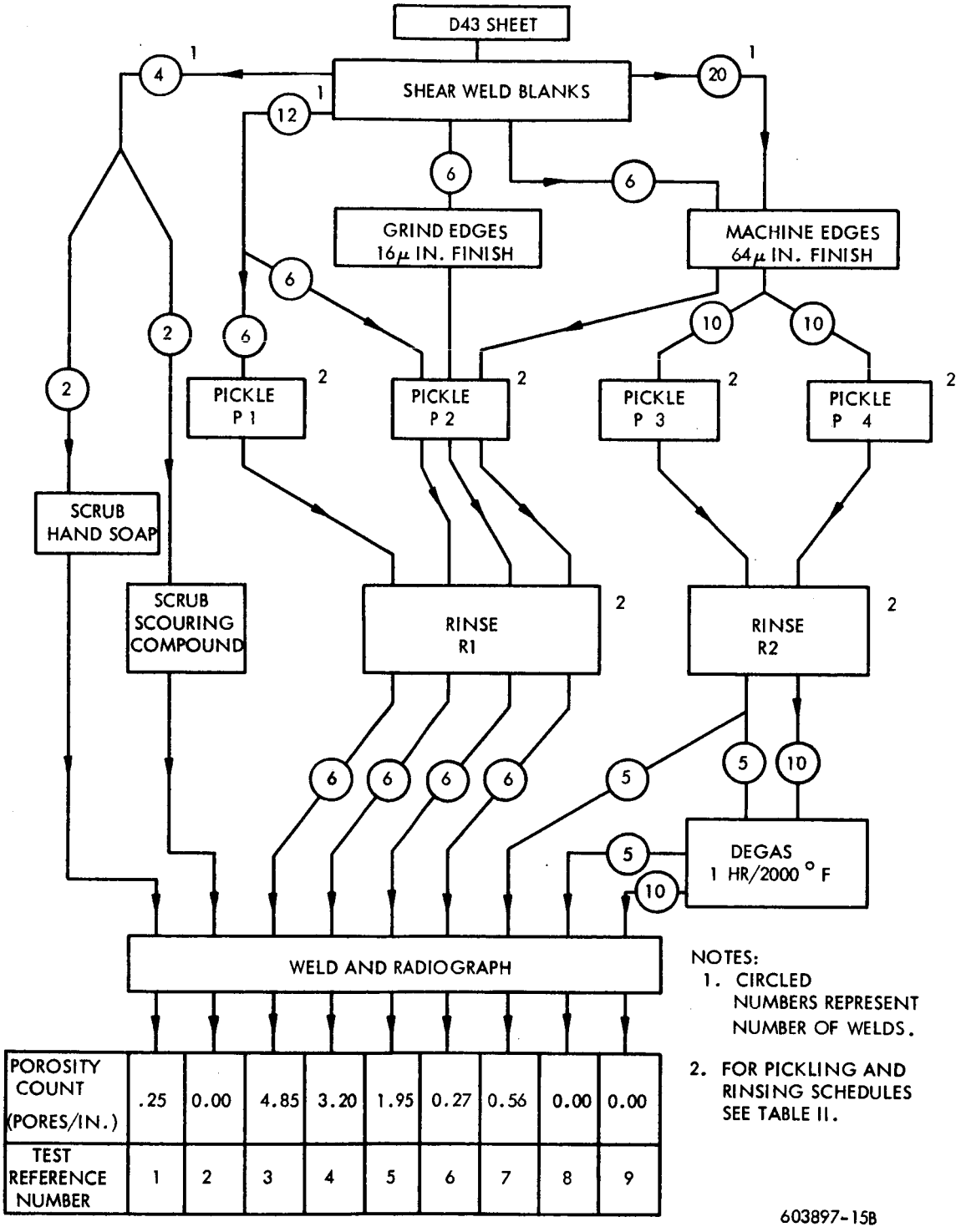

POROSITY COUNT (PORES/IN.)	.25	0.00	4.85	3.20	1.95	0.27	0.56	0.00	0.00
TEST REFERENCE NUMBER	1	2	3	4	5	6	7	8	9

FIGURE 24 - Process Flow Diagram for Weld Porosity Evaluation of D-43

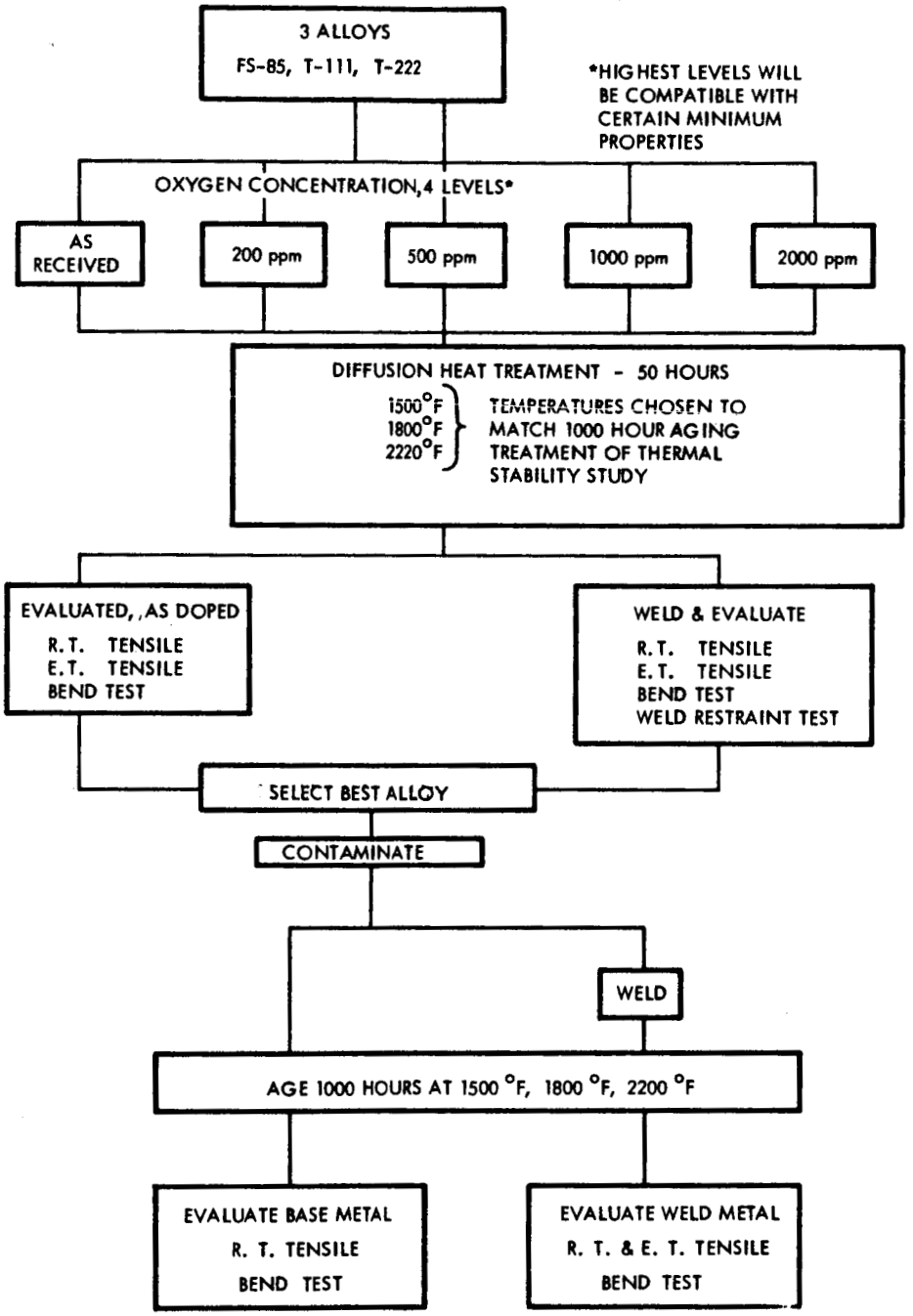

FIGURE 25 - Program Outline for Contaminated Alloy Weldability Evaluation
NOTE: Bead-on Plate Welds Used on this Program

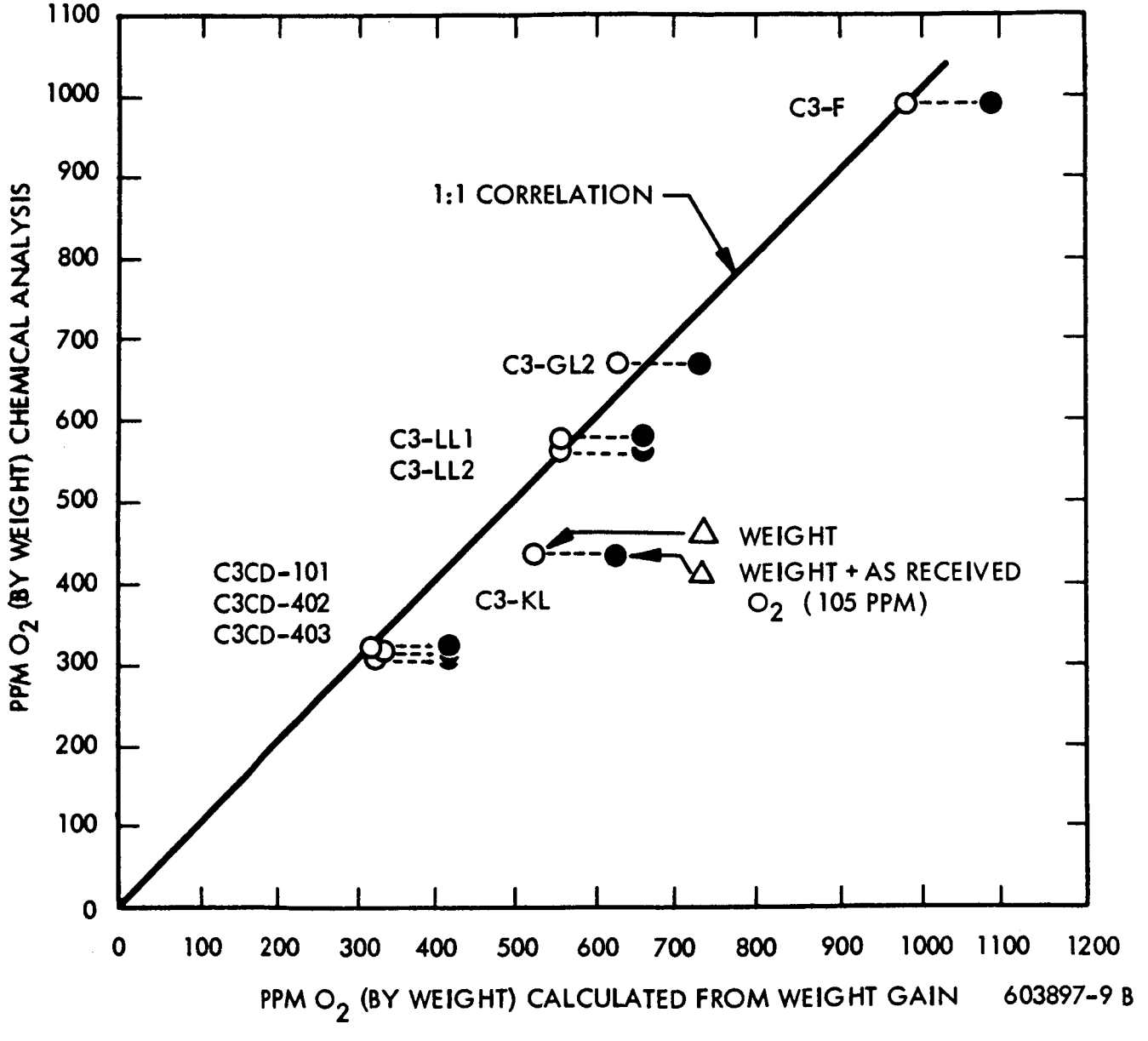

FIGURE 26 - Correlation of Weight Gain with Chemical Analysis

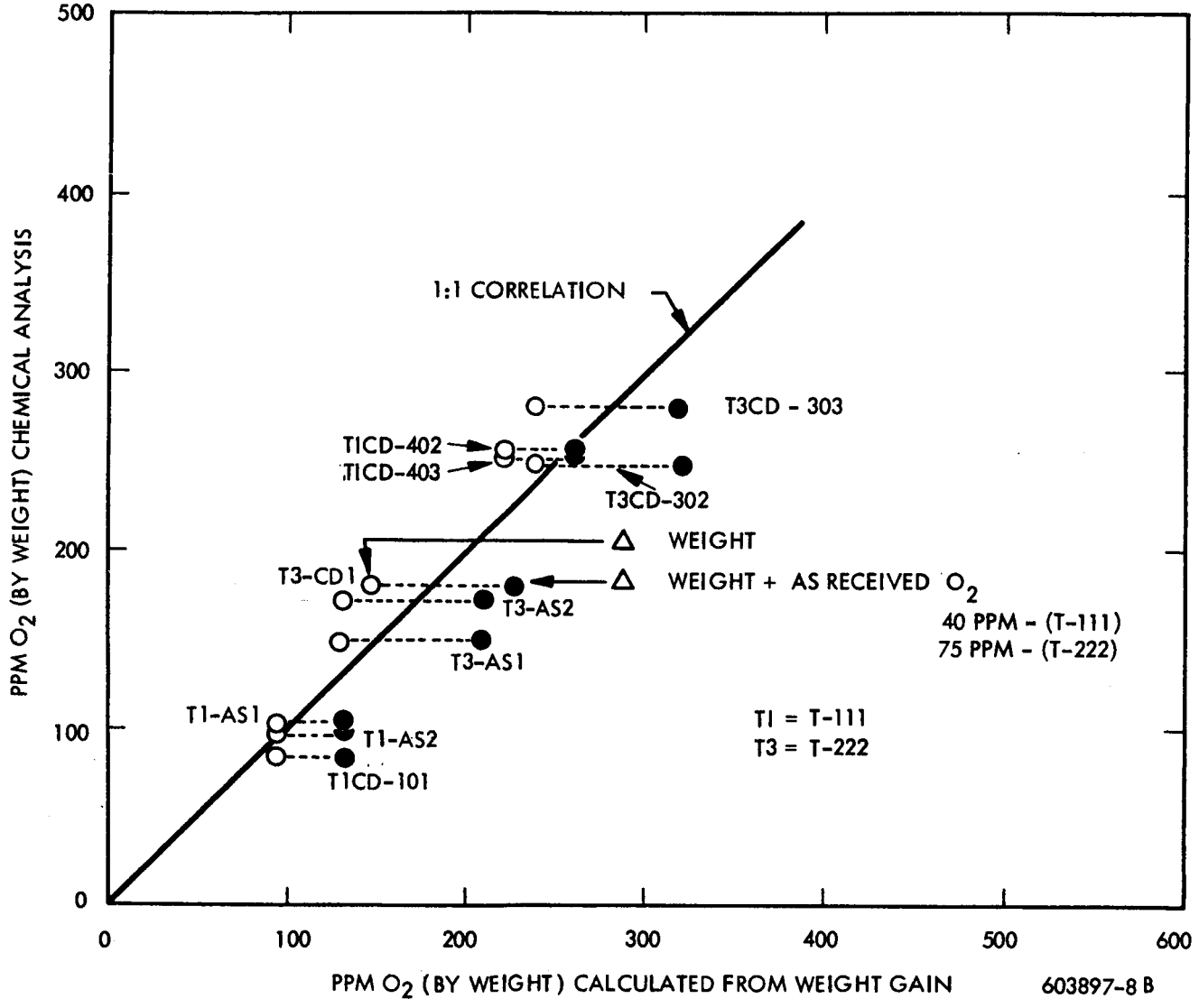

FIGURE 27 - T-111 and T-222 Correlation of Weight Gain with Chemical Analysis

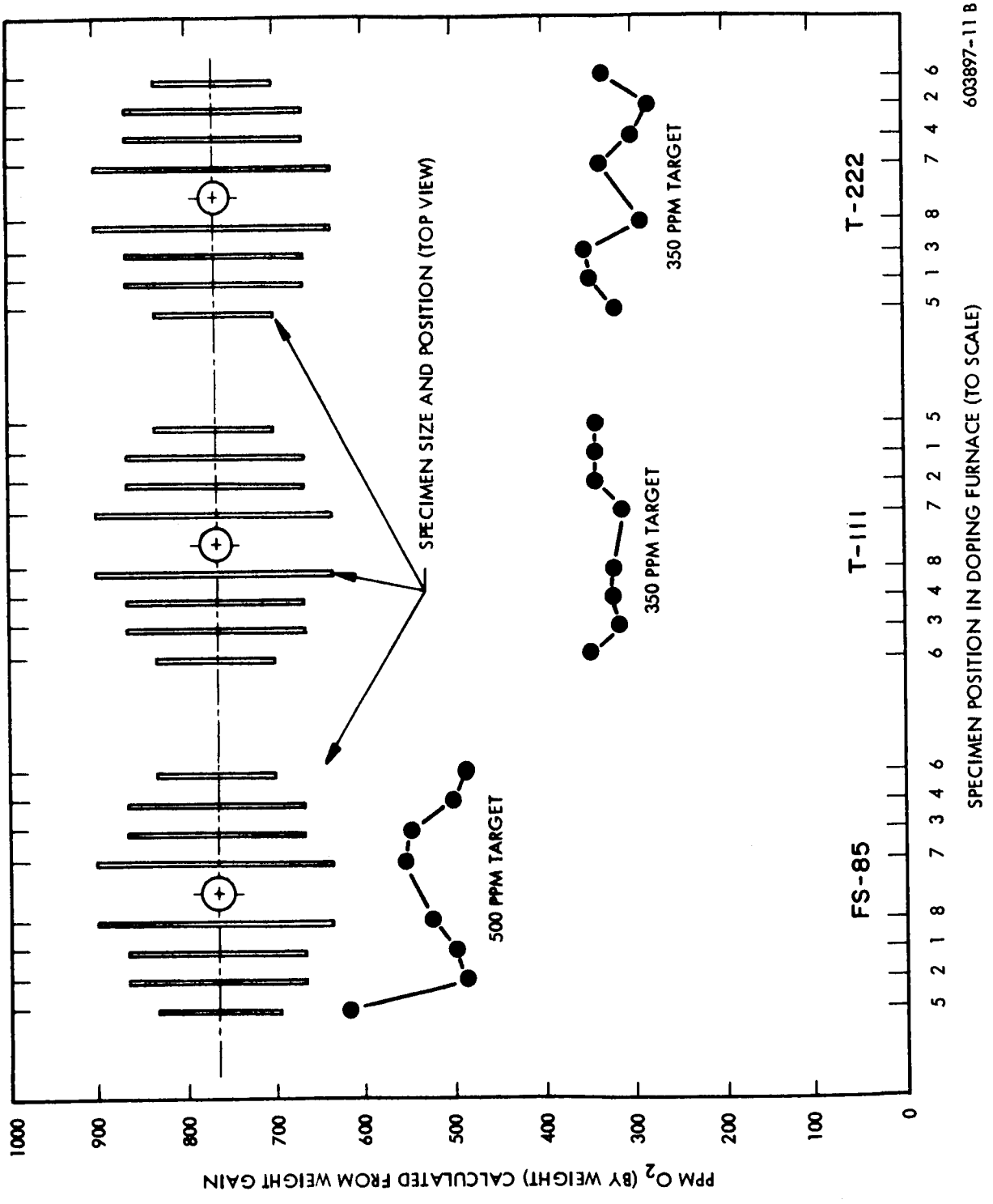

FIGURE 28 - Variation in Oxygen Level Within Furnace Load

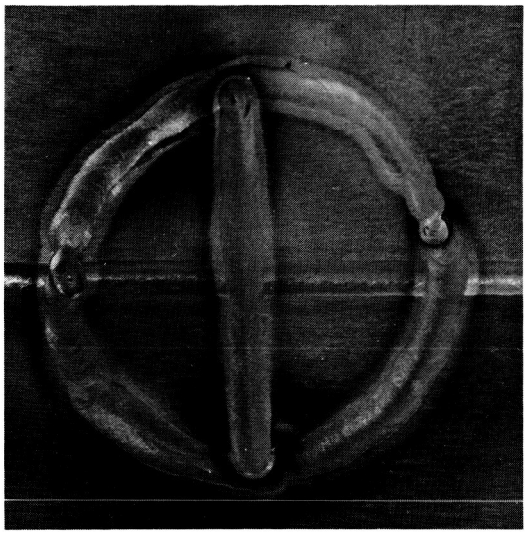

C3CU-7-8 667-2

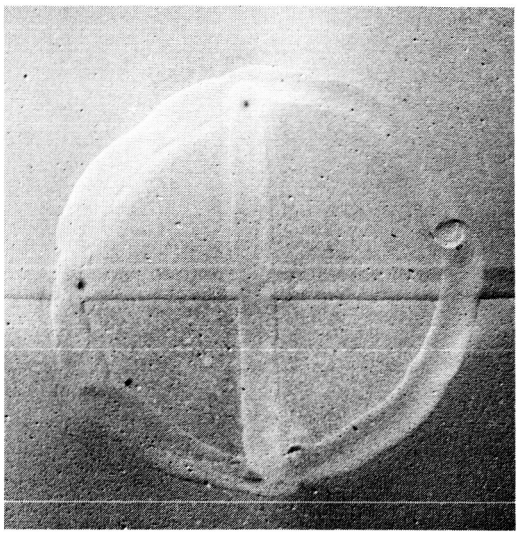

C3CU-7-8 714-3

FS-85 As-Received

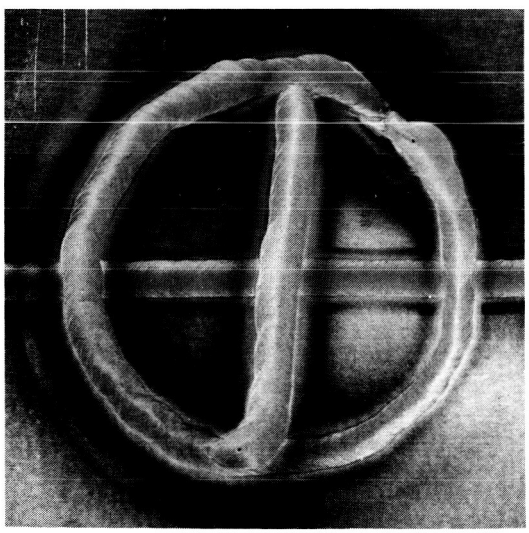

C3CI-7-8 667-7

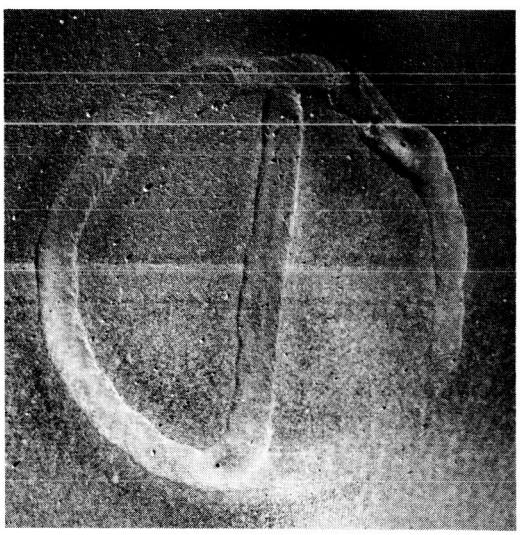

C3CI-7-8 714-5

FS-85 Contaminated to 575 ppm O_2

As-Welded Dye Penetrant Inspected

FIGURE 29 - FS-85 Fabricated Weld Restraint Tests

TICU-7-8 667-5

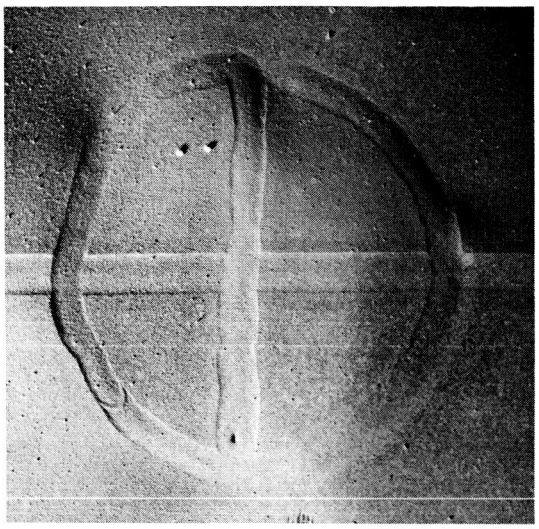

TICU-7-8 714-9

T-111 As-Received

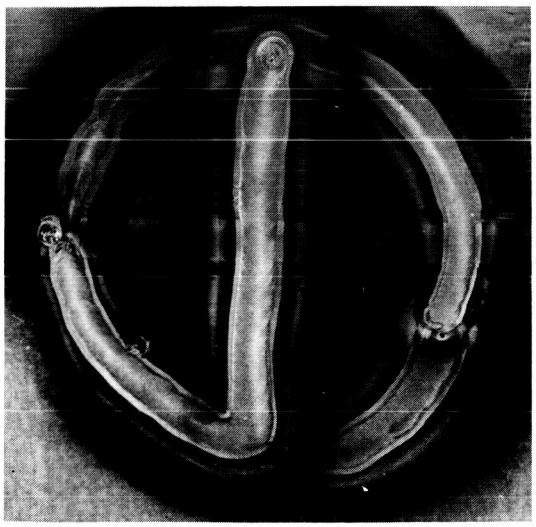

TICI-7-8 668-4

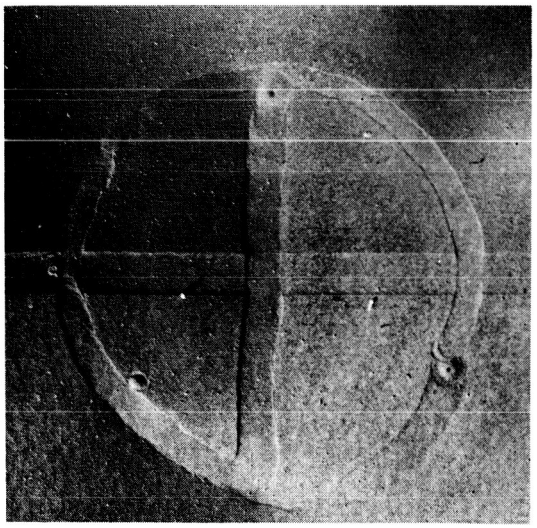

TICI-7-8 714-10

T-111 Contaminated to 335 ppm O_2

As-Welded Dye Penetrant Inspected

FIGURE 30 - T-111 Fabricated Weld Restraint Tests

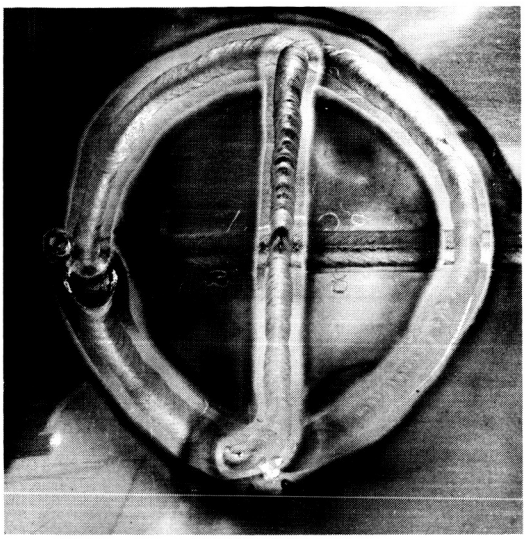

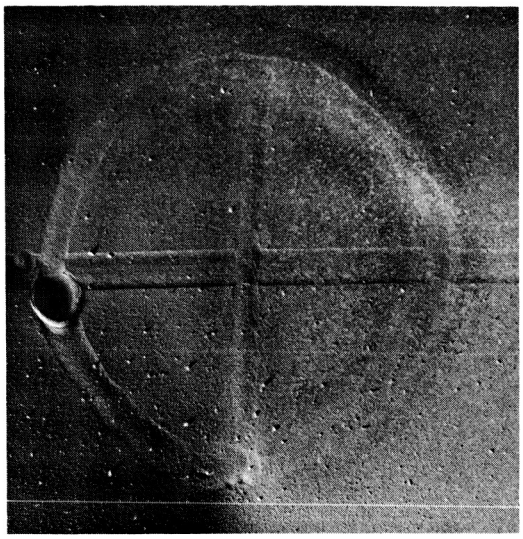

668-6 T3CU-7-8 714-2

T-222 As-Received

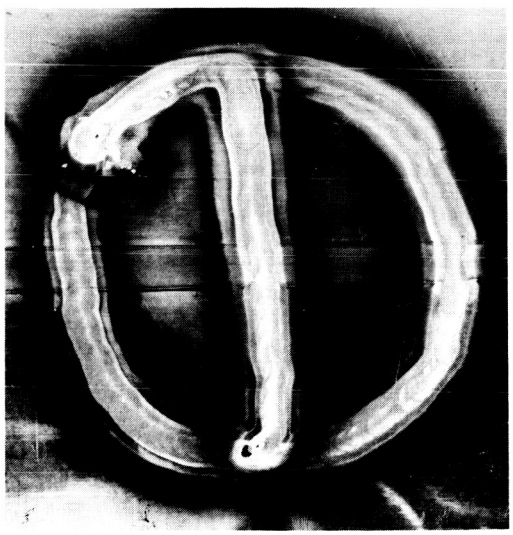

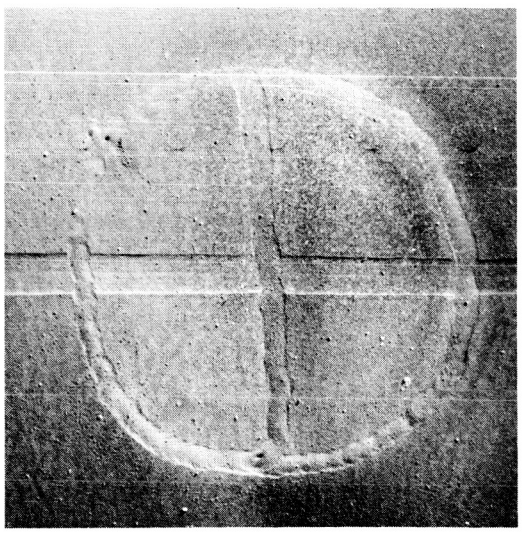

T3CI-7-8 667-1 T3CI-7-8 714-6

T-222 Contaminated to 310 ppm O_2

As-Welded Dye Penetrant Inspected

FIGURE 31 - T-222 Fabricated Weld Restraint Tests

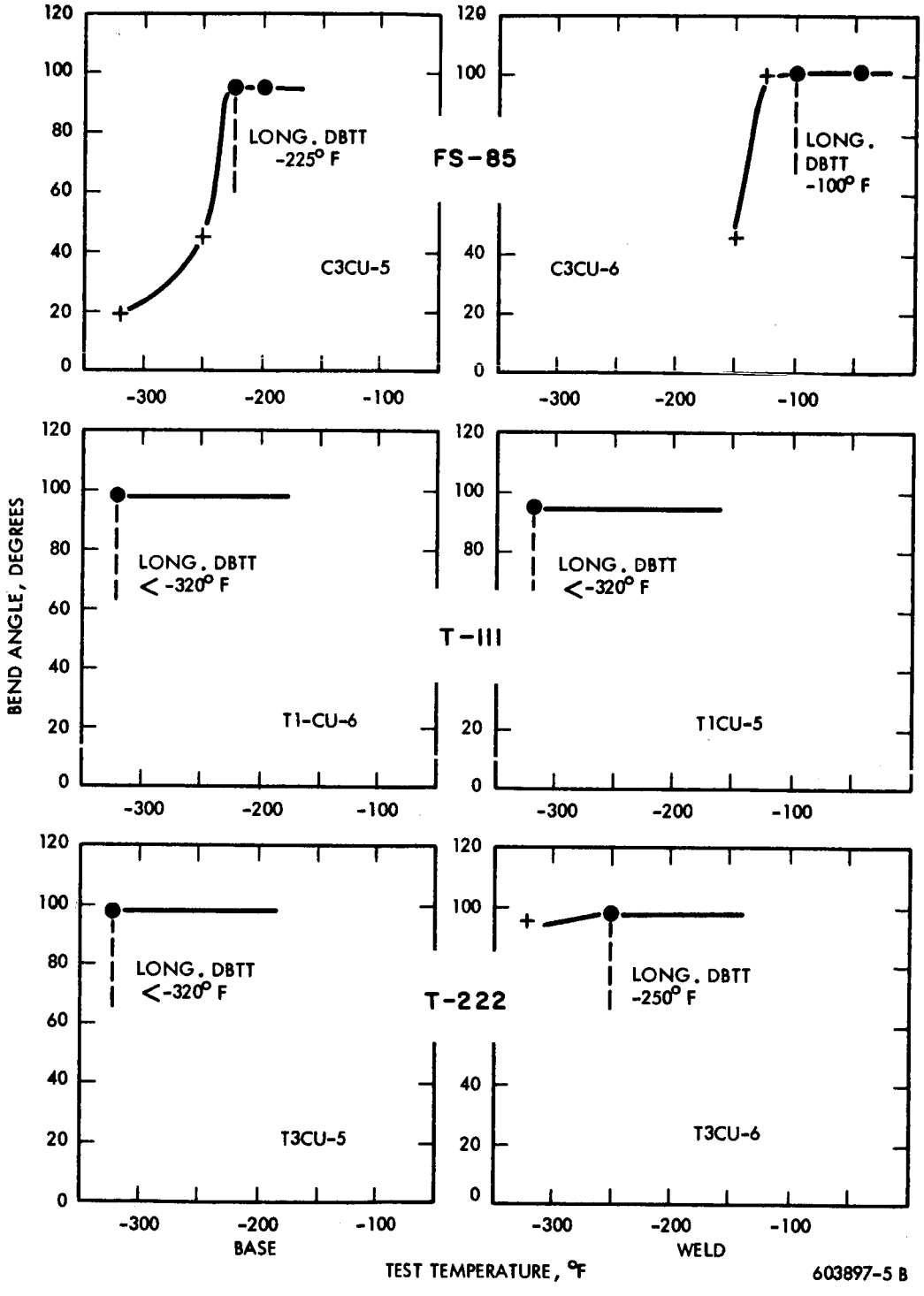

FIGURE 32 - Longitudinal Bend Test Results of Uncontaminated, 1800°F Diffusion Annealed Material

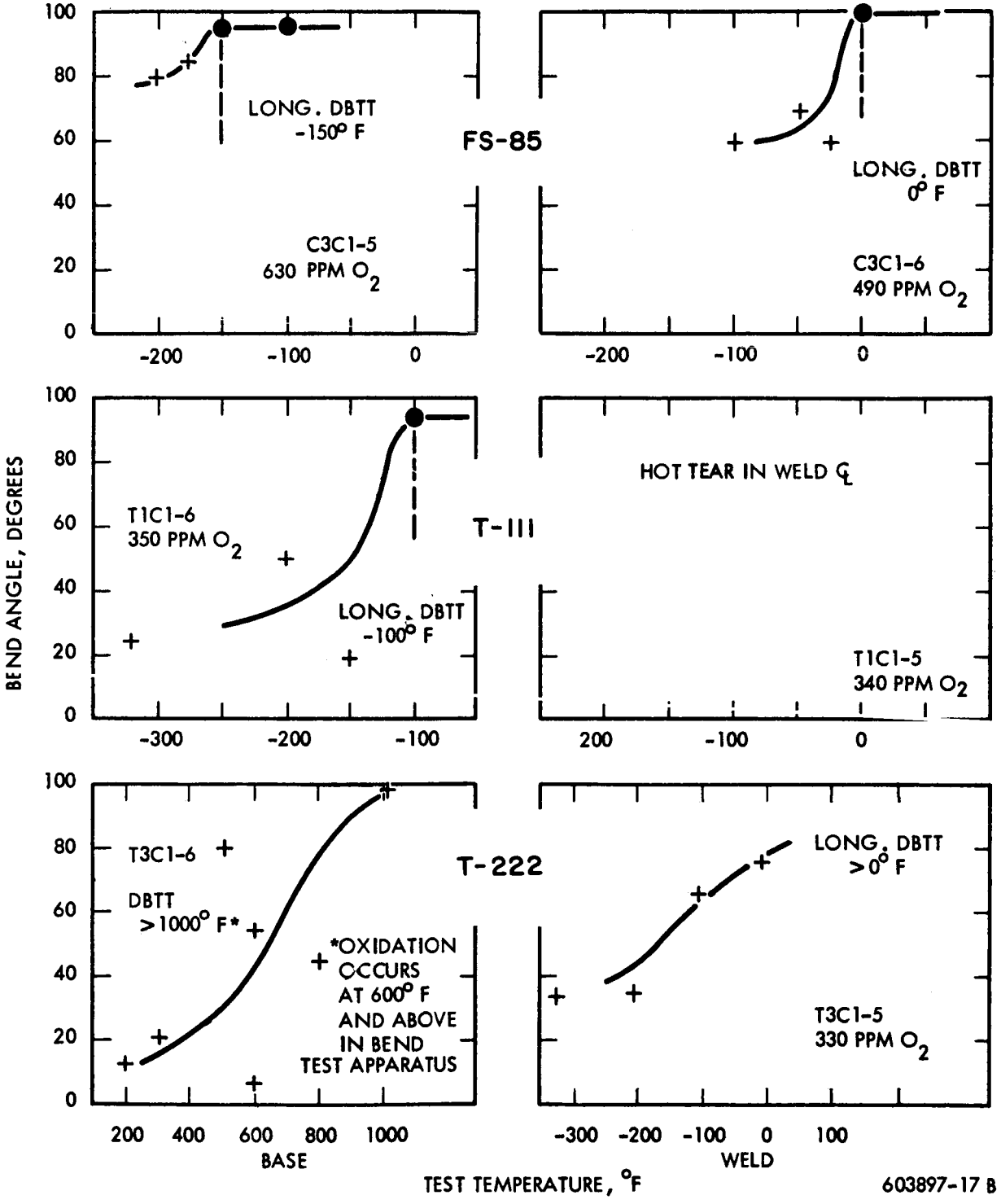

FIGURE 33 - Longitudinal Bend Test Results of 500/350 ppm Oxygen Contaminated, 1800°F Diffusion Annealed Material

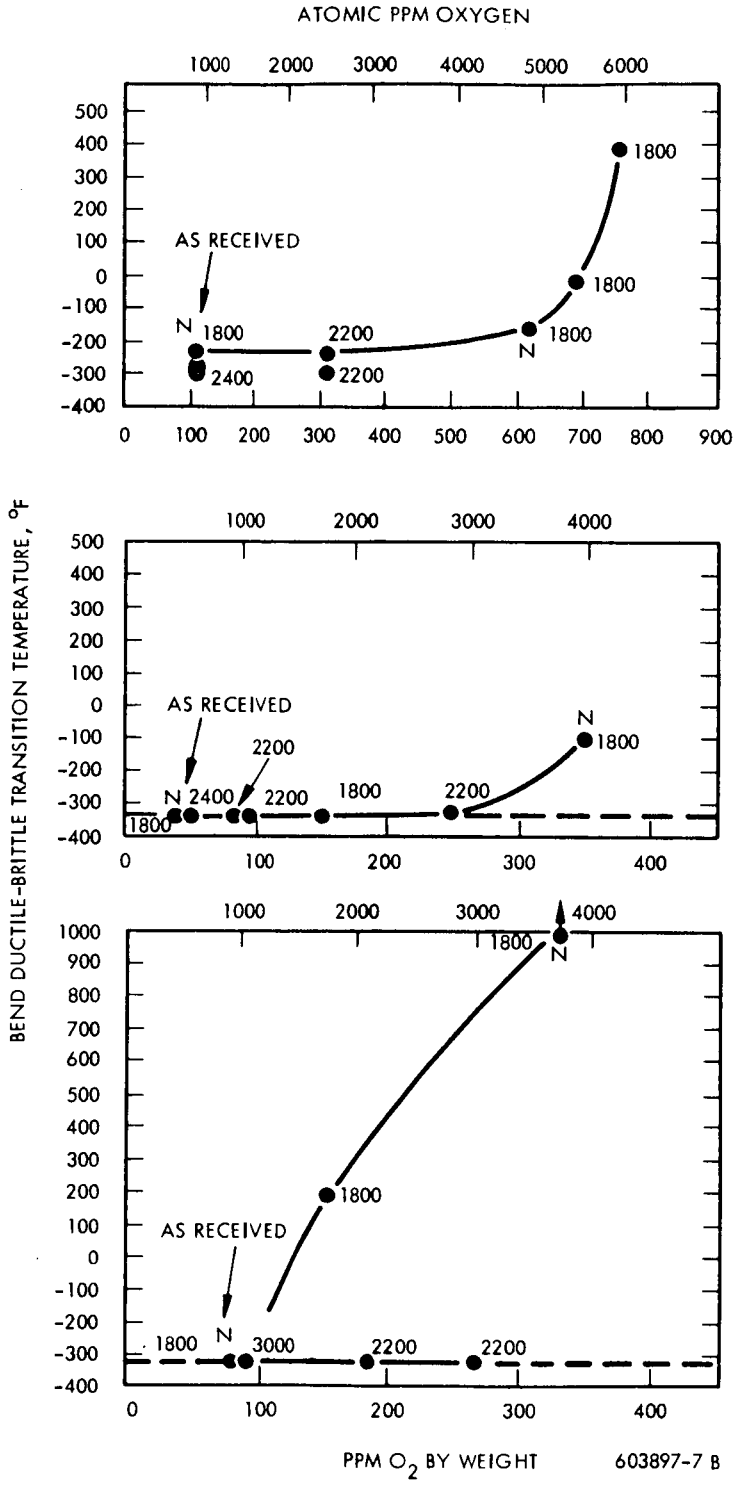

FS-85

T-111

T-222

POINTS MARKED "N" ARE NEW INFORMATION FROM FULL SCALE PROGRAM

LOWEST TEST TEMPERATURE -320° F

DIFFUSION ANNEALING OR PRIOR HEAT TREATING TEMPERATURE LABLED IN °F.

FIGURE 34 - Longitudinal Base Metal Bend Ductility as A Function of Oxygen Content

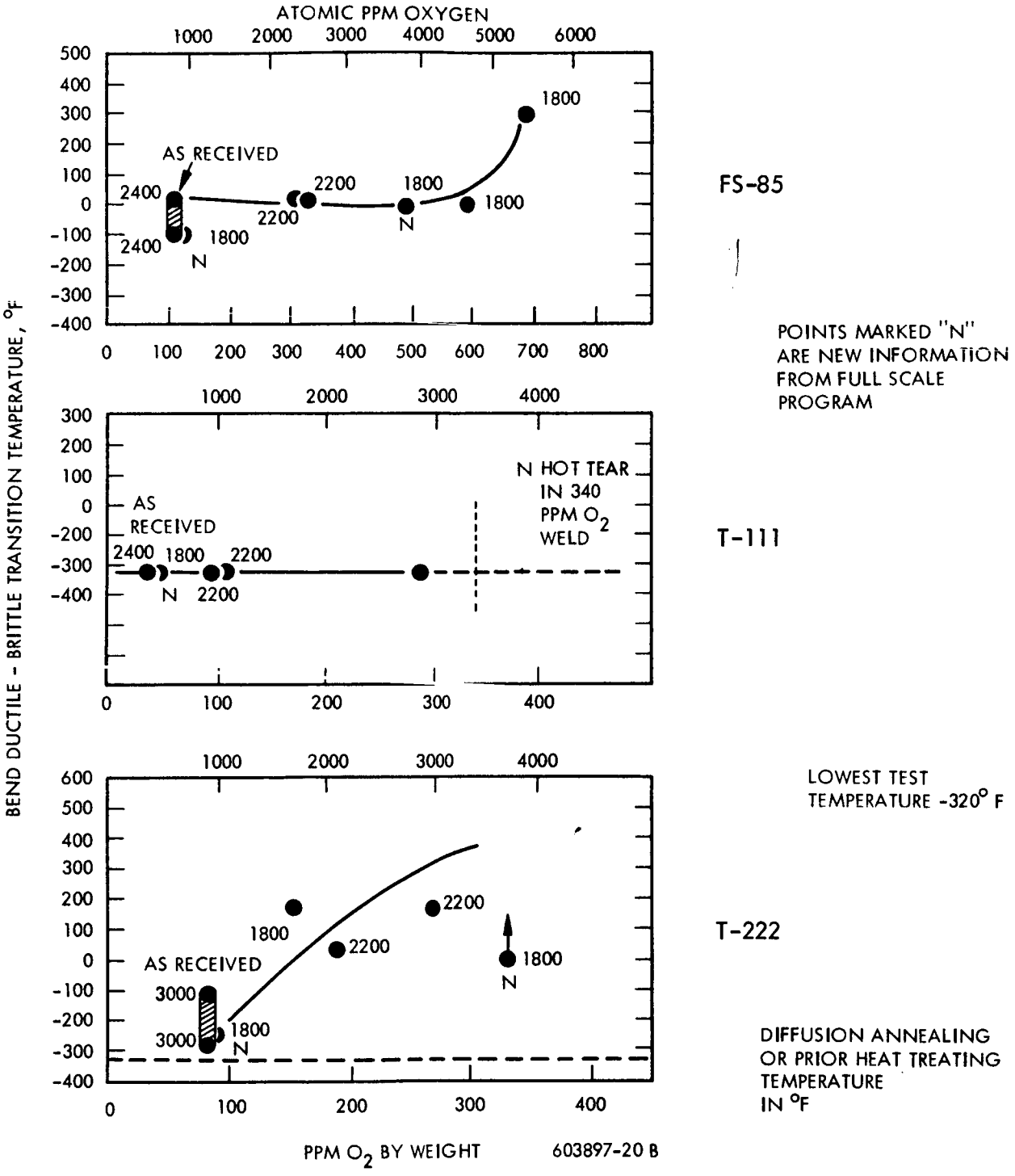

FIGURE 35 - Longitudinal Weld Bend Ductility as a Function of Oxygen Content

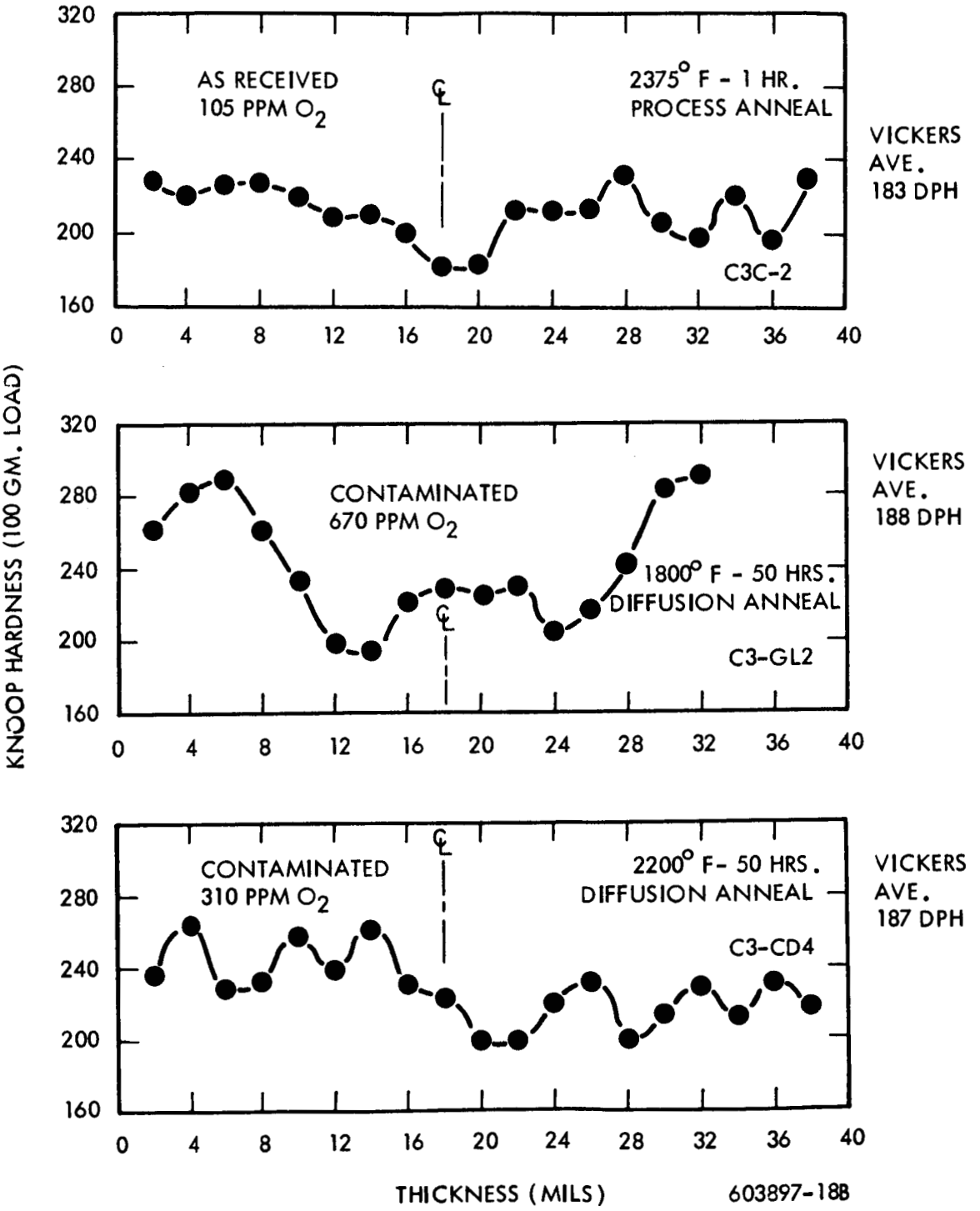

FIGURE 36 - Cross Sectional Hardness Traverse of FS-85

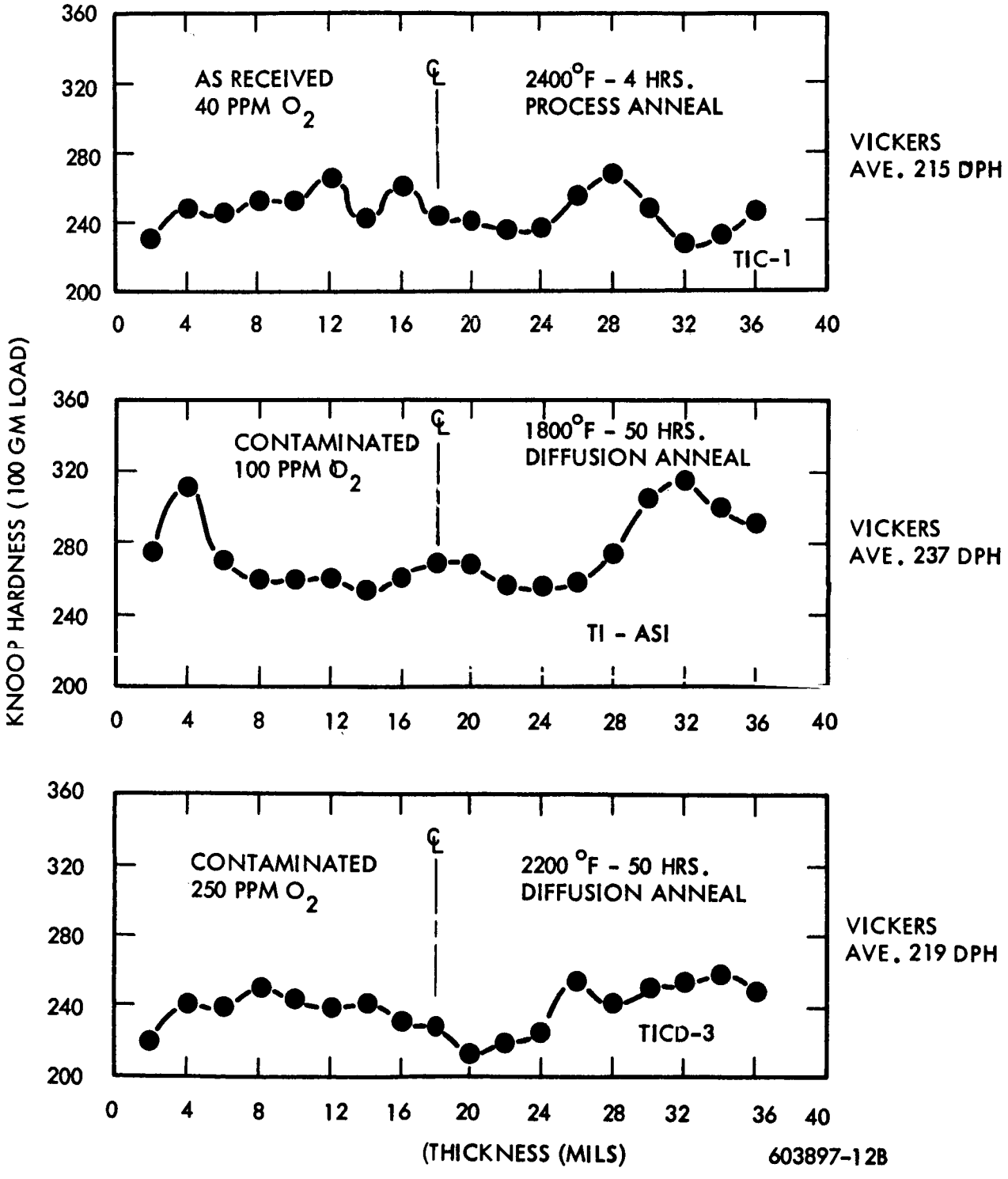

FIGURE 37 - Cross Sectional Hardness Traverse of T-111

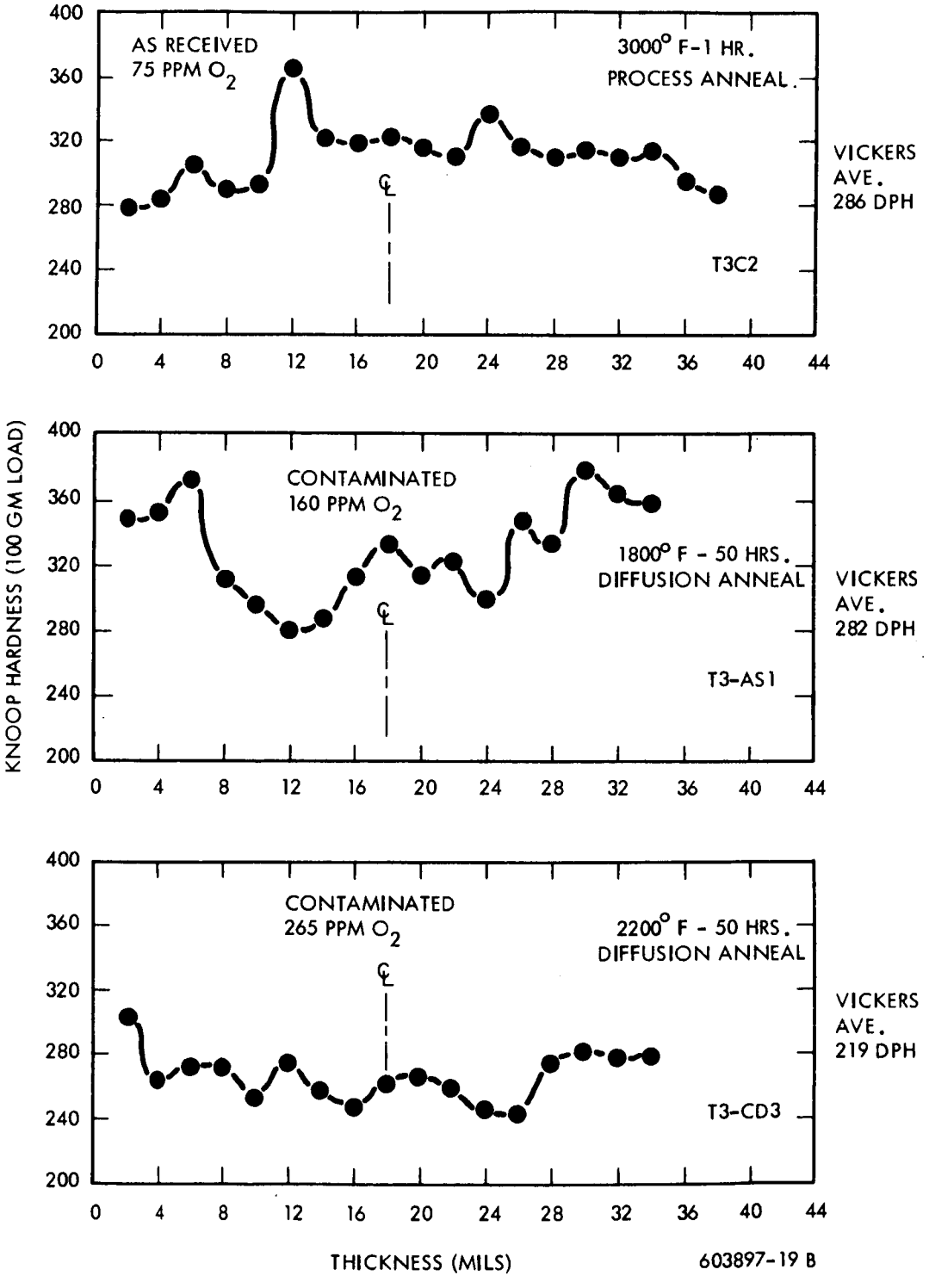

FIGURE 38 - Cross Sectional Hardness Traverse of T-222

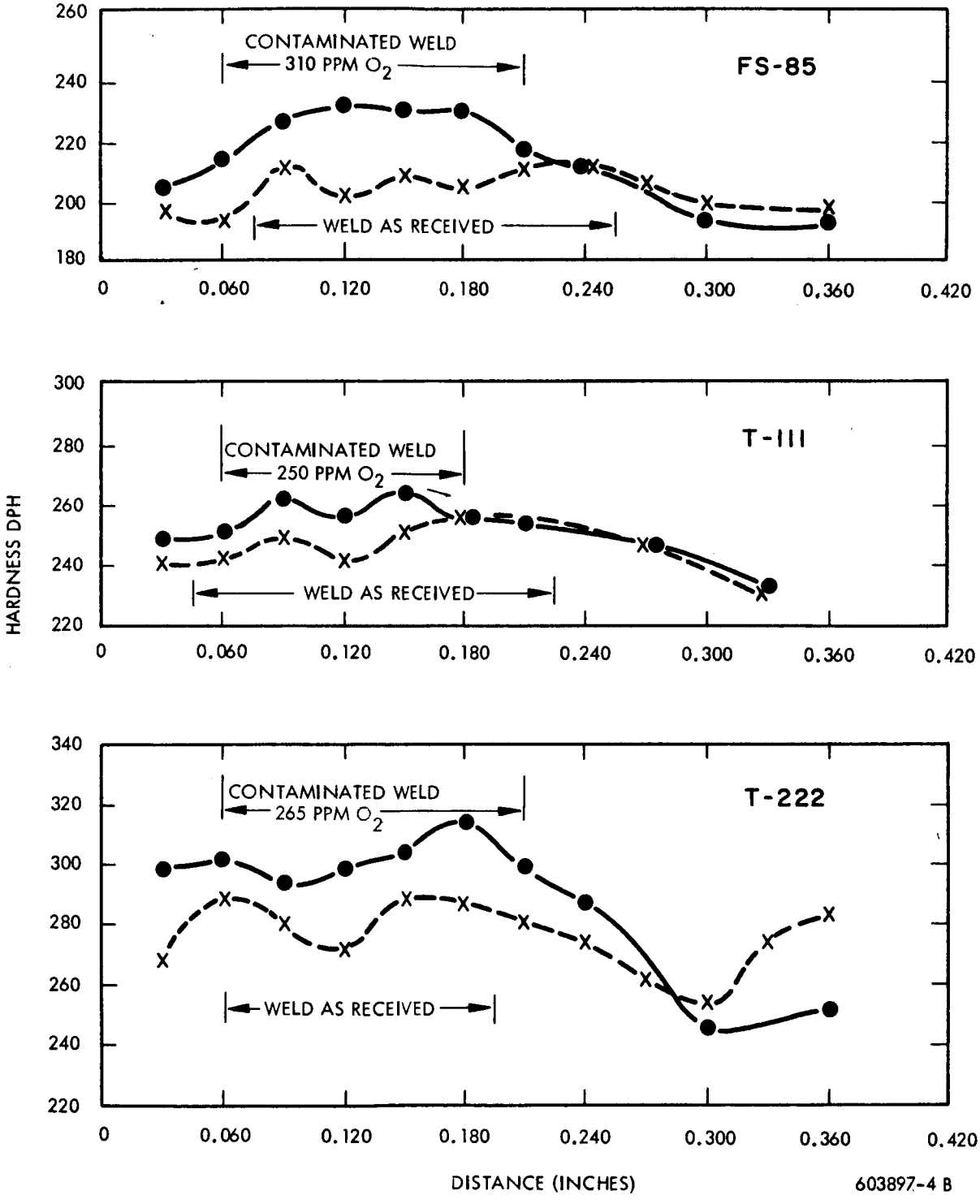

FIGURE 39 - Weld Hardness Traverse of As-Received and Contaminated Material

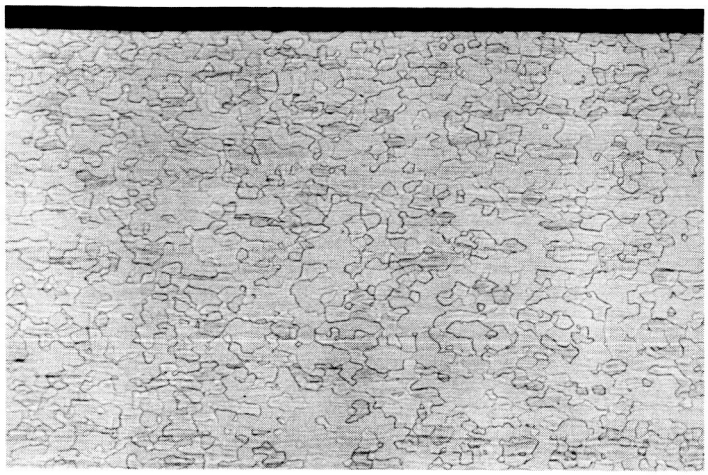

9559 80X

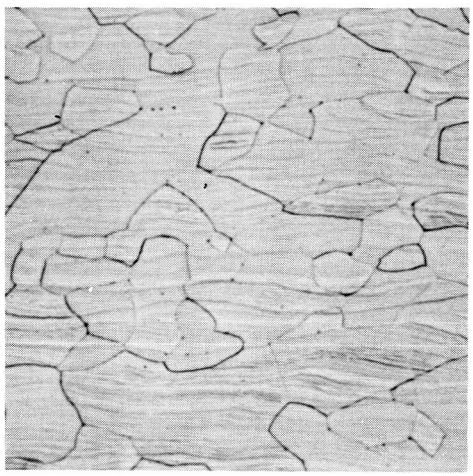

9559 400X

As-Received FS-85 105 ppm O_2
2375°F 1 Hr.

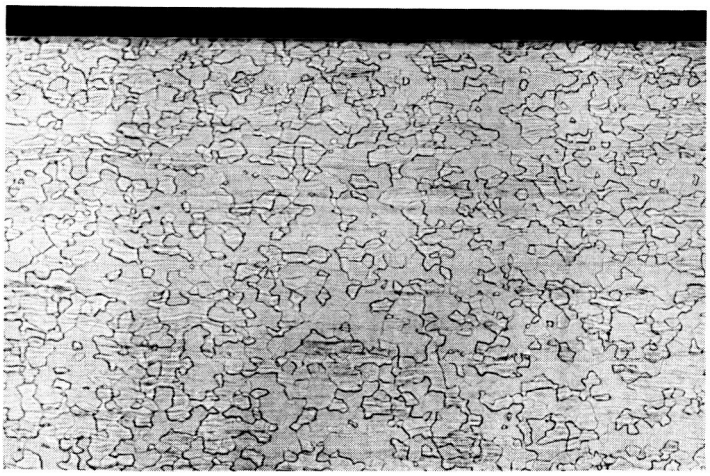

9728 80X

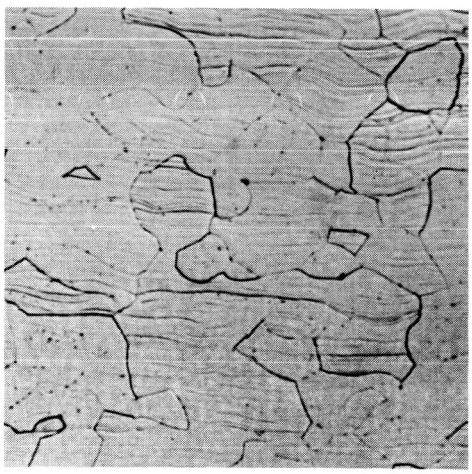

9728 400X

Contaminated FS-85 415 ppm O_2
2200°F 50 Hrs.

FIGURE 40 - Microstructure of As-Received and Contaminated FS-85
(Etch: Glycerine Base $HF-HNO_3 + NH_4F \cdot F$)

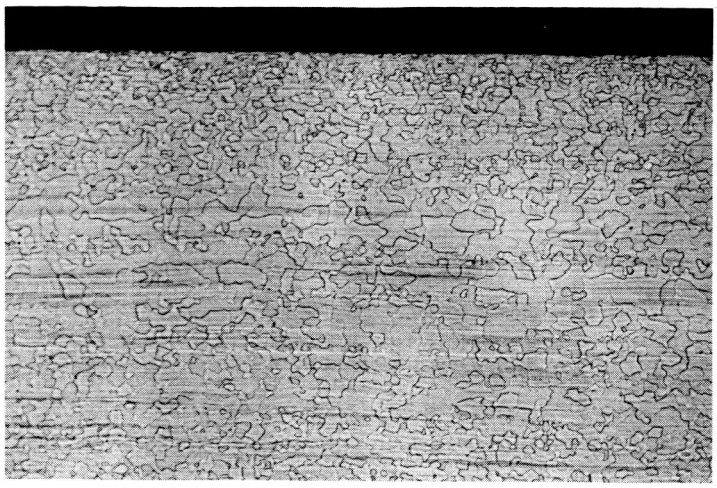

9562 80X

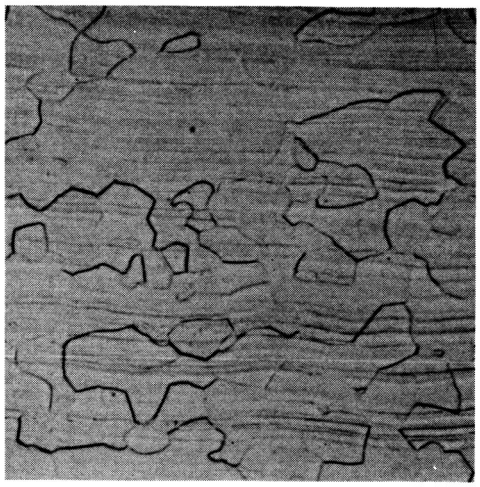

9562 400X

As-Received T-111 2400°F 4 Hours

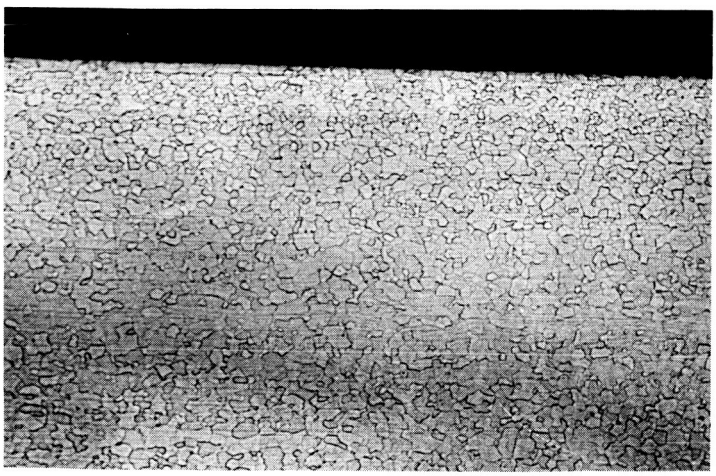

9729 80X

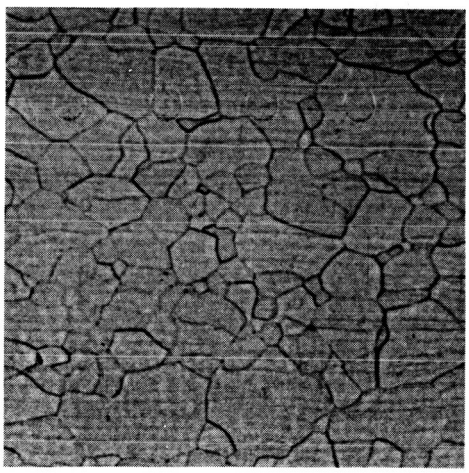

9729 400X

Contaminated T-111 210 ppm O_2
2200°F 50 Hrs.

FIGURE 41 - Microstructure of As-Received and Contaminated T-111
(Etch: 9562 - $NH_4F \cdot HF$, 9729 - Glycerine Base $HF\text{-}HNO_3$
+ $NH_4F \cdot HF$ Wipe)

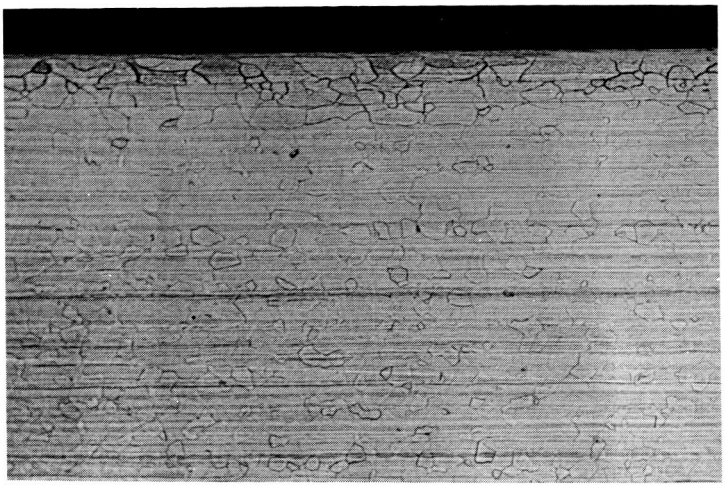

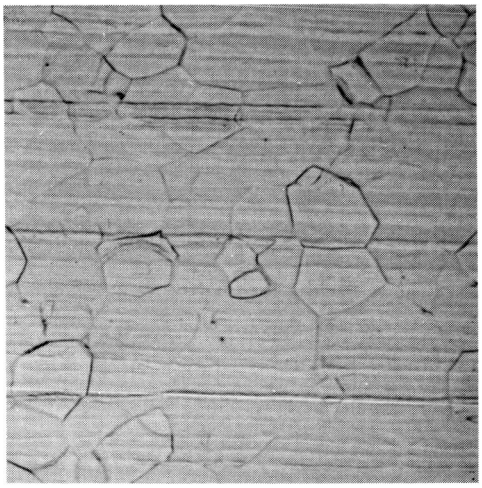

80X 9561 400X

As-Received T-222 3000°F 1 Hr.

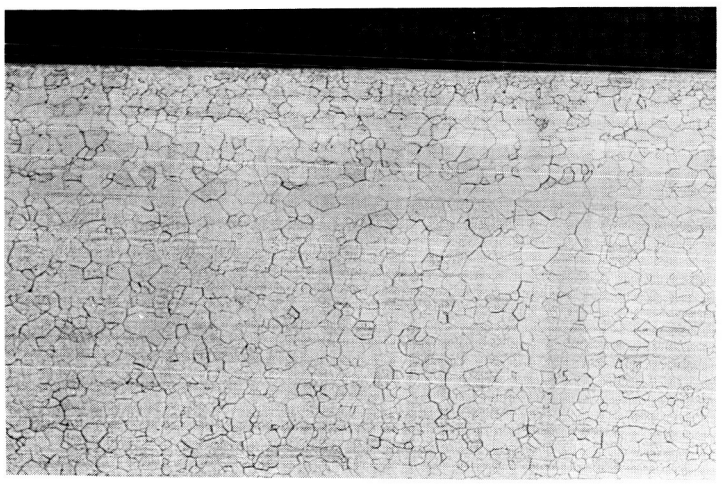

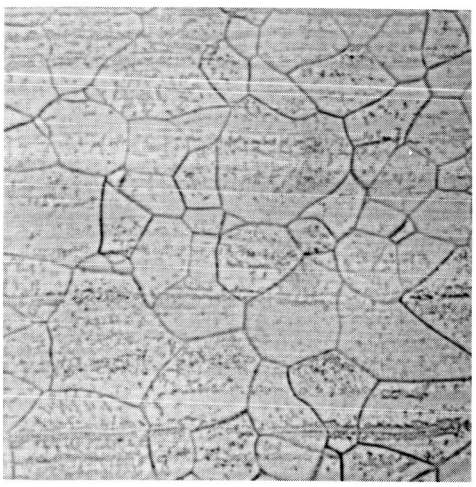

9731 80X 9731 400X

Contaminated T-222 275 ppm O_2
2200°F 50 Hrs.

FIGURE 42 - Microstructure of As-Received and Contaminated T-222
(Etch: Glycerine Base HF-HNO_3 + $NH_4F \cdot HF$ Wipe)

DISTRIBUTION LIST

TRW
Caldwell Research Center
23555 Euclid Avenue
Cleveland, Ohio 44117
Attn: Librarian
Attn: G. J. Guarnieri

TRW
New Devices Laboratories
7209 Platt Avenue
Cleveland, Ohio 44104
Attn: Librarian

National Aeronautics and Space Adm.
Washington, D. C. 20546
Attn: Walter C. Scott
Attn: James J. Lynch (RN)
Attn: George C. Deutsch (RR)

National Aeronautics and Space Adm.
Scientific and Technical Inf. Facility
Box 5700
Bethesda, Maryland 21811

National Aeronautics and Space Adm.
Ames Research Center
Moffet Field, California 94035
Attn: Librarian

National Aeronautics and Space Adm.
Goddard Space Flight Center
Greenbelt, Maryland 20771
Attn: Librarian

National Aeronautics and Space Adm.
Langley Research Center
Hampton, Virginia 23365
Attn: Librarian

National Aeronautics and Space Adm.
Manned Spacecraft Center
Houston, Texas 77001
Attn: Librarian

National Aeronautics and Space Adm.
George C. Marshall Space Flight Center
Huntsville, Alabama 35812
Attn: Librarian
Attn: Wm. A. Wilson

National Aeronautics and Space Adm.
Jet Propulsion Laboratory
4800 Oak Grove Drive
Pasadena, California 91103
Attn: Librarian

National Aeronautics and Space Adm.
21000 Brookpark Road
Cleveland, Ohio 44135
Attn: Librarian
Attn: Dr. Bernard Lubarsky
Attn: Mr. Roger Mather
Attn: Mr. G. M. Ault
Attn: Mr. J. Joyce
Attn: Mr. P. E. Moorhead
Attn: Mr. N. T. Musial
Attn: Mr. T. Strom
Attn: Mr. T. A. Moss
Attn: Dr. Louis Rosenblum
Attn: J. Creagh
Attn: Mr. J. Dilley
Attn: Mr. G. K. Watson
Attn: Mr. T. Moore
Attn: Mr. G. Tulsiak
Attn: NASA-Lewis Laboratory Report Central Section

National Aeronautics and Space Adm.
Western Operations Office
150 Pico Boulevard
Santa Monica, California 90406
Attn: Mr. John Keeler

National Bureau of Standards
Washington 25, D. C.
Attn: Librarian

Aeronautical Systems Division
Wright-Patterson Air Force Base, Ohio
Attn: Charles Armbruster
Attn: T. Cooper
Attn: Librarian
Attn: John L. Morris
Attn: H. J. Middendorp

Army Ordnance Frankford Arsenal
Bridesburg Station
Philadelphia 37, Pennsylvania
Attn: Librarian

Bureau of Ships
Dept. of the Navy
Washington 25, D. C.
Attn: Librarian

Bureau of Weapons
Research and Engineering
Material Division
Washington 25, D. C.
Attn: Librarian

U. S. Atomic Energy Commission
Technical Reports Library
Washington 25, D. C.
Attn: J. M. O' Leary

U. S. Atomic Energy Commission
Germantown, Maryland
Attn: Col. E. L. Douthett
Attn: H. Rochen
Attn: Major Gordon Dicker

U. S. Atomic Energy Commission
Technical Information Service Extension
P. O. Box 62
Oak Ridge, Tennessee

U. S. Atomic Energy Commission
Washington 25, C. C.
Attn: M. J. Whitman

Argonne National Laboratory
9700 South Cross Avenue
Argonne, Illinois
Attn: Librarian

Brookhaven National Laboratory
Upton, Long Island, New York
Attn: Librarian

Oak Ridge National Laboratory
Oak Ridge, Tennessee
Attn: W. O. Harms
Attn: Dr. A. J. Miller
Attn: Librarian
Attn: N. T. Bray

Office of Naval Research
Power Division
Washington 25, D. C.
Attn: Librarian

U. S. Naval Research Laboratory
Washington 25, D. C.
Attn: Librarian

Advanced Technology Laboratories
Division of American Standard
369 Whisman Road
Mountain View, California
Attn: Librarian

Aerojet General Corporation
P. O. Box 296
Azusa, California
Attn: Librarian

Aerojet General Nucleonics
P. O. Box 77
San Ramon, California
Attn: Librarian

AiResearch Manufacturing Company
Sky Harbor Airport
402 South 36th Street
Phoenix, Arizona
Attn: Librarian
Attn: E. A. Kovacevich

AiResearch Manufacturing Company
9851-9951 Sepulveda Boulevard
Los Angeles 45, California
Attn: Librarian

I. I. T. Research Institute
10 W. 35th Street
Chicago, Illinois 60616

Atomics International
8900 DeSoto Avenue
Canoga Park, California

Avco
Research and Advanced Development Dept.
201 Lowell Street
Wilmington, Massachusetts
Attn: Librarian

Babcock and Wilcox Company
Research Center
Alliance, Ohio
Attn: Librarian

Battelle Memorial Institute
505 King Avenue
Columbus, Ohio
Attn: C. M. Allen
Attn: Librarian
Attn: Defense Metals Inf. Center

The Bendix Corporation
Research Laboratories Div.
Southfield, Detroit 1, Michigan
Attn: Librarian

Bell Aerosystems Co.
P. O. Box 1
Buffalo 5, New York
Attn: E. J. King

The Boeing Company
Seattle, Washington
Attn: Librarian

Brush Beryllium Company
17876 St. Clair Avenue
Cleveland, Ohio 44110
Attn: Librarian

Carborundum Company
Niagara Falls, New York
Attn: Librarian

Chance Vought Aircraft Inc.
P. O. Box 5907
Dallas 22, Texas
Attn: Librarian

Clevite Corporation
Mechanical Research Division
540 East 105th Street
Cleveland 8, Ohio
Attn: Mr. N. C. Beerli

Climax Molybdenum Company of Michigan
1600 Huron Parkway
Ann Arbor, Michigan
Attn: Librarian

Convair Astronautics
50001 Kerrny Villa Road
San Diego 11, California
Attn: Librarian

E. I. duPont deNemours and Co., Inc.
Wilmington 98, Delaware
Attn: Librarian

Electro-Optical Systems, Inc.
Advanced Power Systems Division
Pasadena, California
Attn: Librarian

Fansteel Metallurgical, Corp.
North Chicago, Illinois
Attn: Librarian

Ford Motor Company
Aeronutronics
Newport Beach, California
Attn: Librarian

General Dynamics/General Atomic
P. O. Box 608
San Diego, California 92112
Attn: Librarian

General Electric Company
Atomic Power Equipment Div.
P. O. Box 1131
San Jose, California

General Electric Company
Flight Propulsion Laboratory Dept.
Cincinnati 15, Ohio
Attn: Librarian
Attn: Dr. J. W. Semmel

General Electric Company
Missile and Space Vehicle Dept.
3198 Chestnut Street
Philadelphia 4, Pennsylvania
Attn: Librarian

General Electric Company
Vallecitos
Vallecitos Atomic Lab.
Pleasanton, California
Attn: Librarian

Herring Corp.
7356 Greenback Drive
Hollywood, California 91605
Attn: Don Adams

General Dynamics/Fort Worth
P. O. Box 748
Fort Worth, Texas
Attn: Librarian

General Motors Corporation
Allison Division
Indianapolis 6, Indiana
Attn: Librarian

Hamilton Standard
Div. of United Aircraft Corp.
Windsor Locks, Connecticut
Attn: Librarian

Hughs Aircraft Company
Engineering Division
Culver City, California
Attn: Librarian

Lockheed Missiles and Space Div.
Lockheed Aircraft Corp.
Sunnyvale, California
Attn: Librarian

Marquardt Aircraft Co.
P. O. Box 2013
Van Nuys, California
Attn: Librarian

The Martin Company
Baltimore 3, Maryland
Attn: Librarian

The Martin Company
Nuclear Division
P. O. Box 5042
Baltimore 20, Maryland
Attn: Librarian

Martin Marietta Corp.
Metals Technology Laboratory
Wheeling, Illinois

Massachusetts Institute of Technology
Cambridge 39, Massachusetts
Attn: Librarian

Materials Research and Development
Manlabs Inc.
21 Erie Street
Cambridge 39, Massachusetts

Materials Research Corporation
Orangeburg, New York
Attn: Librarian

McDonnell Aircraft
St. Louis, Missouri
Attn: Librarian

MSA Research Corporation
Callery, Pennsylvania
Attn: Librarian

North American Aviation
Los Angeles Division
Los Angeles 9, California
Attn: Librarian

National Research Corp.
Metals Division
45 Industrial Place
Newton, Massachusetts 02164
Attn: Dr. M. L. Torte
Director of Metallurgical Research

Lawrence Radiation Laboratory
Livermore, California
Attn: Dr. James Hadley
Head, Reactor Division

Pratt & Whitney Aircraft
400 Main Street
East Hartford 8, Connecticut
Attn: Librarian

Republic Aviation Corporation
Farmingdale, Long Island, New York
Attn: Librarian

Solar
2200 Pacific Highway
San Diego 12, California

Southwest Research Institute
8500 Culebra Road
San Antonio 6, Texas
Attn: Librarian

Rocketdyne
Canoga Park, California
Attn: Librarian

Superior Tube Co.
Norristown, Pennsylvania
Attn: Mr. A. Bound

Sylvania Electric Products, Inc.
Chem. & Metallurgical
Towanda, Pennsylvania
Attn: Librarian

Temescal Metallurgical
Berkeley, California
Attn: Librarian

Union Carbide Stellite Corp.
Kokomo, Indiana
Attn: Librarian

Union Carbide Metals
Niagara Falls, New York
Attn: Librarian

Union Carbide Nuclear Company
P. O. Box X
Oak Ridge, Tennessee
Attn: X-10 Laboratory Records Department

United Nuclear Corporation
5 New Street
White Plains, New York
Attn: Librarian
Attn: Mr. Albert Weinstein

Universal Cyclops Steel Corp.
Refractomet Division
Bridgeville, Pennsylvania
Attn: C. P. Mueller

TRW Space Technology Laboratories
One Space Park
Redondo Beach, California
Attn: Librarian

University of California
Lawrence Radiation Lab.
P. O. Box 808
Livermore, California
Attn: Librarian

University of Michigan
Department of Chemical & Metallurgical Eng.
Ann Arbor, Michigan
Attn: Librarian

Vought Astronautics
P. O. Box 5907
Dallas 22, Texas
Attn: Librarian

Wolverine Tube Division
Calumet & Hecla, Inc.
17200 Southfield Road
Allen Park, Michigan
Attn: R. C. Cash

Wyman-Gordon Co.
North Grafton, Massachusetts
Attn: Librarian